Bruno Jorge Macedo dos Santos

Development of nonlinear turbulent models based on Reynolds average using objective tensors.

Dissertação de Mestrado

Dissertation presented to the Programa de Pós-Graduação em Engenharia Mecânica of PUC-Rio in partial fulfillment of the requirements for the degree of Mestre em Engenharia Mecânica.

Advisor: Prof. Angela Ourivio Nieckele

Rio de Janeiro

April 2021

Pontifícia Universidade Católica
do Rio de Janeiro

Bruno Jorge Macedo dos Santos

Development of nonlinear turbulent models based on Reynolds average using objective tensors.

Dissertation presented to the Programa de Pós-Graduação em Engenharia Mecânica of PUC-Rio in partial fulfillment of the requirements for the degree of Mestre em Engenharia Mecânica. Approved by the Examination Committee:

Profª. Angela Ourivio Nieckele
Advisor
Departamento de Engenharia Mecânica – PUC-Rio

Prof. Luiz Eduardo Bittencourt Sampaio
Department of Energy Resources Engineering –Stanford University

Prof. Roney Leon Thompson
Departamento de Engenharia Mecânica – UFRJ

Rio de Janeiro, April 6th, 2021

Bruno Jorge Macedo dos Santos

The author graduated in Mechanical Engineering from Universidade Federal Fluminense in December 2014.

Bibliographic data

Santos, Bruno Jorge Macedo dos

Development of nonlinear turbulent models based on Reynolds average using objective tensors / Bruno Jorge Macedo dos Santos ; advisor: Angela Ourivio Nieckele. – 2021.
99 f. : il. color. ; 30 cm

Dissertação (mestrado)–Pontifícia Universidade Católica do Rio de Janeiro, Departamento de Engenharia Mecânica, 2021.
Inclui bibliografia

1. Engenharia Mecânica - Teses. 2. Modelo RANS não linear. 3. Escoamento em canal. 4. Modelo de viscosidade turbulenta. 5. Turbulência. I. Nieckele, Angela Ourivio. II. Pontifícia Universidade Católica do Rio de Janeiro. Departamento de Engenharia Mecânica. III. Título.

CDD: 621

Acknowledgment

I would like, first of all, to thank God for all provision and support during my master course and for this victory in my life.

To my advisor and teacher professor Angela Ourivio Nieckele, for recommending this work to me and for all support provided, helping and guiding me during the work. It was a privilege to work with her. I also thank professor Roney Thompson and Luiz Eduardo Sampaio for the support during the work.

To my dear father Jair and dear mother Licinia for all education, affection and love provided throughout my life.

To my lovely wife Débora, for understanding me in the most difficult moments and believing in my objectives and goals, giving all possible support.

This study was financed in part by the Coordenação de Aperfeiçoamento de Pessoal de Nível Superior - Brasil (CAPES) - Finance Code 001.

Abstract

Santos, Bruno Jorge Macedo dos Santos; Nieckele, Angela O. (orientador). **Development of nonlinear turbulent models based on Reynolds average using objective tensors.** Rio de Janeiro, 2021. 99p. Dissertação de Mestrado – Departamento de Engenharia Mecânica, Pontifícia Universidade Católica do Rio de Janeiro.

Reynolds Average Navier Stokes (RANS) models are among the most employed models to solve turbulent flows, due to their low computational cost. The majority of RANS models use the Boussinesq approximation, based on a linear relation between the deviatoric part of Reynolds stress tensor and the rate of strain tensor, with the turbulent viscosity as the positive proportionality parameter. However, these models fail in several situations, and a great deal of effort has been made by the scientific community aiming to improve model prediction through the development of non-linear models. Analysis of higher-order models employing objective orthogonal tensors has shown that these are very promising to improve the prediction of the normal components of the Reynolds stress. In this work, non-linear models based on the square of the rate-strain tensor and non-persistence tensor were examined for a range of friction Reynolds number from 395 to 5200. New wall damping functions were developed, employing the turbulent kinetic energy and intensity of the rate of strain tensor to determine the turbulent characteristic velocity and length. Further, a new one-equation turbulent model based only on the turbulent kinetic energy transport equation was proposed coupled with an algebraic closure equation to model the turbulent kinetic energy dissipation. The models prediction for a channel flow were compared with DNS data and presented a better adherence to the DNS data, than the results of other RANS models available in the literature.

Keywords

Non-Linear RANS Model; Channel Flow; Eddy Viscosity Model; Turbulence.

Resumo

Santos, Bruno Jorge Macedo dos Santos; Nieckele, Angela O. (orientador). **Desenvolvimento de modelos turbulentos não lineares baseados na média de Reynolds usando tensores objetivos.** Rio de Janeiro, 2021. 99p. Dissertação de Mestrado – Departamento de Engenharia Mecânica, Pontifícia Universidade Católica do Rio de Janeiro.

Modelos RANS (Reynolds Average Navier-Stokes) estão entre os modelos mais empregados para resolver escoamentos turbulentos, devido a seu baixo custo computacional. A maioria dos modelos RANS usa a aproximação de Boussinesq, baseada em uma relação linear entre a parte deviatórica do tensor de Reynolds e o tensor taxa de deformação, com a viscosidade turbulenta sendo o parâmetro positivo de proporcionalidade. Contudo, esses modelos falham em várias situações, e um grande esforço tem sido feito pela comunidade científica com intuito de melhorar a previsibilidade do modelo desenvolvendo modelos não lineares. Análises de modelos de ordem superior empregando tensores ortogonais objetivos têm mostrado que estes são muito promissores para melhorar a previsão dos componentes normais do tensor de Reynolds. No presente trabalho, modelos não lineares baseados no quadrado do tensor taxa de deformação e no tensor não persistência de deformação foram avaliados para uma faixa de número de Reynolds baseados na velocidade de atrito, variando de 395 até 5200. Novas funções de parede foram desenvolvidas, utilizando energia cinética turbulenta e o módulo do tensor taxa de deformação para determinar a velocidade e comprimento característicos. Além disso, um novo modelo turbulento de uma-equação baseado somente na equação de transporte da energia cinética turbulenta foi proposto juntamente com uma equação de fechamento algébrica para modelar a dissipação da energia cinética turbulenta. Os resultados dos modelos para escoamento em canal foram comparados com os dados DNS, apresentando uma melhor aderência aos dados DNS em comparação com os resultados de outros modelos RANS encontrados na literatura.

Palavras-chave

Modelo RANS Não Linear; Escoamento em Canal; Modelo de Viscosidade Turbulenta; Turbulência.

Summary

Figure List

Table List

Nomenclature

$\boldsymbol{A}$	Original tensor
$\boldsymbol{a}$	Dimensionless Reynolds stress tensor
$\boldsymbol{a}^*$	Reynolds stress tensor
$\boldsymbol{B}$	Decomposition tensor
$\boldsymbol{B}^{\perp}$	Orthogonal decomposition tensor
$C_{\mu}^{\kappa-\varepsilon}, C_{\mu 2}^{\kappa-\varepsilon}, C_{\beta}^{\kappa-\varepsilon}$	Constant reference parameters for $\kappa-\varepsilon$ model
$\boldsymbol{D}$	Rate of strain tensor
E^+	Dimensionless source term of rate of dissipation of turbulent kinetic energy equation
$f_{\mu}, f_{\mu 2}, f_{\beta}$	Damping function of the new model
$f_{\mu}^{\kappa-\varepsilon}, f_{\mu 2}^{\kappa-\varepsilon}, f_{\beta}^{\kappa-\varepsilon}, f_1, f_2$	Wall damping functions for $\kappa-\varepsilon$ model
g	Gravity acceleration
G_{κ}^{+}	Dimensionless production terms
ℓ_c	Characteristic length
$\boldsymbol{P}$	Non-persistence of strain tensor
p^*	Pressure
$\hat{p}$	Modified pressure
Re_{τ}	Friction Reynolds number
t	Time
$\boldsymbol{U}$	Mean dimensionless velocity tensor
u_{τ}	Friction velocity
u^*	Axial velocity
$\overline{u_i}$	Mean velocity
V_c	Characteristic velocity
x_i	Dimensionless coordinate system
x_i^*	Dimensional coordinate system
$\boldsymbol{W}$	Vorticity tensor
$\widehat{\boldsymbol{W}}$	Relative vorticity tensor

Symbols

α	Constant
$\alpha_D, \alpha_{D2}, \alpha_\beta$	Parameters
$\hat{\alpha}_D, \hat{\alpha}_{D2}, \hat{\alpha}_\beta$	Dimensionless parameters
$\dot{\gamma}$	Dimensionless intensity of the rate of strain tensor
$\dot{\gamma}^*$	Intensity of the rate of strain tensor
ε	Rate of dissipation of the turbulent kinetic energy
ε^+	Dimensionless rate of dissipation of the turbulent kinetic energy
κ	Turbulent kinetic energy
κ^+	Dimensionless kinetic energy
μ	Molecular Viscosity
μ_T	Eddy Viscosity
ν	Kinematic Viscosity
ν_t	Turbulent viscosity
ρ	Density
σ_κ	Constant of turbulent kinetic energy equation
$\sigma_\varepsilon\ c_{\varepsilon 1}\ c_{\varepsilon 2}$	Constant of rate of dissipation of turbulent kinetic energy equation
τ_w	Wall shear stress
$\mathbf{\Omega}^{\mathrm{D}}$	Rate of strain eigenvectors' tensor

Acronym

CFD	Computational Fluid Dynamics
DNS	Direct Numerical Simulation
LES	Large Eddy Simulation
NLEVM	Non-Linear Eddy Viscosity Model
TB	Tensorial Base
NLT_{ij}^*	Non-linear terms
RANS	Reynolds-Averaged Navier-Stokes

1 . Introduction

Most flows occurring in nature and in engineering applications are turbulent. The boundary layer in the earth's atmosphere is turbulent (except possibly in very stable conditions), the water currents below the surface of the oceans are turbulent, interstellar gas clouds (gaseous nebulae) are turbulent. Boundary layers growing on aircraft wings or around any vehicle are turbulent, as well as natural gas and oil flow in pipelines (Tennekes & Lumley, 1972). However, in spite the abundance of turbulent flow in nature and industry, it is still a challenge to predict this type of flow.

The flow is classified as turbulent when it is unstable, i.e., small perturbations are amplified by the non-linear convective terms of the momentum equation. Often turbulent flows are called random since they are irregular and chaotic. The flow becomes turbulent when a parameter such as Reynolds number Re, Rayleigh number Ra, or the inverse Richardson number Ri^{-1}, exceed a critical value.

The nonlinearity of a turbulent flow is also directly related with vortex stretching, a key process by which three-dimensional turbulent flows maintain their angular momentum. The vortex stretching mechanism transfers energy and vorticity to increasingly smaller scales. Thus, a characteristic feature of turbulence is the existence of an enormous range of eddy sizes. The size of the largest eddies is in the order of the object of interest, e.g., in a boundary layer it corresponds to the thickness of the layer. The large eddies contain most of the energy. The energy is transferred from large to small eddies by nonlinear interactions, until it is dissipated by viscous diffusion in the smallest eddies. These smallest scales, called Kolmogorov scales (Pope, 2000), depend on the dissipation of turbulent kinetic energy ε and kinematic viscosity υ. Turbulent flows therefore require a continuous supply of energy to make up for the viscous losses. Even the smallest scales occurring in a turbulent flow are ordinarily far larger than any molecular length scale (Tennekes & Lumley, 1972), so it is a continuum phenomenon, governed by the equation of fluid mechanics.

Due to the macroscopic mixing of fluid particles, turbulent flows are

characterized by a rapid rate of diffusion of momentum and heat. Given the importance of the damping or enhancing turbulence in engineering applications, it is no surprise that a substantial amount of research effort is dedicated to the development of methodologies and models to capture the important effects due to turbulence.

Presently the most common methodologies to analyze a turbulent flow are (Pope, 2000): Direct Numerical Simulation (DNS), Large eddy simulation (LES) and Reynolds-Averaged Navier-Stokes (RANS). For these three methodologies, as the simulation cost is reduced, the level of modeling increases.

Direct Numerical Simulation (DNS) computes all flow quantities in all scales directly. The continuity and momentum equations are solved on spatial grids and time steps that are sufficiently fine that they can resolve the Kolmogorov scales (length ℓ, time τ, and velocity v). However, the Kolmogorov scales are inversely proportional to the Reynolds number ($\ell/L \sim Re^{-3/4}$, $\tau / t \sim Re^{-1/2}$ and $v/u \sim Re^{-3/4}$), and its computational demand increases substantially as the Reynolds number grows. Therefore, presently this approach is limited to flows of low or moderate Reynolds numbers. Since the DNS approach is highly costly in terms of computing resources, its main application is to study and understand the turbulent phenomena, as well as to aid in the development of improved LES or RANS models.

Large eddy simulation (LES) is based on space filtering of the conservation equations, which passes the larger eddies and rejects the smaller eddies. The effects on the resolved flow (spatial average flow plus large eddies) due to the smallest, unresolved eddies are included by means of a so-called sub-grid scale model. The sub-grid modelling introduces a modeling error, which, although smaller than in RANS, should not be disregarded. Avoiding the requirement of accurate resolution of small-scale motions significantly reduces the computational cost in comparison to DNS and makes it possible to simulate flows in realistically complex geometries at realistically high Reynolds numbers. On the other hand, the computational cost of LES is much higher than the cost of the RANS methods, since it is always 3D and transient and it requires small mesh size and time step (although larger than for DNS). Currently the use of LES in practical engineering analysis is limited, but with the fast development of larger and faster computers, this technique is beginning to be employed to determine complex flow in industry.

Reynolds-Averaged Navier-Stokes (RANS) modeling is focused on the effects of turbulence on mean flow properties. In RANS methodology, transport equations for the time average variables of interest (or ensemble averaged in flows with time-dependent boundary conditions) are obtained by introducing a time averaging procedure to the conservation equation. Within this methodology, one can introduce the approximation of steady state flow and/or reduce the flow dimension, leading to less costly solution than the previous cases. However, through this procedure, additional unknown variables (called turbulent transport flux) related to instantaneous fluctuations appear. In the momentum equation, those are called Reynolds stresses and are responsible for representing the effects of turbulence on the mean flow (Pope, 2000). Thus, to compute a turbulent flow with the RANS equations it is necessary to develop turbulence models to predict the Reynolds stresses and any other turbulent scalar transport terms, related to the application, and all flow scales are modeled.

The majority of engineers are almost always satisfied with information about the time-averaged properties of the flow, e.g., mean velocities, mean pressures, mean stresses etc., that is, it is unnecessary to resolve the details of the turbulent fluctuations. Thus, according to Versteeg & Malalasekra (2007), the vast majority of applied turbulent flow computations has been and will continue, in the foreseeable future, to be carried out with procedures based on the RANS equations.

There are several levels of approximation to determine the turbulent stress tensor and turbulent fluxes. A transport equation can be written directly for these quantities, i.e., the Reynolds stress model consists of solving a transport equation for each of the Reynolds stress tensor components. This model has also a high computing cost, due to elevated number of differential equations to be solved. The majority of RANS turbulence models are based on the Boussinesq hypothesis, where the Reynolds stress tensor is defined through an analogy with the constitutive equation for a Newtonian fluid, i.e., the Reynolds stress tensor is defined as proportional to the mean rate of strain tensor and a coefficient of proportionality called the turbulent viscosity μ_t, which remains to be modelled.

There are also several levels of modeling for the turbulent viscosity μ_t. It is usually modelled as proportional to a characteristic velocity V_c and a characteristic length ℓ_c. These quantities can be determined employing algebraic equations (zero differential equations) like the Prandtl mixing length model. One, two, three, etc.

differential equations can also be employed. A large number of models employ two differential equations to evaluated the characteristic length and velocity. Often, the turbulent kinetic energy is selected to estimate the characteristic velocity ($V_c = \kappa^{0.5}$). The characteristic length is more difficult to be estimated. Among the most popular two equations model are the models based on the turbulent kinetic energy κ and its dissipation ε, the $\kappa - \varepsilon$ family models (Rodi & Mansur, 1993) or turbulent kinetic energy κ and its specific rate of dissipation ω, called $\kappa - \omega$ family models (Menter, 1994).

There are several applications that the Boussinesq hypothesis fails as flows in the presence of separation, swirl flow, flow with sudden changes in mean strain rate, rapid dilatation, out of plane straining, or significant streamline curvature, all of which give rise to unequal normal Reynolds stresses, (Bradshaw, 1973).

Through a rigorous procedure to determine the turbulent viscosity within the Boussines hypothesis, the turbulent viscosity should be a fourth order tensor, because to get a second order tensor (Reynolds stress tensor), it is necessary to make the product of a fourth order tensor (turbulent viscosity) with a second order tensor (rate of strain tensor). By approximating the turbulent viscosity as a scalar, the contribution of some of the components of fourth order tensor is lost, therefore, linear models of the Reynolds stress tensor are not able to predict the existence of its normal components. Thus, a simple way to improve the deficiencies of the linear models is to develop a "Non-linear eddy viscosity model" (NLEVM) to represent the Reynolds stress, i.e., by assuming that the Boussinesq Hypothesis is simply the leading term in a series of expansion of functions (Wilcox, 1994). These additional nonlinear terms can be defined as combinations of the rate of strain tensor and vorticity tensor (Lien *et al.*, 1996). Thompson *et al.* (2010) argue that the suitable tensors to model the Reynolds stress are the strain rate and non-persistence tensor, due to its objectivity and frame indifference form. Nieckele *et al*. (2016) presented a priori investigation of six different models based on combinations of these two tensors getting a high predictability of the flow. They also suggested to employ the turbulent kinetic energy κ and its dissipation ε to evaluate the characteristic turbulent velocity and length.

Since the transport equation for ε is difficult to obtain and several empirical strong approximation are needed, Alves (2014) recommended to base the

characteristic length on the norm of strain deformation tensor ($\dot{\gamma}$), aiming also to obtain more smooth damping functions.

Murad (2018) and Santos (2019) performed a posteriori analysis of four models presented on Nieckele *et al.* (2016), considering a channel flow and pipe flow, respectively. They considered both combinations of turbulent characteristic velocity and length: $\kappa - \varepsilon$ and $\kappa - \dot{\gamma}$, with good results. However, for the $\kappa - \dot{\gamma}$ case, complicated adjustment functions based on the wall distance very defined by both authors throughout the flow.

1.1 Objective

The main objective of this work is to develop and evaluate RANS models to improve the prediction of turbulent shear flows. To this end, non-linear models were selected, considering on its tensorial base the rate of deformation tensor $\boldsymbol{D}$, the square of the rate of deformation tensor $\boldsymbol{D^2}$ and the non-persistence tensor $\boldsymbol{P}$. To close the models definition, the proportionality parameters of each tensor from the tensorial base were defined employing characteristic turbulent velocity and length based on the turbulent kinetic energy, κ, and the norm of strain deformation tensor, $\dot{\gamma}$. Additionally, new near wall damping functions were developed for each tensor. To determine the turbulent kinetic energy the Modified Rodi-Mansur model (Michelassi *et al*., 1993) was selected, and the resulting models were classified as two equations $\kappa - \dot{\gamma}$ models.

Although, the characteristic variables are based on κ and $\dot{\gamma}$, the dissipation of turbulent kinetic energy, ε, is still needed in the transport equation of κ. To eliminate the need to solve a transport equation for ε, a model for the dissipation rate of κ is proposed, resulting in one-equation $\kappa - \dot{\gamma}$ models. The model developed for ε is based on the production of κ, being dependent on κ and on the norm of strain deformation tensor $\dot{\gamma}$.

The models were developed based on a fully developed channel flow, where DNS data is available aiding in the modeling definition and their evaluation. To evaluated the models, the predictions for a channel flow are compared with DNS data of Thais *et al.* (2012) and Lee and Moser (2015) for a wide range of friction Reynolds numbers Re_τ, and the predictions of non-linear models of Murad (2018) obtained with the open source code OpenFoam, for $Re_\tau = 1000$.

1.2 Manuscript Organization

This work is divided in five chapters. In the first one, objective and motivation are exposed. In the second, a literature review related to turbulence models is presented.

Mathematical and numerical modeling that were used in the simulations can be found in Chapter 3. Low Reynolds models as $\kappa - \varepsilon$ model and a new model for turbulent kinetic energy dissipation are discussed. Numerical details used in the simulation are also shown.

The results are presented in Chapter 4. Initially some preliminary tests are shown. Then, both $\kappa - \dot{\gamma}$ models proposed here (2 equations $\kappa - \dot{\gamma}$ model and 1 equation $\kappa - \dot{\gamma}$ model) are examined for different non-linear models of the tensorial base and are compared with DNS data. In the sequence, the best non-linear model of the tensorial base, with 1 and 2 equations $\kappa - \dot{\gamma}$ formulations are compared with data found in the literature.

Finally, in Chapter 5, the conclusions of the work are presented, summarizing the work's contributions for the turbulence modeling area. Suggestion for future work are also discussed.

Additional information regarding the models coefficients adjustments, a grid test and a comparison of 1D and 2D formulation are shown in the Appendix.

2 . Literature Review

The present literature review is focused in the RANS methodology, based on the analysis of time average quantities.

The turbulent viscosity was introduced by Boussinesq in 1877, while Reynolds in 1894 derived the time average equations (Pope, 2000). The deviatoric Reynolds stress tensor was defined as proportional to the mean rate of strain, employing a positive scalar coefficient named as eddy viscosity (or turbulent viscosity) as the proportionality parameter. If the Boussinesq hypothesis is accepted as a good approximation, eddy viscosity has to be determined, that can be written as the product of the velocity and a length (Pope, 2000).

Although some models based on Boussinesq hypothesis provide excellent predictions for many flows of engineering interest, there are some applications that these models do not satisfactorily predict the flow, getting differ from corresponding measurements. Generally speaking, according to Bradshaw (1973), such models are inaccurate for flows with sudden changes in mean strain rate and for flows with rapid dilatation, out of plane straining or significant streamline curvature, all which give rise to unequal normal Reynolds stresses, and the Boussinesq hypothesis fails (Wilcox, 1994).

Park *et al.* (2002) developed a new non-linear model on the basis of realizability constraints to predict turbulent flow with heat transfer. The linear $\kappa - \varepsilon - f_\mu$ model developed by Park and Sung (1997) was extended to a non-linear formulation and the stress-strain relationship was derived from the Cayley-Hamilton theorem in a homogeneous flow. The model performance well for a channel flow, backward-step and imping jet problem

Abe *et al.* (2003) proposed new closure approximations, within the framework of non-linear eddy-viscosity modeling, aiming specifically to improve the representation of near-wall anisotropy in shear flows (fully developed channel flow at $Re = 6875$ and $Re = 21200$ and a spanwise-homogeneous flow in a periodically constricted channel. The main novel element was the introduction of tensorial terms, alongside strain and vorticity, which depend on wall-direction

indicators and which reproduce the correct asymptotic near-wall behavior of the Reynolds stresses. The new model elements result in a substantially improved representation of the Reynolds stress field at the wall, especially in the wall-normal Reynolds stress.

Based on the assumption of wall layer universality, Kalitzin *et al.* (2005) proposed a novel wall-function formulation applicable to any RANS turbulence model applied to the entire model. The behavior of RANS turbulence models in the near wall region was also analyzed for a flow over in a flat plane. Their work considered 1 equation Spalart-Allmaras model, and two equation models $\kappa - \omega$ and $\kappa - g$, and 4 equations $v^2 - f$ model. The analysis of the latter resulted in a new analytical solution in the viscous sublayer and logarithmic layer. The analytical solution for the Spalart-Allmaras model can be used directly as a simple wall function. The existing wall functions for $\kappa - \omega$ model showed significant deficiencies, the transformation from ω to g circumvents the difficulties with ω in the viscous sublayer.

Thompson (2008) developed a mathematical concept of tensor decomposition, showing two types of orthogonal decomposition. Bacchi (2009) studied non-persistence of straining tensor, vortex definition and their applications in the flow. Then, based on these two works, Thompson *et al.* (2010) presented a methodology to quantify the dependence of linear and non-linear Reynolds stress tensor on mean kinematic tensor basis using rate of strain and non-persistence tensor, proposing six different models.

Mukin *et al.* (2011) presented an explicit algebraic Reynolds stress for a non-linear turbulent viscosity model (NLEVM) combined with modified $\kappa - \varepsilon$ turbulence model to take into account particles effect on turbulence for calculating the main turbulent characteristic of two-phase flow in a circular tube. The developed model adequately described turbulence anisotropy and the influence of particles inertia and concentration on the turbulence intensity.

Chen *et al.* (2011) have develop a NLEVM model for the prediction of flows in the presence of cavitation, which are accompanied by large density ratio and large- swirling flow structures around a complex submerged vehicle. They proposed a quadratic and cubic non-linear eddy-viscosity turbulence models with low Reynolds number correction to improve the prediction of anisotropic turbulence stresses. These non-linear models were capable of capturing more

accurate macroscopic shape and hydrodynamic property of supercavition of benchmark problems.

Fu *et al.* (2011) develop a framework to aid in the development of NLEVM, based on the Cayley-Hamilton theory, which resulted in a five-term model expression. An explicit algebraic stress model (EASM) was formulated in a compact vorticity tensor to a form a minimal representation. The model was tested for a few classical problems like channel flow, boundary layer flow, flow over obstacles, as well as a fully developed flow inside a rotating pipe, presenting reasonable results.

BenSaid *et al.* (2012) evaluated the performance prediction of near wall flow with algebraic linear models ($\kappa - \varepsilon$ and $v^2 - f$ models) and a non-linear model of Shih, performing *a priori* and *a posteriori* analysis, by comparing the model predictions with DNS data of a plane channel flow. The results suggested that $v^2 - f$ model is an efficient model to capture the turbulent shear stress component of the Reynolds stress for this type of flow, but is unable to predict correctly the level of anisotropy of the Reynolds stress tensor. Furthermore, it is shown that the presence of non-linear terms in a turbulent model improves the ability to predict the flow anisotropy.

Using DNS data from Thais *et al.* (2012), Nieckele *et al.* (2016) performed a priori analysis of the six different models proposed by Thompson *et al.* (2010) and formulated expressions for damping functions for the dimensionless non-linear terms in a channel flow. They defined the characteristic velocity and length as a function of the turbulent kinetic energy and its dissipation rate to obtain dimensionless coefficients for the Reynolds stress tensor. The results showed that the non-linear models improved the representation of the normal components of the traceless Reynolds stress tensor. The best results were obtained with a combination of the non-persistence tensor and the square of mean rate of strain tensor.

Alves (2014) proposed a new characteristic length based on the strain tensor intensity, aiming to obtain more smooth damping functions applied to a channel flow, and to reduce the influence of the dissipation of turbulent kinetic energy ε in the model. The new set of coefficients presented a more universal behavior for the Reynolds numbers tested.

Wei *et al.* (2015) developed a non-linear model and a scalable hybrid URANS/LES strategy to improve the capability of the RANS model to simulate

complex flows featuring separations and unsteady motions. Calculated results of the flow around a triangular cylinder showed that the non-linear model was able to improve the flow prediction, but the error was still considerable, and small turbulence structures were not clearly captured by the model.

Weatheritt *et al.* (2016) developed an algorithm based on Machine Learning to develop a mathematical model for tensors, using DNS data and applied to the backward facing step and periodic hills flows. This mathematical model was applied in turbulence modelling, in the formulation of non-linear RANS stress-strain relationships, with promising results.

Ribeiro *et al.* (2018) employed a tensorial decomposition technique as a mean to evaluate the Boussinesq hypothesis based on Thompson *et al.* (2010) work. The technique projects the anisotropic Reynolds stress tensor onto the rate of strain tensor, enabling an estimate for the turbulent viscosity and the error associated with the assumption. The authors examined a convergent-divergent channel flow and the flow around a sphere and showed large errors in the prediction with Boussinesq based models. The best performance was achieve using $\kappa - \omega$ model in comparison to $\kappa - \varepsilon$ model.

Luo *et al.* (2018) proposed an hybrid RANS/LES model based on κ equation with the quadratic stresses to improve the coupling between the methods at the RANS/LES interface. The model was validated in a Taylor-Couette flow and the results obtained were close to the experimental values.

Murad (2018) and Murad *et al.* (2020) performed an evaluation of available linear RANS models by comparing to DNS data for a channel flow, followed by an analysis of the non-linear models recommended by Nieckele *et al.* (2016). New damping near wall functions were developed based on the turbulent kinetic energy and its dissipation rate as characteristic velocity and length, for several Reynolds number for a channel flow. For friction Reynolds equal to a 1000, the characteristic length proposed for Alves (2014) was also tested, with promising results, although the damping functions were too complicated. Santos (2019) performed similar analysis, with the same damping functions for circular ducts flow, obtaining equivalent results as it was found for the channel flow.

Otereo *et al.* (2018) presented a novel methodology for the prediction of wall-bounded flows in the presence of thermos-physical properties strong gradients in

the fully develop channel flow. The modification of the diffusion term of the turbulent kinetic energy equation resulted improved results.

Tian *et al.* (2019) proposed a model to directly determine turbulent viscosity through a variable denominated R, by the solution of its differential equation. The model is based on the work of Elkhoury (2017), and relates R with the turbulent kinetic energy and its dissipation, as $R = C_\mu \kappa^2/\varepsilon$ by deriving R equation from these variables equations. This simplified model presents coefficients and functions constructed such as to preserve the anisotropic characteristic of turbulence encountered in non-equilibrium flows. To evaluate the accuracy of the model, it was applied to the fully developed, asymmetric plane diffuser and a flow over Onera-M6 wing. Comparisons indicate that the new model improves the accuracy of flow predictions compared to the widely used Spalart-Allmaras model and remains competitive with SST $\kappa - \omega$ model.

Rahman *et al.* (2019) proposed an approach to devise a consistent formulation for production-to-dissipation ratio to obtain a non-singular coefficient of eddy-viscosity embedded in the one-equation model based on the turbulent kinetic energy. The dissipation rate was evaluated with an algebraically prescribed length scale having only one adjustable coefficient, accompanied by an anisotropic function enhancing the dissipation in non-equilibrium flow regions. To validate the new model, it was applied in developed channel flow, flat plane boundary layer flow with zero pressure gradient, backward facing step flow, an asymmetric diffuser plane flow, flow over a 3D axisymmetric hill, flow past an NACA 4412 airfoil, the flow over an ONERA-M6 wing and free shear flow. Although promising results were obtained, the authors indicate the need of additional validations are necessary to gain confidence in the proposed approach.

Using a quadratic stress-strain relation for the Reynolds stress tensor Fadhila *et al.* (2020) proposed and formulated a new ω −based non-linear eddy viscosity model, based on the original $\kappa - \omega$ model and applied in zero pressure gradient flat plate, curved channel, planar diffuser with a downstream monolith and swirling flow. For enhanced treatment of near-wall turbulence anisotropy, a formulation that scales only with the turbulent Reynolds number is proposed for the first time. This new model outperformed the standard $\kappa - \omega$ model.

Alegre *et al.* (2020) developed a nonlinear model that represents what is generally found in a Hole-Pattern machine seal. The methodology consists mainly in translating the coefficients obtained via orthogonal projection of the Reynolds stress that are calculated from LES onto a given basis tensor. The results showed a better performance of the model than the linear Boussinesq model, but with some limitations.

Beetham *et al.* (2020) presented a data-driven framework for formulation of closures of the RANS equations. His work has leveraged a sparse regression framework while the body of work has primarily leveraged neural networks. The data-driven framework was applied in sections of a Hole-Pattern seal with one hole, three holes and five holes. The sparse regression framework results a closed model in algebraic form, allowing for direct physical inferences to be drawn and naive integration into existing computational fluid dynamics solvers.

Kaandorp *et al.* (2020) have also used machine learning algorithm, called the Tensor Basis Random Forest (TBRF), to predict the Reynolds-stress anisotropy tensor, an improvement is observed with respect to the base line $\kappa - \omega$ simulations. The authors argue that the TBRF algorithm presented is relatively easy to implement because some machine learning issues can be avoided. They have applied the algorithm in curved backward facing step, backward facing step and square duct. Both works guarantee Galilean invariance by making use of a tensor basis.

Yang *et al.* (2020) developed a new turbulent viscosity definition which inherits the advantages of the elliptic blending turbulence models and the SST turbulence models. The new model was applied to near-wall, separated and impinging jet flows and associated heat transfer problems. The current new model yields better results than the SST $\kappa - \omega$ model for separated and impinging jet flows and the associated heat transfer problems.

Li *et al.* (2020) developed a modified expression for the eddy viscosity, combining a proposed non-linear constitutive equation between the Reynolds stress and mean strain rate with the analytical solution of the pressure strain term in the Reynolds stress transport equation. This new model was developed for turbulent flow of supercritical fluid. Improved results were obtained in vertical flow and horizontal flow with respect to heat transfer and turbulent statistics of supercritical fluids.

Zhang *et al.* (2020) formulated a new low-Reynolds-number turbulence model also based on the based on R parameter ($R = \kappa^2/\varepsilon$) computing a fully-developed turbulent channel and flat plane flows. Most of the diffusion terms emerging from the transformation have been preserved in the derivation of the new model, maintaining the closest relationship with its parent $\kappa - \varepsilon$ model. The coefficients and functions are constructed aiming to guarantee the original anisotropic characteristics of turbulence. The prediction of this new model presented a good correlation with experimental data.

This literature review has shown the existence of countless turbulent models. Each model focus in improving the representation of some specific turbulent flow, with different geometries, in the presence or not of heat transfer or particles in the flows. It is clear the difficulty to develop one model able to predict any type of flow, leading the scientific community to continue to search more accurate and general models or models specifically designed for a particular engineering problem.

Among the different developed models available in the literature, higher order models employing objective orthogonal tensors seem to be very promising to improve the flow prediction, and have been selected to be further examined in the present work. Further, it is clear that the transport equation of the turbulent kinetic energy dissipation is a drawback in the available models, thus in the present work a simple model to this variable is proposed to avoid the solution of its transport equation, and render a simpler and cheaper model.

3 . Mathematical and Numerical Modeling

In this chapter, the mathematical and numerical models employed in the present work to analyzed a turbulent flow are described. Initially the time average conservation equations are introduced, followed by the description of the non-linear Reynolds Average Turbulence Models selected to be examined.

Two different characteristic velocities and lengths are selected to define the models coefficients, and are described. A modification of the non-linear models is proposed aiming to obtained a more robust and accurate model, by eliminating the determination of the dissipation of turbulent kinetic energy.

The configuration employed to evaluate the models is a fully developed channel flow, and DNS data (Thais *et al.*, 2012 and Lee and Moser, 2015) are available for comparison, and details of this test case are discussed.

The last section of this chapter presents information related with the numerical model employed.

3.1 Conservation Equations

Considering a Newtonian and incompressible fluid, the mass conservation and momentum equations can be written as

$$\frac{\partial u_i^*}{\partial x_i^*} = 0 \tag{3.1}$$

$$\frac{\partial(\rho\, u_i^*)}{\partial t} + \frac{\partial\left(\rho\, u_i^* u_j^*\right)}{\partial x_j^*} = -\frac{\partial p^*}{\partial x_i^*} + \rho g_i + \frac{\partial\left(2\,\mu\, D_{ij}^*\right)}{\partial x_j^*} \tag{3.2}$$

where u_i^* is the velocity component, x_i^* is the coordinate system, ρ is the density, p^* is the pressure, g_i is the gravity acceleration component, μ is the molecular viscosity and D_{ij}^* is the rate of strain tensor, written as

$$D_{ij}^* = \frac{1}{2}\left(\frac{\partial u_j^*}{\partial x_i^*} + \frac{\partial u_i^*}{\partial x_j^*}\right) \tag{3.3}$$

According to RANS (Reynolds Average Navier-Stokes) methodology, all variables, whether tensors or scalars, can be written as a sum of Reynolds time average term $\bar{\phi}$ with fluctuation around it, ϕ', as shown in Eq. (3.4). It is important to note that the time average of the fluctuation is zero, but the product of fluctuations of correlated variables is not zero.

$$\phi^* = \bar{\phi} + \phi' \qquad ; \qquad \bar{\phi} = \frac{1}{\Delta t}\int_{\Delta t} \phi^* \, dt \tag{3.4}$$

The RANS equations are obtained by replacing all variable by its mean value plus its fluctuation and applying time average in the conservation equations, resulting in the following set for time average steady state situations

$$\frac{\partial \, \overline{u_j}}{\partial x_j^*} = 0 \tag{3.5}$$

$$\frac{\partial \left(\rho \, \overline{u_i u_j} \right)}{\partial x_j^*} = \rho g_i - \frac{\partial \bar{p}}{\partial x_i^*} + \frac{\partial}{\partial x_j^*}\left(2 \, \mu \, \overline{D_{ij}}\right) + \frac{\partial}{\partial x_j^*}\left(- \rho \, \overline{u_i' u_j'}\right) \tag{3.6}$$

where the term $\left(-\rho \overline{u_i' u_j'}\right)$ is the Reynolds Stress Tensor. The deviatoric part of the Reynolds Stress Tensor (traceless tensor) is

$$a_{ij}^* = - \, \overline{u_i' u_j'} + \frac{2}{3} \, \kappa \, \delta_{ij} \tag{3.7}$$

where κ is the turbulent kinematic energy and δ_{ij} is the Delta Kronecker.

$$\kappa = \frac{1}{2} \overline{u_k' u_k'} \tag{3.8}$$

The momentum equation can be rewritten as:

$$\frac{\partial \left(\overline{u_i u_j} \right)}{\partial x_j^*} = - \frac{\partial \hat{p}}{\partial x_i^*} + \frac{\partial}{\partial x_j^*}\left(2 \, \nu \, \overline{D_{ij}}\right) + \frac{\partial a_{ij}^*}{\partial x_j^*} \tag{3.9}$$

where $\nu = \mu \, / \, \rho$ is the kinematic viscosity and $\hat{p}$ is a modified pressure, defined as

$$\hat{p} = \frac{1}{\rho}\left[\bar{p} - \rho \, g_k \, x_k^* + \frac{2}{3} \, \rho \, \kappa\right] \tag{3.10}$$

3.1.1 Dimensionless momentum equation

The conservation equations can be written in dimensionless form as

$$\frac{\partial\, U_j}{\partial x_j} = 0 \quad ; \quad \frac{\partial\left(U_i U_j\right)}{\partial x_j} = -\frac{\partial P}{\partial x_i} + \frac{\partial}{\partial x_j}\left(2\, D_{ij}\right) + \frac{\partial a_{ij}}{\partial x_j} \tag{3.11}$$

where the following dimensionless variables were employed

$$x_i = \frac{x_i^*\, u_\tau}{\nu} \quad ; \quad U_i = \frac{\overline{u_\iota}}{u_\tau} \quad ; \quad P = \frac{\hat{p}}{u_\tau^2} \quad ; \quad a_{ij} = \frac{a_{ij}^*}{u_\tau^2} \tag{3.12}$$

with the characteristic velocity as the friction velocity, defined as:

$$u_\tau = \sqrt{\frac{\tau_w}{\rho}} \tag{3.13}$$

where τ_w is the wall shear stress.

To define the traceless Reynolds stress tensor a_{ij}, a turbulence model is required and it is discuss in the next section.

3.2 Turbulent Models

The development of a turbulent model has two distinct levels of modeling. The first is related to the definition of the relationship between the Reynolds stress tensor and the kinematic tensors, i.e., the selection of the tensorial basis (TB) to model the tensor. The second level is related with the selection of the turbulent characteristic velocity V_C and length ℓ_c, to defined the proportionality between tensors.

Within the first level is the traditional approach based on the Boussinesq hypothesis, where an analogy with the viscous stress tensor is employed. This model of the tensorial base is classified as linear, since the Reynolds stress tensor is assumed as proportional to the mean rate of strain, where the positive scalar coefficient of proportionality is the turbulent viscosity μ_t, given by the follow equation

$$a_{ij}^* = \frac{\mu_t}{\rho}\, 2\, D_{ij}^* \tag{3.14}$$

If the Boussinesq hypothesis is accepted as an adequate approximation, the

next step is to determine an appropriate specification of the turbulent viscosity μ_t. The turbulent viscosity μ_t can be written as the product of a characteristic velocity (V_C) and a characteristic length (ℓ_c) of an eddy, given by

$$\frac{\mu_t}{\rho} \sim V_C \, \ell_c \tag{3.15}$$

There are a large variety of turbulence models of the second level, depending on the specification of the characteristic velocity and length (Pope, 2000). Several models specify the characteristic velocity based on the turbulent kinetic energy as $V_C = \sqrt{\kappa}$, for which a transport equation is relatively easy to obtain. However, it is a challenge to specify the characteristic length, leading to a large variety of models, like the $\kappa - \varepsilon$ where ℓ_c is related to dissipation of the turbulent kinetic energy, ε.

Although linear models are very popular, it is well known that these models fail in a large number of situations. Therefore, there is a large effort to develop more accurate models for the Reynolds stress tensor.

To obtain a better representation of the turbulent flow, some researchers invest in working directly with a transport equation for the Reynolds stress tensor (Pope, 2000). With this approach, several new terms appear that need further closure. In addition to this difficulty, this approach requires great computational effort, due to the need to solve a large number of differential equations, without bringing great benefits in relation to precision, when compared to Large Eddy Simulations (LES), for example.

Another approach within the tensorial basis level is called *Non-linear turbulent viscosity models* (NLEVM), and it consists on extending the base of the Reynolds tensor for its representation beyond the Boussinesq structure (Lumley, 1970, Pope, 1975, Gatski *et al*., 2000, Wallin & Johanson, 2002).

$$a_{ij}^* = \frac{\mu_t}{\rho} \, 2 \, D_{ij}^* + NLT_{ij}^* \tag{3.16}$$

where NLT_{ij}^* is the non-linear stress tensor. There are several non-linear models, for each one, the definition of NLT_{ij} is different. Within NLEVM, a base of independent tensors is defined, applying representation theorems, ending with a set of tensors that are obtained from the combination of the originals. In the next section, a brief description of the non-linear models selected to be studied here is presented.

3.2.1 Non-Linear Models

A question related to the *Non-linear turbulent viscosity models* approach is whether the selected tensor base respects the conditions of Euclidean invariance, objectivity and frame invariance.

Thompson (2008) developed a mathematical concept of tensor decomposition, showing two types of orthogonal decomposition. In the first decomposition, the tensor A_{ij} is written as the sum of a linear component αB_{ij} plus an orthogonal component $B_{ij}^{\perp}$ as

$$A_{ij} = \alpha B_{ij} + B_{ij}^{\perp} \tag{3.17}$$

In the second decomposition the tensor is divided into in-phase and out-phase parts. The in-phase part is composed of a tensor $B_{ij}^{H}{}_{A}$ (H denotes that the term is written in the base of H_{ij} eigenvalues) that has the same eigenvectors as A_{ij}. Because of that, the $B_{ij}^{H}{}_{A}$ component is able to sweep a broader tensor field than the linear term of the first decomposition (αB_{ij}). However, the out-phase $\widetilde{B_{ij}^{H}}_{A}$ has different eigenvectors than A_{ij}, therefore:

$$A_{ij} = B_{ij}^{H}{}_{A} + \widetilde{B_{ij}^{H}}_{A} \tag{3.18}$$

Using Cayley-Hamilton theorem, the in-phase term can be rewritten as:

$$B_{ij}^{H}{}_{A} = \alpha_0 I + \alpha_h H + \alpha_{h_2} H^2 \tag{3.19}$$

Bacchi (2009) showed the importance of non-persistence of straining tensor translating rotational effects of the flow in a discussion of flow types and vortex definition. This is an important tensor because it can measure the ability of the fluid to avoid been stretched in the flow and it is given by:

$$P_{ij} = D_{ij}\widehat{W_{ij}} - \widehat{W_{ij}}D_{ij} \tag{3.20}$$

where $\widehat{W_{ij}}$ is the relative vorticity defined as:

$$\widehat{W_{ij}} = W_{ij} - \Omega_{ij}^{D} \tag{3.21}$$

W_{ij} is the skew symmetric of the velocity gradient, given by:

$$W_{ij} = \frac{1}{2}\left(\frac{\partial U_j}{\partial x_i} - \frac{\partial U_i}{\partial x_j}\right) \tag{3.22}$$

and Ω_{ij}^{D} is the rate of rotation of the eigenvalues of the rate of strain, given by:

$$\Omega_{ij}^{\mathrm{D}} = \sum_{k=1}^{3} \dot{e_k^D} e_k^D \tag{3.23}$$

where e_k^D is the unit eigenvector of rate of strain tensor and $\dot{e_k^D}$ is its material derivation.

Thompson *et al.* (2010), based on Thompson, (2008) and Bacchi, (2009), showed the dependence of linear and non-linear Reynolds stress tensor on mean kinematic tensor basis using in-phase decomposition (strain rate tensor) and out-phase decomposition (non-persistence of straining tensor) and presented a methodology to quantify this dependence.

Six models of the tensorial basis were evaluated by Nieckele *et al.* (2016) using some combinations of mean kinematic tensors by employing a priori analysis by comparing the prediction of each model with experimental (Carlier *et al.*, 2005, and Stanislas *et al.*, 2008) and DNS data (Thais *et al.*,2012).

A priori analysis is to apply DNS or experimental data directly in the model and verify if the prediction of Reynolds tensor is acceptable. In contrast, a posteriori analysis is to apply the model in the conservation equations and solve them

In the present work, four models of the tensorial basis (TB) were selected to be analyzed with a posteriori analysis: a linear model and three of the best models non-linear models studied by Nieckele *et al.* (2016).

$$\boldsymbol{TB_I}: \quad a_{ij}^* = \alpha_D \, 2 \, D_{\boldsymbol{ij}}^* \tag{3.24}$$

$$\boldsymbol{TB_{II}}: \quad a_{ij}^* = \alpha_0 \, \delta_{ij} + \alpha_D \, 2 \, D_{\boldsymbol{ij}}^* + \alpha_{D2} \, D_{\boldsymbol{ij}}^{*2} \tag{3.25}$$

$$\boldsymbol{TB_{III}}: \quad a_{ij}^* = \alpha_0 \, \delta_{ij} + \alpha_D \, 2 \, D_{\boldsymbol{ij}}^* + \alpha_{D2} \, D_{\boldsymbol{ij}}^{*2} + \beta_P \, P_{ij}^* \tag{3.26}$$

$$\boldsymbol{TB_{IV}}: \quad a_{ij}^* = \alpha_D \, 2 \, D_{\boldsymbol{ij}}^* + \beta_P \, P_{ij}^* \tag{3.27}$$

Model I of the tensorial baseis a linear model, with the Reynolds tensor directly proportional to D_{ij}. Model II, III and IV of the tensorial base are non-linear,

Model II is in-phase/out-phase decomposition of the D_{ij}, the error associated to this model is lower than ModelI. Model III is another non-linear model with in-phase/out-phase decomposition, the orthogonal tensor is modeled by a linear decomposition using P_{ij}, the error associated to this model is lower than Model II. Model IV is non-linear model too, similar to Model I, but with the orthogonal tensor being modeled by a linear decomposition using P_{ij} and added to the linear decomposition of Model I.

The non-linear tensor D_{ij}^2 is

$$D_{ij}^2 = D_{ik}D_{kj} = \frac{1}{4}\left(\frac{\partial U_i}{\partial x_k}\frac{\partial U_k}{\partial x_j} + \frac{\partial U_k}{\partial x_i}\frac{\partial U_k}{\partial x_j} + \frac{\partial U_i}{\partial x_k}\frac{\partial U_j}{\partial x_k} + \frac{\partial U_k}{\partial x_i}\frac{\partial U_j}{\partial x_k}\right) \tag{3.28}$$

For the particular case of a channel flow, $\widehat{W_{ij}} = W_{ij}$, and the non-linear tensors P_{ij} is

$$P_{ij} = D_{ik}W_{kj} - W_{ik}D_{kj} = \frac{1}{2}\left(\frac{\partial U_k}{\partial x_i}\frac{\partial U_k}{\partial x_j} - \frac{\partial U_i}{\partial x_k}\frac{\partial U_j}{\partial x_k}\right) \tag{3.29}$$

The coefficient α_0 present in Models II and III of the tensorial base is defined in order to guarantee that the tensor a_{ij} is trace free, as

$$\alpha_0 = -\frac{\alpha_{D2}}{3}\,\mathrm{tr}\,(\boldsymbol{D^2}) = -\frac{\alpha_{D2}}{6}\left(\frac{\partial U_i}{\partial x_k}\frac{\partial U_k}{\partial x_i} + \frac{\partial U_k}{\partial x_j}\frac{\partial U_j}{\partial x_k}\right) \tag{3.30}$$

The coefficients α_D, α_{D2} and β_P were determined by Nieckele *et al.* (2016) employing experimental and DNS data. Since these coefficients have dimensions, it is convenient to normalize them, by selecting a characteristic velocity V_c and characteristic length ℓ_c (second modeling level).

3.2.2 Characteristic velocity and length, based on κ and ε

As already mentioned the turbulent kinetic energy is very often employed as a characteristic velocity. The characteristic length can be related with the dissipation of the turbulent kinetic energy, ε, as it is employed in the popular $\kappa - \varepsilon$ model. These two parameters were employed by Nieckele *et al.* (2016). The first parameter is the turbulent viscosity ($\nu_t = \mu_t/\rho$), defined as

$$\alpha_D = \nu_t = f_\mu^{\kappa-\varepsilon} C_\mu^{\kappa-\varepsilon} \frac{\kappa^2}{\varepsilon} \tag{3.31}$$

The non-linear parameters were defined as

$$\alpha_{D2} = f_{\mu 2}^{\kappa-\varepsilon} C_{\mu 2}^{\kappa-\varepsilon} \frac{\kappa^3}{\varepsilon^2} \quad ; \quad \alpha_\beta = f_\beta^{\kappa-\varepsilon} C_\beta^{\kappa-\varepsilon} \frac{\kappa^3}{\varepsilon^2} \tag{3.32}$$

The dimensionless parameters are

$$\hat{\alpha}_D = \frac{\alpha_D}{\nu} = \frac{\nu_t}{\nu} = \frac{\mu_t}{\mu} = f_\mu^{\kappa-\varepsilon} C_\mu^{\kappa-\varepsilon} \frac{{\kappa^+}^2}{\varepsilon^+} \tag{3.33}$$

$$\hat{\alpha}_{D2} = \frac{\alpha_{D2}}{\nu\,(\nu / u_\tau)^2} = f_{\mu 2}^{\kappa-\varepsilon} C_{\mu 2}^{\kappa-\varepsilon} \frac{{\kappa^+}^4}{{\varepsilon^+}^2} \tag{3.34}$$

$$\hat{\beta}_P = \frac{\beta_P}{\nu\,(\nu / u_\tau)^2} = f_\beta^{\kappa-\varepsilon} C_{\beta\,\beta}^{\kappa-\varepsilon} \frac{{\kappa^+}^4}{{\varepsilon^+}^2} \tag{3.35}$$

where

$$\kappa^+ = \frac{\kappa}{u_\tau^2} \quad ; \quad \varepsilon^+ = \frac{\nu\,\varepsilon}{u_\tau^4} \tag{3.36}$$

In the previous definitions, $C_\mu^{\kappa-\varepsilon}$, $C_{\mu 2}^{\kappa-\varepsilon}$ and $C_\beta^{\kappa-\varepsilon}$ are constant reference parameters, and $f_\mu^{\kappa-\varepsilon}$; $f_{\mu 2}^{\kappa-\varepsilon}$ and $f_\beta^{\kappa-\varepsilon}$ are wall damping functions. These quantities were obtained by Nieckele *et al*, (2016) based on the DNS channel flow (Thais *et al.*, 2012) and experimental boundary layer flow (Carlier *et al.*, 2005, and Stanislas *et al.*, 2008). The reference values corresponding to friction Reynolds number $Re_\tau = u_\tau\, H/\nu$ equal to 1000 (H is the half distance between the plates) are shown in Table 3.1, and the variation of the damping functions with the dimensionless wall distance $y^+ = u_\tau\, y^*\,/\,\nu$ are present in Figure 3.1 and Figure 3.2. Examining these curves, it is possible to observe the strong variation near the wall. As a result, it is difficult to create correlations for the damping functions, so that them can be easily employed in a turbulence model.

Table 3.1 – Constant parameters $C_\mu^{\kappa-\varepsilon}$, $C_{\mu 2}^{\kappa-\varepsilon}$ and $C_\beta^{\kappa-\varepsilon}$, $Re_\tau = 1000$.

$C_\mu^{\kappa-\varepsilon}$	$C_{\mu 2}^{\kappa-\varepsilon}$	$C_\beta^{\kappa-\varepsilon}$
0.072	– 0.050	0.049

Since, the coefficient α_D corresponds to the turbulent viscosity of the linear models, Nieckele *et al*. (2016) evaluated several damping function by comparing with the DNS (Thais *et al*., 2012) and experimental (Carlier *et al*., 2005 and Stanislas *et al*., 2008) as shown in Figure 3.1a.The behavior of the function is shown in log-scale in Figure 3.1b to better visualized the wall region. As mentioned, the steep increase of the function near the wall is very difficult to represent by a simple equation, and as it can be seen in the Figure 3.1a, very often, it is discarded. Nieckele *et al*. (2016) recommended the Rodi Mansour model (Michelassi *et al*., 1993) and therefore, it was also employed here. The damping function for $y^+ \leq 100$ is

$$f_\mu^{\kappa-\varepsilon} = 1 - \exp\left(-2.10^{-4}y^+ - 6.10^{-4}{y^+}^2 + 2.5.10^{-7}{y^+}^3\right) \tag{3.37}$$

while $f_\mu = 1$ when $y^+ > 100$.

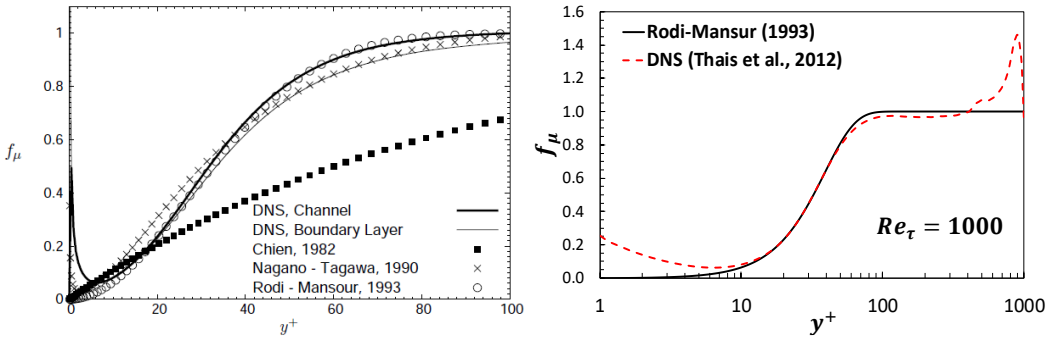

(a) linear scale (Nieckele et al, 2016) (b) log-scale

Figure 3.1 – Damping function ($f_\mu^{\kappa-\varepsilon}$) obtained from DNS data of Thais et al (2012) for a channel flow (a) linear scale and compared several propositions from the literature (Nieckele et al, 2016) (b) log scale.

Michelassi *et al*. (1993) defined the reference $C_\mu^{\kappa-\varepsilon}$ as 0.09, however, here, the value that presented the best adjustment with the DNS channel flow data of Thais *et al.* (2012) is 0.072, and it was employed in the present work.

Figure 3.2 shows the damping function of the non-linear terms, $Re_\tau = 1000$ obtained from the DNS data and the proposition of Murad (2018). Nieckele *et al.* (2016) proposed the following damping functions of the non-linear terms,

$$f_{\mu 2}^{\kappa-\varepsilon} = f_\beta^{\kappa-\varepsilon} = \frac{\tanh\left(8.5\times10^{-4}\left(y^+\right)^{2.01}\right)}{\tanh\left(1.8\times10^{-5}\left(y^+\right)^{5.35}\right)} \tag{3.38}$$

However, Murad (2018) examined the previous expressions and proposed new damping expressions to better adjust with the DNS data as

$$f_{\mu 2}^{\kappa-\varepsilon} = \frac{\tanh\left(6.15 \times 10^{-4}(y^{+})^{2.135}\right)}{\tanh\left(10^{-5}(y^{+})^{5.8}\right)} + 6.1 \times 10^{-2} e^{\left(-\frac{y^{+}}{300}\right)^{2}} \tag{3.39}$$

$$f_{\beta}^{\kappa-\varepsilon} = \frac{\tanh(2.56 * 10^{-4}(y^{+})^{2.305})}{\tanh(1.3 * 10^{-5}(y^{+})^{6.5})} + 1.818 * 10^{-2} e^{\left(-\frac{y^{+}}{300}\right)^{2}} + \frac{60.6}{(y^{+})^{4}} + 0.02727 \tag{3.40}$$

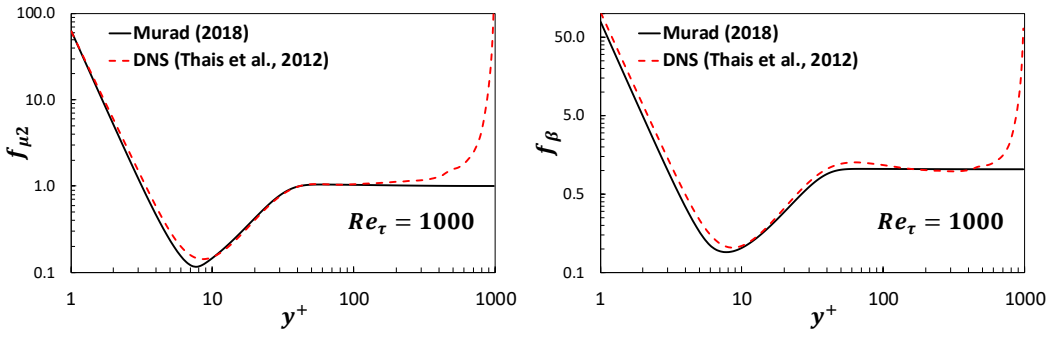

(a) $f_{\mu 2}^{\kappa-\varepsilon}$ (b) $f_{\beta}^{\kappa-\varepsilon}$

Figure 3.2 – Damping function ($f_{\mu 2}^{\kappa-\varepsilon}$and $f_{\beta}^{\kappa-\varepsilon}$) obtained from DNS data of Thais *et al.* (2012) for a channel flow and adjusted by Murad (2018).

To be able to employ these models, it is necessary to determine the turbulent kinetic energy κ and its dissipation rate ε. Their transport equations are shown in the next section.

3.2.3 Transport equations for κ and ε

The transport equations for κ and ε can be obtained from manipulations of the momentum equation (Pope,2000). However, different approximations can be made, and different closure models can be applied, resulting in a large variety of $\kappa - \varepsilon$ models.

Murad (2018) evaluated the performance of four different linear models (Lam & Bremhost, 1981; Launder Sharma, 1977; Lien Leschziner, 1996 and Modified Rodi Mansour, 1993) to predict the channel flow, and also recommended the Modified Rodi Mansour model (Michelassi *et al.*, 1993). Therefore, this model was selected to be employed in the present work to determine κ and ε.

The dimensionless transport equations for κ and ε, corresponding to the Modified Rodi-Mansur model (Michelassi *et al*., 1993) are

$$\frac{\partial(U_j\,\kappa^+)}{\partial x_j} = \frac{\partial}{\partial x_j}\left[\left(1+\frac{\mu_t/\mu}{\sigma_\kappa}\right)\frac{\partial \kappa^+}{\partial x_j}\right] + G_k^+ - \varepsilon^+ \tag{3.41}$$

$$\frac{\partial(U_j\,\varepsilon^+)}{\partial x_j} = \frac{\partial}{\partial x_j}\left[\left(1+\frac{\mu_t/\mu}{\sigma_\varepsilon}\right)\frac{\partial \varepsilon^+}{\partial x_j}\right] + c_{\varepsilon 1} f_1 \frac{\varepsilon^+}{\kappa^+}\,G_k^+ - c_{\varepsilon 2}\,f_2\,\frac{\varepsilon^{+2}}{\kappa^+} + E^+ \tag{3.42}$$

The production of turbulent kinetic energy G_k^+ is

$$G_k^+ = a_{ij}\frac{\partial U_i}{\partial x_j} \tag{3.43}$$

Michelassi et al, (1993) presented the model for a 2D shear flow, thus

$$G_k^+ = \frac{\mu_t}{\mu}\left(\frac{\partial U}{\partial y}\right)^2 \tag{3.44}$$

and the source term E^+ of the dissipation equation is

$$E^+ = \left\{1.2\frac{\mu_t}{\mu}\left(\frac{\partial^2 U}{\partial y^2}\right)^2 + 0.0075\,\frac{\kappa^+}{\varepsilon^+}\frac{\partial \kappa^+}{\partial y}\frac{\partial U}{\partial y}\frac{\partial^2 U}{\partial y^2}\right\} \tag{3.45}$$

Damping functions f_1 and f_2 are also introduced in the dissipation equation to damp the production and destruction of ε at the near wall region, and are shown in Table 3.2. The model constants are: $\sigma_\kappa = 1.3$, $\sigma_\varepsilon = 1.3$, $C_{\varepsilon 1} = 1.44$, $C_{\varepsilon 2} = 1.92$.

Table 3.2 – Damping functions (Michelassi *et al.*, 1993).

Damping functions	$\mathbf{y^+ \leq 100}$
$\boldsymbol{f_1}$	1
$\boldsymbol{f_2}$	$f_2^1.f_2^2 + f_3 - 1$
$\boldsymbol{f_2^1}$	$1 - 0.22\exp\left(-0.3357\,R_t^{\frac{1}{2}}\right)$
$\boldsymbol{f_2^2}$	$1 - \exp(-0.095\,R_y)$
$\boldsymbol{f_3}$	$\exp(1.8\,R_p^3)$

The dimensionless variables used in the damping functions are:

$$R_t = \frac{{\kappa^*}^2}{\nu\,\varepsilon^*}; \quad R_y = \frac{y\sqrt{\kappa^*}}{\nu^*}; \quad R_p = \frac{G_\kappa^*}{\kappa^*\sqrt{\frac{C_\mu \varepsilon^*}{\nu^*}}}; \quad y^+ = \frac{u_\tau\, y^*}{\nu} \tag{3.46}$$

or

$$R_t = \frac{{\kappa^+}^2}{\varepsilon^+}; \quad R_y = y^+\sqrt{\kappa^+}; \quad R_p = \frac{G_\kappa^+}{\kappa^+\sqrt{C_\mu\,\varepsilon^+}} \tag{3.47}$$

3.2.4 Characteristic velocity and length, based on κ and $\dot{\gamma}$

As shown in the previous section, the transport equation for the dissipation involves a high number of damping and empirical coefficients. This equation has a high level of uncertainties, and this is one of the reasons why there are many variants of the $\kappa - \varepsilon$ model. Thus, Alves *et al.* (2014) proposed dimensionless coefficients of the models using the turbulent kinetic energy (κ) and the intensity of the rate of strain tensor ($\dot{\gamma}^*$) to avoid the influence of the ε field in the model.

The definition of $\dot{\gamma}^*$ is:

$$\dot{\gamma}^* = \sqrt{\frac{1}{2}\gamma_{ij}^*\gamma_{ij}^*} \quad ; \quad \gamma_{ij}^* = 2\,\overline{D_{ij}^*} \tag{3.48}$$

Note that

$$\mathrm{tr}\left(\overline{D^{*2}}\right) = \frac{\dot{\gamma}^{*2}}{2} \tag{3.49}$$

Murad (2018), based on the proposition of Alves *et al.* (2014), used the following dimensionless coefficients:

$$\alpha_D = f_\mu C_\mu \frac{\kappa}{\dot{\gamma}^*} \tag{3.50}$$

$$\alpha_{D2} = f_{\mu 2} C_{\mu 2} \frac{\kappa}{\dot{\gamma}^{*2}} \quad ; \quad \alpha_\beta = f_\beta C_\beta \frac{\kappa}{\dot{\gamma}^{*2}} \tag{3.51}$$

Here, as in the previous definitions, C_μ, $C_{\mu 2}$ and C_β are constant reference parameters, and f_μ; $f_{\mu 2}$ and f_β are wall damping factors. The dimensionless parameters are

$$\hat{\alpha}_D = \frac{\alpha_D}{\nu} = \frac{\nu_t}{\nu} = \frac{\mu_t}{\mu} = f_\mu C_\mu \frac{\kappa^+}{\dot{\gamma}} \tag{3.52}$$

$$\hat{\alpha}_{D2} = \frac{\alpha_{D2}}{\nu\,(\nu\,/\,u_\tau)^2} = f_{\mu 2} C_{\mu 2} \frac{\kappa^+}{\dot{\gamma}^2} \tag{3.53}$$

$$\hat{\beta}_P = \frac{\beta_P}{\nu\,(\nu\,/\,u_\tau)^2} = f_\beta C_\beta \frac{\kappa^+}{\dot{\gamma}^2} \tag{3.54}$$

$$\dot{\gamma} = \frac{\nu\,\dot{\gamma}^*}{u_\tau^2} \tag{3.55}$$

At the present work, correlations for the damping functions f_μ, $f_{\mu 2}$, f_β were developed based on the DNS data of Thais *et al*. (2012) and Lee and Moser (2015) for a channel flow, for several friction Reynolds numbers, $Re_\tau = u_\tau\, H/\nu$, where H is a characteristic dimension. For the channel flow, H is half distance between the plates. Details can be found in Appendix A. Murad (2018) also proposed damping functions for the non-linear model, based on κ and $\dot{\gamma}$. These expression were quite complicated and they are shown in Appendix A.

The constants C_μ, $C_{\mu 2}$ and C_β are different for each Re_τ and are shown in Table 3.3.

Table 3.3 – Constant parameters C_μ, $C_{\mu 2}$ and C_β.

Re_τ	C_μ	$C_{\mu 2}$	C_β
395	0.298	-0.79	0.76
590	0.283	-0.75	0.75
1000	0.261	-0.75	0.73
2000	0.256	-0.75	0.72
5200	0.242	-0.70	0.72

The functions that describe the damping functions are:

$$f_\mu = \tanh\left(a_1 y^{+^{b_1}}\right) \tag{3.56}$$

$$f_{\mu 2} = a_2\left\{b_2 + \exp\left[c_2 + d_2 y^+ + g_2 y^{+^2}\right]\right\}^{h_2} \tag{3.57}$$

$$f_\beta = a_3\{b_3 + \exp[c_3 + d_3 y^+ + g_3 y^{+2}]\}^{h_3} \tag{3.58}$$

The coefficients of damping function correlation f_μ vary with the friction Reynolds number Re_τ and are shown in Table 3.4. However, the constants a_i, b_i, c_i, d_i, g_i and h_i used in the damping functions $f_{\mu 2}$ and f_β are equals for all Re_τ.

$$a_2 = 0.0155; b_2 = 1.2;\ c_2 = -0.0425;\ \ d_2 = -0.0013; \tag{3.59}$$
$$g_2 = 0.21; h_2 = 2.4$$

$$a_3 = 0.0155; b_3 = -0.32;\ c_3 = -0.02;\ d_3 = -0.0013; \tag{3.60}$$
$$g_3 = 0.21; h_3 = 2.4$$

Table 3.4 – Constants for f_μ.

Re_τ	a_1	b_1
395	0.040	0.890
590	0.062	0.772
1000	0.070	0.750
2000	0.091	0.639
5200	0.049	0.870

Figure 3.3 illustrates the variation of the damping function with the dimensionless wall distance, for $Re_\tau = 1000$. In each figure de damping function determined from the DNS data is compared with the correlation proposed in the present work. Note, that the damping curves present a smoother behavior, which is another advantage in comparison with the previous dimensionless variables.

The variation of the damping coefficients with wall distance employing the DNS data and the adjusted functions are shown in the Appendix A.1 for all friction Reynolds number.

It should be mentioned here, that although the models coefficients do not depend on ε, the transport equation for κ depends on this variable. However, its influence is reduced, since it is only in an indirect manner, through the turbulent kinetic energy equation.

Aiming to develop a model completely independent of ε, at the present work, a model was proposed and it is presented in the next section.

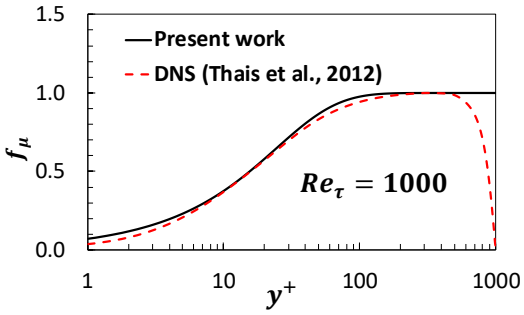

(a) f_μ

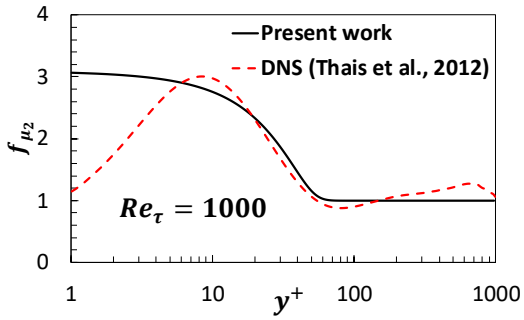

(b) $f_{\mu 2}$

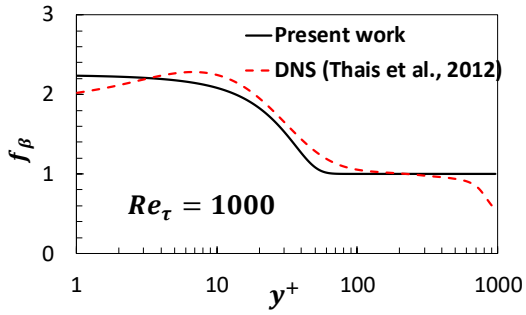

(c) f_β

Figure 3.3 – Damping function (f_μ, $f_{\mu 2}$ and f_β) obtained from DNS data of Thais *et al.* (2012) for a channel flow, $Re_\tau = 1000$.

3.3 Model for the Dissipation of Turbulent Energy

To completely eliminate the influence of the dissipation of turbulent kinetic energy ε in the turbulence models based on κ and $\dot{\gamma}$, a model is proposed here evaluating the two-equation models for one-equation model. To this end, it was considered that there is a balance between production and destruction of κ. Proceeding in a similar way as Michelassi *et al.* (1993), for a shear flow, the turbulent kinetic energy production is $G_k^+ = \mu_t / \mu \, (\partial U / \partial y)^2$ (Eq. 3.44). Thus,

$$G_k^+ = \varepsilon^+ \rightarrow \frac{\mu_t}{\mu} \dot{\gamma}^2 = \varepsilon^+ \tag{3.61}$$

Recalling that the turbulent viscosity is $\mu_t/\mu = f_\mu C_\mu \, \kappa^+ / \dot{\gamma}$, the dissipation can be written as

$$\varepsilon^+ = f_\varepsilon \, C_\varepsilon \, \kappa^+ \, \dot{\gamma} \tag{3.62}$$

where, to better adjust the dissipation behavior in the wall region, the wall function is defined based on the DNS data (Thais *et al.*, 2012 and Lee and Moser, 2015).

Figure 3.4 presents the wall function for the dissipation obtained from the DNS data of Thais *el al.* (2012), for $Re_\tau = 1000$.

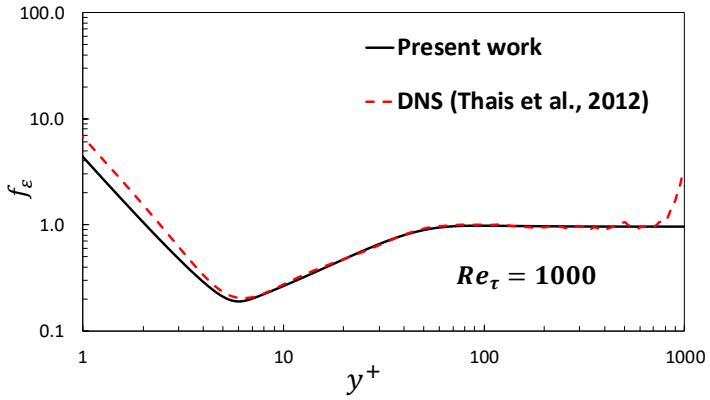

Figure 3.4 – Dissipation damping f_ε from DNS data of Thais *et al.* (2012) for a channel flow, and fitted for $Re_\tau = 1000$

The limiting parameter is $C_\varepsilon = 0.26$, and the wall function is limited to the wall region $y^+ \leq 100$. A correlation of the following form and for all $Re_\tau$was propose for the dissipation damping

$$f_\varepsilon = \left\{ a \frac{\tanh[b(y^+)^c]}{\tanh[d(y^+)^e]} \right\}^\Theta + g \left\{ \exp\left[\lambda - \frac{y^+}{h} \right] \right\} \tag{3.63}$$

Its coefficients and the constant C_ε are independent of the friction Reynolds number and are presented in Table 3.5. Appendix A shows a comparison of the correlation with DNS data for all Re_τ.

Table 3.5 – Constants for f_ε.

a	b	c	d	e	Θ	g	λ	h
0.95	0.0035	1.5	0.00038	4.6	0.68	0.05	0.1	100

3.4 Channel Flow

The configuration selected to test the non-linear turbulence models is the channel flow, i.e., fully developed flow between two parallel plates (Figure 3.5). The distance between the plates is $y^*_{max} = 2\,H$, or in dimensionless units $2\,y^+_{max} = 2\,Re_\tau$. The mean flow is in the axial direction (x^* direction), y^* is the normal direction and z^* the transversal one. The bottom and top walls are at $y^* = 0$ and $y^* = 2\,H$, respectively, with the mid-plane being $y = H$ defining the center line.

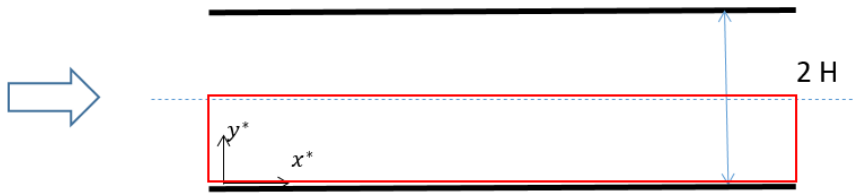

Figure 3.5 – Scheme of a Channel Flow.

Considering that the pressure can be written as an area average value p_m and a perturbation around it,

$$\bar{p} = p_m(x^*) + \tilde{p}(x^*, y^*, z^*) \tag{3.64}$$

and defining a new modified dimensionless pressure as

$$\tilde{P} = \frac{1}{\rho\, u_\tau^2}\left[\tilde{p} - \rho\, g_k\, x_k^* + \frac{2}{3}\,\rho\,\kappa\right] \tag{3.65}$$

The dimensionless pressure gradient is

$$\frac{\partial P}{\partial x_i} = \frac{\nu}{u_\tau^3}\frac{1}{\rho}\frac{\partial p_m}{\partial x_i^*} + \frac{\partial \tilde{P}}{\partial x_i} \tag{3.66}$$

Since the flow is time-average 2D, steady state and fully developed, there is no acceleration. Therefore, there is a force balance equilibrium, i.e., the axial pressure force is equal to the viscous force

$$\frac{\partial p_m}{\partial x^*} = \frac{\partial \tau}{\partial y^*} \tag{3.67}$$

Integrating the shear stress in the above equation and knowing that the shear stress in the symmetry line is null, the resulting equation is:

$$\tau = -\frac{\partial p_m}{\partial x^*} H\left(1 - \frac{y^*}{H}\right) \tag{3.68}$$

And the wall shear stress is

$$\tau_w = \tau(y = 0) = -\frac{\partial p_m}{\partial x^*} H \tag{3.69}$$

Thus,

$$-\frac{\partial p_m}{\partial x^*} = \frac{\tau_w}{H} \tag{3.70}$$

So, one can write

$$\frac{\partial P}{\partial x} = \frac{1}{Re_\tau} + \frac{\partial \tilde{P}}{\partial x} \qquad ; \qquad \frac{\partial P}{\partial y} = \frac{\partial \tilde{P}}{\partial y} \tag{3.71}$$

The conservation equations employed to test the four selected models for the channel flow are

$$\frac{\partial\, U}{\partial x} + \frac{\partial\, V}{\partial y} = 0 \tag{3.72}$$

$$\frac{\partial\,(U\,U)}{\partial x} + \frac{\partial\,(V\,U)}{\partial y} = \frac{1}{Re_\tau} - \frac{\partial \tilde{P}}{\partial x} + \frac{\partial NLT_{xx}}{\partial x} + \frac{\partial NLT_{xy}}{\partial y} + \tag{3.73}$$

$$\frac{\partial}{\partial x}\left[\left(1+\frac{\mu_t}{\mu}\right)\frac{\partial U}{\partial x}\right] + \frac{\partial}{\partial y}\left[\left(1+\frac{\mu_t}{\mu}\right)\frac{\partial U}{\partial y}\right] + \frac{\partial}{\partial x}\left[\left(1+\frac{\mu_t}{\mu}\right)\frac{\partial U}{\partial x}\right] + \frac{\partial}{\partial y}\left[\left(1+\frac{\mu_t}{\mu}\right)\frac{\partial V}{\partial x}\right]$$

$$\frac{\partial\,(U\,V)}{\partial x} + \frac{\partial\,(V\,V)}{\partial y} = -\frac{\partial \tilde{P}}{\partial y} + \frac{\partial NLT_{xy}}{\partial x} + \frac{\partial NLT_{yy}}{\partial y} + \tag{3.74}$$

$$\frac{\partial}{\partial x}\left[\left(1+\frac{\mu_t}{\mu}\right)\frac{\partial V}{\partial x}\right] + \frac{\partial}{\partial y}\left[\left(1+\frac{\mu_t}{\mu}\right)\frac{\partial V}{\partial y}\right] + \frac{\partial}{\partial x}\left[\left(1+\frac{\mu_t}{\mu}\right)\frac{\partial U}{\partial y}\right] + \frac{\partial}{\partial y}\left[\left(1+\frac{\mu_t}{\mu}\right)\frac{\partial V}{\partial y}\right]$$

where the dimensionless non-linear terms are

$$\boldsymbol{TB_I}: \quad NLT_{ij} = 0 \tag{3.75}$$

$$\boldsymbol{TB_{II}}: \quad NLT_{ij} = \hat{\alpha}_{D2}\; D_{ij}^2 \tag{3.76}$$

$$\boldsymbol{TB_{III}}: \quad NLT_{ij} = \hat{\alpha}_{D2}\; D_{ij}^2 + \hat{\beta}_P\, P_{ij} \tag{3.77}$$

$$\boldsymbol{TB_{IV}}: \quad NLT_{ij} = \hat{\beta}_P\, P_{ij} \tag{3.78}$$

The 2D non-linear tensor components are

$$D_{xx}^2 = \left(\frac{\partial U}{\partial x}\right)^2 + \frac{1}{4}\left(\frac{\partial U}{\partial y} + \frac{\partial V}{\partial x}\right)^2 \;;\; D_{yy}^2 = \left(\frac{\partial V}{\partial y}\right)^2 + \frac{1}{4}\left(\frac{\partial U}{\partial y} + \frac{\partial V}{\partial x}\right)^2 \tag{3.79}$$

$$D_{xy}^2 = D_{yx}^2 = \frac{1}{2}\left(\frac{\partial U}{\partial x} + \frac{\partial V}{\partial y}\right)\left(\frac{\partial\, U}{\partial y} + \frac{\partial\, V}{\partial x}\right) \tag{3.80}$$

$$P_{xx} = \frac{1}{2}\left[\left(\frac{\partial V}{\partial x}\right)^2 - \left(\frac{\partial U}{\partial y}\right)^2\right] \;;\; P_{yy} = -P_{xx} \tag{3.81}$$

$$P_{xy} = P_{yx} = \frac{1}{2}\left[\left(\frac{\partial U}{\partial x} - \frac{\partial V}{\partial y}\right)\left(\frac{\partial U}{\partial y} - \frac{\partial V}{\partial x}\right)\right] \tag{3.82}$$

The 2D turbulent kinetic energy transport equation is

$$\frac{\partial\,(U\,\kappa^+)}{\partial x} + \frac{\partial\,(V\,\kappa^+)}{\partial y} = \tag{3.83}$$

$$= \frac{\partial}{\partial x}\left[\left(1 + \frac{\mu_t/\,\mu}{\sigma_\kappa}\right)\frac{\partial \kappa^+}{\partial x}\right] + \frac{\partial}{\partial y}\left[\left(1 + \frac{\mu_t/\,\mu}{\sigma_\kappa}\right)\frac{\partial \kappa^+}{\partial y}\right] + G_k^+ - \varepsilon^+$$

where the production of $\kappa^+$is $G_k^+ = a_{ij}\,\partial U_i/\,\partial x_j$ with $a_{ij} = (\mu_t/\mu\;2)\,D_{ij} + NLT_{ij}$,

$$G_k^+ = \frac{\mu_t}{\mu}\frac{1}{2}\left(\frac{\partial U_i}{\partial x_j} + \frac{\partial U_j}{\partial x_i}\right)^2 + NLT_{ij}\frac{\partial U_i}{\partial x_j} \tag{3.84}$$

For a 2D flow

$$G_k^+ = \frac{\mu_t}{\mu}\left[2\left(\frac{\partial U}{\partial x}\right)^2 + 2\left(\frac{\partial V}{\partial y}\right)^2 + \left(\frac{\partial U}{\partial y} + \frac{\partial V}{\partial x}\right)^2\right] + NLT_{xx}\frac{\partial U}{\partial x} \tag{3.85}$$
$$+ NLT_{xy}\left(\frac{\partial U}{\partial y} + \frac{\partial V}{\partial x}\right) + NLT_{yy}\frac{\partial V}{\partial y}$$

The 2D dissipation of the turbulent kinetic energy transport equation is

$$\frac{\partial\,(U\,\varepsilon^+)}{\partial x} + \frac{\partial\,(V\,\varepsilon^+)}{\partial y} = \frac{\partial}{\partial x}\left[\left(1 + \frac{\mu_t\,\mu}{\sigma_\varepsilon}\right)\frac{\partial \varepsilon^+}{\partial x}\right] + \frac{\partial}{\partial y}\left[\left(1 + \frac{\mu_t\,\mu}{\sigma_\varepsilon}\right)\frac{\partial \varepsilon^+}{\partial y}\right] \tag{3.86}$$

$$+ c_{\varepsilon 1} f_1 \frac{\varepsilon^+}{\kappa^+}\,G_k^+ - c_{\varepsilon 2}\,f_2\,\frac{\varepsilon^{+2}}{\kappa^+} + E^+$$

Due to the symmetry of the configuration, the solution was obtained for only half domain, from the inferior plate to the symmetry line, as indicated in Figure 3.5. At the inferior plate, no slip was imposed

$$y = 0\;;\;\; U = V = \kappa^+ = 0\,;\varepsilon^+ = 2\left(\frac{\partial\sqrt{\kappa^+}}{\partial y}\right)^2 \tag{3.87}$$

and symmetry at $y^* = H$ $(y = y^+ = Re_\tau)$

$$y = Re_\tau \;;\; V = 0 \,; \frac{\partial U}{\partial y} = \frac{\partial \kappa^+}{\partial y} = \frac{\partial \varepsilon^+}{\partial y} = 0 \tag{3.88}$$

Further, since the flow is fully developed, a periodic boundary condition was imposed in the axial direction, what means that all variables at the inlet of the domain are equal to the variables at the outlet of the domain, with the average pressure gradient imposed.

3.4.1 1D formulation

Although the channel flow problem has been solved as 2D flow, in fact, it is 1D flow, since $\boldsymbol{U} = U(y)\boldsymbol{e_x}$. The intensity of the rate of strain tensor is

$$\dot{\gamma} = \frac{\partial U}{\partial y} \tag{3.89}$$

The Reynolds stress tensor components are

$$\boldsymbol{TB_I}: \quad a_{xx} = a_{yy} = a_{zz} = 0 \;\; ; \;\; a_{xy} = \frac{\mu_t}{\mu}\,\dot{\gamma} \tag{3.90}$$

$$\boldsymbol{TB_{II}}: a_{xx} = a_{yy} = \frac{\hat{\alpha}_{D2,III}}{12}\,\dot{\gamma}^{\boldsymbol{2}} \;\; ; \;\; a_{zz} = -\frac{\hat{\alpha}_{D2,III}}{6}\,\dot{\gamma}^{\boldsymbol{2}} \,; \;\; a_{xy} = \frac{\mu_t}{\mu}\,\dot{\gamma} \tag{3.91}$$

$$\begin{aligned} \boldsymbol{TB_{III}}: \quad & a_{xx} = \left(\frac{\hat{\alpha}_{D2,III}}{12} - \frac{\beta_{P,III}}{2}\right)\dot{\gamma}^{\boldsymbol{2}} \;\; ; \;\; a_{yy} = \left(\frac{\hat{\alpha}_{D2,III}}{12} + \frac{\beta_{P,III}}{2}\right)\dot{\gamma}^{\boldsymbol{2}} \\ & a_{zz} = -\frac{\hat{\alpha}_{D2,III}}{6}\,\dot{\gamma}^{\boldsymbol{2}} \quad ; \quad a_{xy} = \frac{\mu_t}{\mu}\,\dot{\gamma} \end{aligned} \tag{3.92}$$

$$\boldsymbol{TB_{IV}}: a_{xx} = -\frac{\beta_{P,III}}{2}\,\dot{\gamma}^{\boldsymbol{2}} \;\; ; \;\; a_{yy} = \frac{\beta_{P,III}}{2}\,\dot{\gamma}^{\boldsymbol{2}} \;\; ; \;\; a_{zz} = 0 \;\; ; \; a_{xy} = \frac{\mu_t}{\mu}\,\dot{\gamma} \tag{3.93}$$

Note that for all models considered, the non-linear part of the Reynolds stress component xy is null, ($NLT_{xy} = 0$).

The velocity field can also be obtained with 1D formulation, and only the axial momentum equation needs to be solved, with the turbulent quantities.

$$0 = \frac{1}{Re_\tau} + \frac{\partial}{\partial y}\left[\left(1 + \frac{\mu_t}{\mu}\right)\frac{\partial U}{\partial y}\right] \tag{3.94}$$

$$0 = \frac{\partial}{\partial y}\left[\left(1 + \frac{\mu_t / \mu}{\sigma_\kappa}\right)\frac{\partial \kappa^+}{\partial y}\right] + G_k^+ - \varepsilon^+ \tag{3.95}$$

$$0 = \frac{\partial}{\partial y}\left[\left(1 + \frac{\mu_t\, \mu}{\sigma_\varepsilon}\right)\frac{\partial \varepsilon^+}{\partial y}\right] + c_{\varepsilon 1} f_1 \frac{\varepsilon^+}{\kappa^+} G_k^+ - c_{\varepsilon 2} f_2 \frac{\varepsilon^{+2}}{\kappa^+} + E^+ \tag{3.96}$$

$$G_k^+ = \frac{\mu_t}{\mu} \dot{\gamma}^2 \tag{3.97}$$

3.5 Numerical Model

The governing conservation equation were solved with an in-house code developed by the Group *Dinâmica dos Fluidos Computacional*, written in Fortran and extensively tested was used. The code is based on the Finite Volume Method (Patankar, 1980). The Finite Volume Method consists of dividing the domain of interest in control volumes and integrating the conservation equation in each control volume, resulting on a global conservation equation. The code is based on a staggered mesh, where scalar quantities are stored at the control volume central point, and velocities at the control volume faces.

All conservation equations can be written in the following general form

$$\frac{\partial\,(U\varphi)}{\partial x} + \frac{\partial\,(V\,\varphi)}{\partial y} = \frac{\partial}{\partial x}\left(\Gamma_\varphi \frac{\partial \varphi}{\partial x}\right) + \frac{\partial}{\partial y}\left(\Gamma_\varphi \frac{\partial \varphi}{\partial y}\right) + Sc_\varphi + Sp_\varphi \varphi \tag{3.98}$$

For each variables φ the corresponding diffusion coefficient Γ_φ and the source terms Sc_φ and Sp_φ, shown in Table 3.6 were implemented in the USER routine. One important observation to be made here, is that since κ^+ and ε^+ must always be positive, the source terms for these variables are implemented guaranteeing that $Sc_\varphi \geq 0$ and $Sp_\varphi \leq 0$.

The convective-diffusive flux was approximated with the Power-law scheme (Patankar, 1980) and the pressure-velocity coupling was solved with the SIMPLE (Semi-Implicit Method for Pressure-Linked Equations) algorithm.

To solve the system equations, the Cyclic Line-by-line TDMA algorithm (Patankar *et al.*,1977) was employed. In order to accelerate convergence, the block correction algorithm (Settari & Aziz, 1973) was used.

Table 3.6 – Diffusion coefficient and source terms of conservation equation terms.

$\boldsymbol{\varphi}$	$\boldsymbol{\Gamma_\varphi}$	$\boldsymbol{Sc_\varphi}$	$\boldsymbol{Sp_\varphi}$
Axial Momentum, *U*	$1+\frac{\mu_t}{\mu}$	$\frac{1}{Re}+\frac{\partial}{\partial x_j}\left(\Gamma_\varphi \frac{\partial U_j}{\partial x}\right)+\frac{\partial\, NLT_{xj}}{\partial x_j}$	
Normal Momentum, *V*	$1+\frac{\mu_t}{\mu}$	$\frac{\partial}{\partial x_j}\left(\Gamma_\varphi \frac{\partial U_j}{\partial y}\right)+\frac{\partial\, NLT_{yj}}{\partial x_j}$	
Turbulent kinetic energy, κ^+	$1+\frac{\mu_t/\,\mu}{\sigma_\kappa}$	G_k^+	$-\frac{\varepsilon^+}{\kappa^+}$
Dissipation of κ, ε^+	$1+\frac{\mu_t/\,\mu}{\sigma_\varepsilon}$	$c_{\varepsilon 1} f_1 \frac{\varepsilon^+}{\kappa^+}\, G_k^+ + E^+$	$-c_{\varepsilon 2}\, f_2\, \frac{\varepsilon^+}{\kappa^+}$

Sub relaxation factors were applied to all transport equations. At the beginning of the simulations, these factors were very small to control the convergence evolution and were slowly increased up to 0.9.

The solution was considered converged when variation of the wall shear stress was inferior to 1%, and the residues of all conservation equations were inferior to 10^{-6}.

One important note to the model is that the turbulent viscosity as well as the non-linear coefficients, Eqs. (3.52)–(3.54), are inversely proportional to $\dot{\gamma}$. Therefore, as $\dot{\gamma} \to 0$, these variables approach ∞. Therefore, to bound the model, a small number is added in the denominator of these coefficients to avoid division by zero. After some investigation, the chosen constant for the turbulent viscosity was defined as 10^{-3}, while for the non-linear terms 10^{-6} was sufficient to avoid the problem.

4 . Results

The results obtained with the 2 equations $\kappa - \dot{\gamma}$ and 1 equation $\kappa - \dot{\gamma}$ models proposed in this work, based on the characteristic velocity $V_c = \kappa^{1/2}$ and length $\ell_c = \kappa/\dot{\gamma}$, are presented here. To validate the methodology, DNS channel flow data of two different sets were employed: Thais *et al.* (2012), corresponding to friction Reynolds numbers Re_τ =395, 590 and 1000 and Lee and Moser (2015), Re_τ =2000 and 5200.

All tests presented in this section were obtained with the same mesh as the DNS reference for each friction Reynolds number to allow a direct comparison. However, a grid test was performed and it is shown in Appendix B illustrating that the same results were obtained with a courser mesh as desired in RANS simulations.

Before testing the numerical simulation of the models proposed, a few tests were performed with $Re_\tau = 1000$. First, a DNS-reference solution is obtained, i.e., the mean velocity field based on the actual DNS data for the Reynolds stress tensor components is obtained and compared with the DNS data. Then, tests were performed to determine the impact of approximating different terms of the model in the flow field prediction, leading to a new 2 equations $\kappa - \dot{\gamma}$.

As shown in section 3.4.1, the channel flow is actually a 1D situation. Therefore, one additional preliminary test was performed by comparing the solution obtained by solving the 2D set of conservation equations with the solution obtained by solving the 1D set of conservation equations. This test is presented in Appendix C, where the prediction of all flow variables, for all friction Reynolds number, employing Model III of the tensorial base is discussed. As expected, perfect agreement was obtained, and the 1D formulation was employed for the following tests, since it requires less computing effort.

At the two following sections, the solution obtained for $Re_\tau = 1000$, with the proposed 2 equations $\kappa - \dot{\gamma}$ model and 1 equation $\kappa - \dot{\gamma}$ model and all models of the tensorial basis, are presented. In both sections, the proposed models predictions are compared with DNS data of Thais *et al.* (2012).

In the sequence, it is presented a comparison of the proposed 2 equations $\kappa -$

$\dot{\gamma}$ and 1 equation $\kappa - \dot{\gamma}$ non-linear models with RANS predictions obtained by Murad (2018), with Model III of the tensorial basis with $\kappa - \varepsilon$ model and $\kappa - \dot{\gamma}$ with his proposed damping coefficients, coupled with the solution of κ and ε transport equations of the Modified Rodi Mansour model (Michelassi *et al.*, 1993). Finally, the models prediction for the different Reynolds numbers are presented.

4.1 Mean velocity field with DNS Reynolds stress tensor

The first test performed was designed to evaluate the quality of the mean velocity field obtained by the solution of the momentum equation, employing the DNS Reynolds stress tensor components data directly in the conservation equations. This test was motivated by the work of Thompson *et al.* (2016), who have presented a careful evaluation of statistical errors in DNS data of plane channel flow. Assuming a perfectly converged DNS Reynolds tensor field, the main idea is to obtain a reference velocity field corresponding to this tensor, which would be the best velocity field that one can obtained with a turbulent RANS model, if the model is able to completely mimic the DNS Reynolds stress tensor components.

Figure 4.1a presents the dimensionless mean axial velocity profile U^+ along the vertical dimensionless coordinated y^+, obtained by the solution of momentum equations with $a_{xy} = a_{xy}^{DNS}$ of Thais *et al.* (2012). The velocity profile is plotted in log and linear scales to allow a deeper observation of the profile details close to the wall and symmetry line. The acronym SL in the figures stands for symmetry line. Analyzing the results in Figure 4.1(a), it can be seen an under prediction of the axial velocity for the "DNS-reference" based on Thais *et al.* (2012) data. A closer look to the DNS data shows that at the symmetry line, the DNS value of Thais *et al.* (2012) is $a_{xy} = a_{xy}^{DNS} = -5.44 \times 10^{-3}$. However, at the symmetry line, the time average value of a_{xy} is expected to be zero. Thus, another simulation was performed by changing only the a_{xy} value at the symmetry line to zero. It can be seen in Figure 4.1b a slightly better profile, but now an overestimation of the velocity was obtained near the symmetry. The DNS data (Thais *et al.*, 2012) presents a value for a_{xy} at the symmetry line very close to zero, but this small disturbance causes a significant change in the reference velocity field.

To investigate further the matter, the same simulation was performed using the DNS data from Lee & Moser (2015) for $Re_\tau = 1000$, where at the symmetry line the

DNS value is $a_{xy} = a_{xy}^{DNS} = 4.99 \times 10^{-4}$. Figure 4.1a shows a perfect agreement of the DNS data for the mean axial velocity profile of the two references, further, the reference solution obtained with Lee & Moser (2015) also agrees perfectly.

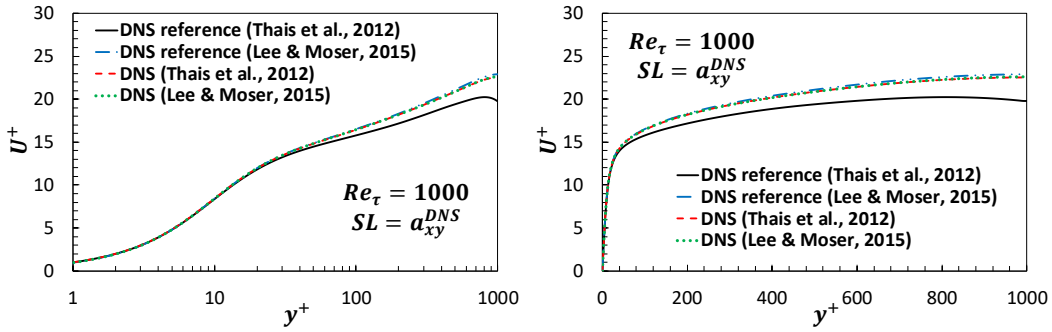

(a) at symmetry: $a_{xy} = a_{xy}^{DNS}$

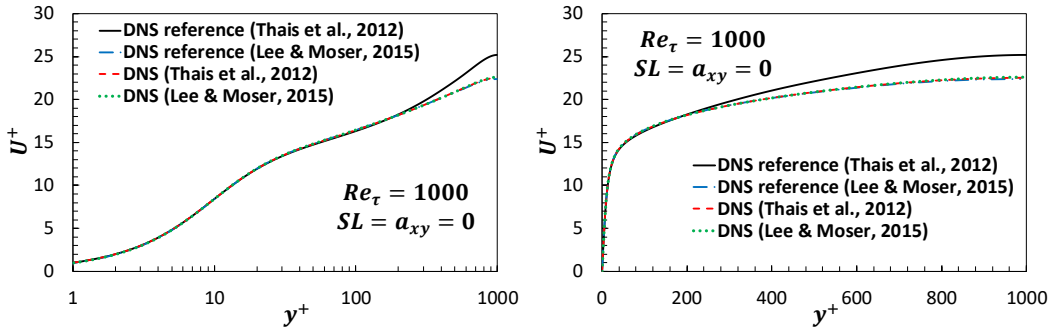

(b) at symmetry: $a_{xy} = 0$

Figure 4.1 – Velocity field obtained with DNS a_{xy} (a) $a_{xy} = a_{xy}^{DNS}$ in the symmetry line (b) $a_{xy} = 0$ in the symmetry line. $Re_\tau = 1000$.

One more test was performed, applying $a_{xy} = 0$ at the symmetry line, and using $a_{xy} = a_{xy}^{DNS}$ of Lee & Moser (2015) for the rest of the domain (Figure 4.1b). The agreement between predictions is also almost perfect, since at the symmetry line, the a_{xy}^{DNS} value of Lee & Moser (2015) is not only closer to zero than a_{xy}^{DNS} of Thais *et al.* (2012), but it is positive, indicting perhaps that the convergence of Thais *et al.* (2012) should have been improved.

The conclusion is that the numerical solution of the velocity field is very sensitive to the value of a_{xy} at the symmetry line, since it has a direct impact on its derivative, what is really necessary for the solution.

For all following simulations, the boundary condition for the velocity at the symmetry line was set equal to zero, corresponding to $a_{xy} = 0$. It was also decided to compare the models prediction directly with the available DNS data, not only because both DNS data set presented equal data, but the reference solution obtained with Lee & Moser (2015) data was also the same.

4.2 Preliminary Tests

Preliminary tests were performed for friction Reynolds number Re_τ =1000, and employed Thais *et al.* (2012) DNS data. The objective of the tests was to determine the impact of different terms in the flow field prediction, by determining the mean velocity field and Reynolds stress components. Model III of the tensorial base was selected, since it presents the contribution of all non-linear terms, i.e., $\boldsymbol{D}^2$ and $\boldsymbol{P}$.

Three cases were examined to evaluate the contribution of different terms on the non-linear model proposed, solving the kinematic tensors:

- Case 1: DNS near wall damping function coefficients, DNS turbulent kinetic energy and DNS dissipation rate of the turbulent kinetic energy
- Case 2: DNS turbulent kinetic energy and its dissipation rate, with the proposed near wall damping coefficients
- Case 3: DNS dissipation rate of turbulent kinetic energy, solving Modified Rodi-Mansur turbulent kinetic energy equation, with the proposed near wall damping coefficients

4.2.1 Case 1: Impact of rate of strain for $\kappa - \dot{\gamma}$ model

The first preliminary test consisted in determining the velocity field employing the coefficients obtained for the model from the DNS data (Thais *et al.*, 2012) and solving the conservation equations with the kinematic tensors. Model III of the tensor base was selected, and all model coefficients were directly obtained from the DNS data, and the Reynolds stress tensor components were defined as

$$a_{xy} = \hat{\alpha}_{D,DNS}\, 2\, D_{xy} + \hat{\alpha}_{D2,DNS}\, D_{xy}^2 + \hat{\beta}_{P,DNS} P_{xy} \tag{4.1}$$

$$a_{xx} = \hat{\alpha}_{o,DNS} + \hat{\alpha}_{D,DNS}\, 2\, D_{xx} + \hat{\alpha}_{D2,DNS} D_{xx}^2 + \beta_{P,DNS} P_{xx} \tag{4.2}$$

$$a_{yy} = \hat{\alpha}_{o,DNS} + \hat{\alpha}_{D,DNS}\, 2\, D_{yy} + \hat{\alpha}_{D2,DNS} D_{yy}^2 + \beta_{P,DNS} P_{yy} \tag{4.3}$$

$$a_{zz} = \hat{\alpha}_{o,DNS} + \hat{\alpha}_{D,DNS}\, 2\, D_{zz} + \hat{\alpha}_{D2,DNS} D_{zz}^2 + \beta_{P,DNS} P_{zz} \tag{4.4}$$

Figure 4.2 presents for Case 1, a comparison of the velocity field, in log and linear scales to better examine the profile. Figure 4.3 shows a comparison of all Reynolds stress components obtained with Model III with DNS data of Thais *et al.*

(2012).

In this test, the turbulent kinetic energy and the damping functions are DNS fields, and perfect agreement was obtained for all variables, indicating that Model III is able to capture the anisotropic behavior of the flow, by employing the square of the rate of strain tensor as well as the non-persistence tensor. Further, it also indicates that all velocity derivatives are well implemented and perfectly captured.

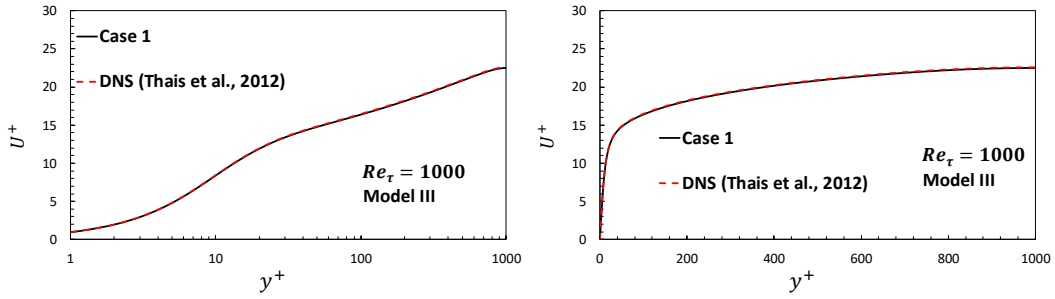

Figure 4.2 – Case 1: Comparison of mean axial velocity with DNS data (Thais *et al.*, 2012). $Re_\tau = 1000$, Model III of the tensorial model.

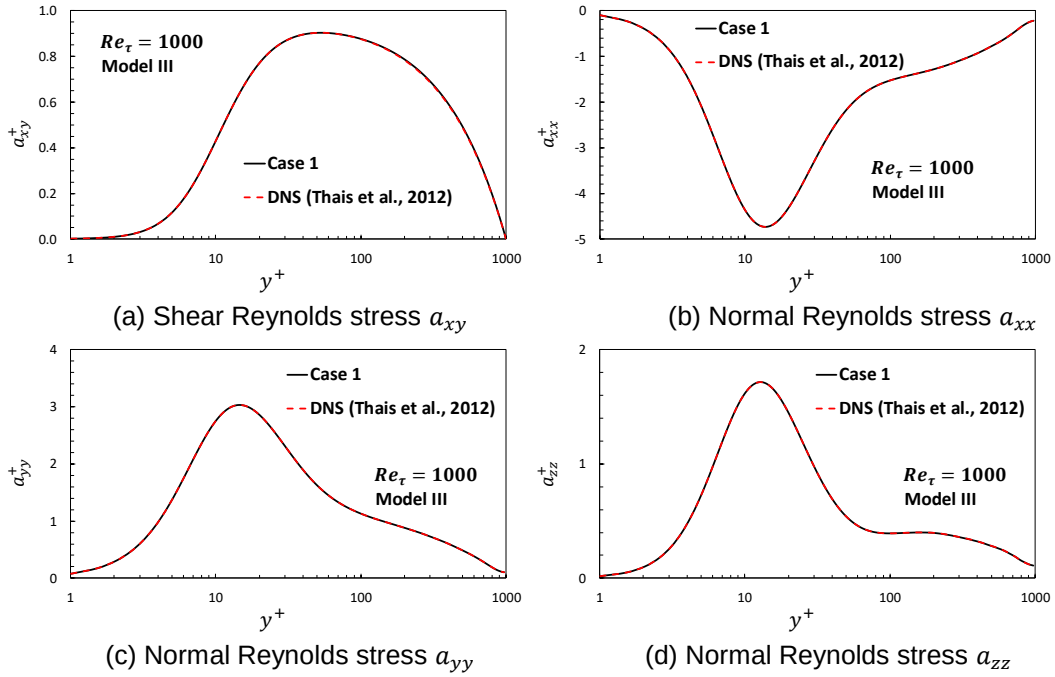

(a) Shear Reynolds stress a_{xy}

(b) Normal Reynolds stress a_{xx}

(c) Normal Reynolds stress a_{yy}

(d) Normal Reynolds stress a_{zz}

Figure 4.3 – Case 1: Comparison of Reynolds stress tensor components with DNS data (Thais *et al.*, 2012). $Re_\tau = 1000$, Model III of the tensorial model.

4.2.2 Case 2: Impact of near wall damping functions for $\kappa - \dot{\gamma}$ model

To evaluate the impact in the solution of the proposed $\kappa - \dot{\gamma}$ turbulent viscosity model, with the developed damping functions, without uncertainties of

the turbulent kinetic energy equation, the velocity field was obtained by solving the momentum equation with

$$\hat{\alpha}_{D_D} = \frac{\mu_t}{\mu} = f_\mu C_\mu \frac{\kappa_{DNS}^+}{\dot{\gamma}};\ \hat{\alpha}_{D2} = f_{\mu 2} C_{\mu 2} \frac{\kappa_{DNS}^+}{\dot{\gamma}^2};\ \hat{\beta}_P = f_\beta C_\beta \frac{\kappa_{DNS}^+}{\dot{\gamma}^2} \tag{4.5}$$

The velocity field obtained with this test is shown in Figure 4.4 and the normal Reynolds stress components are shown in Figure 4.5.

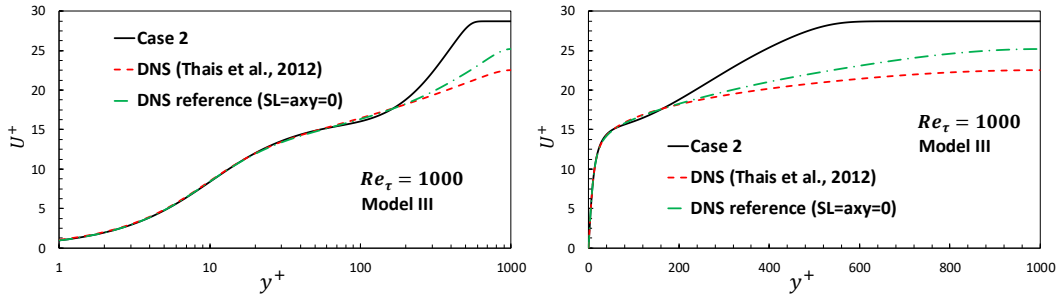

Figure 4.4– Case 2: Comparison of mean axial velocity with DNS data (Thais *et al.*, 2012). $\boldsymbol{Re_\tau = 1000}$, Model III of the tensorial model.

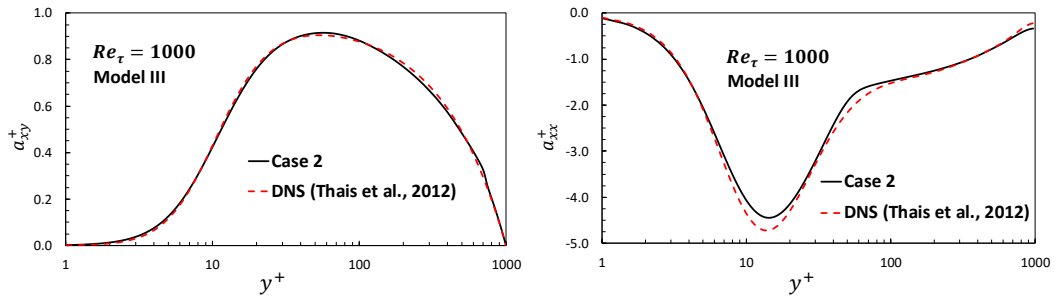

(a) Shear Reynolds stress a_{xy} (b) Normal Reynolds stress a_{xx}

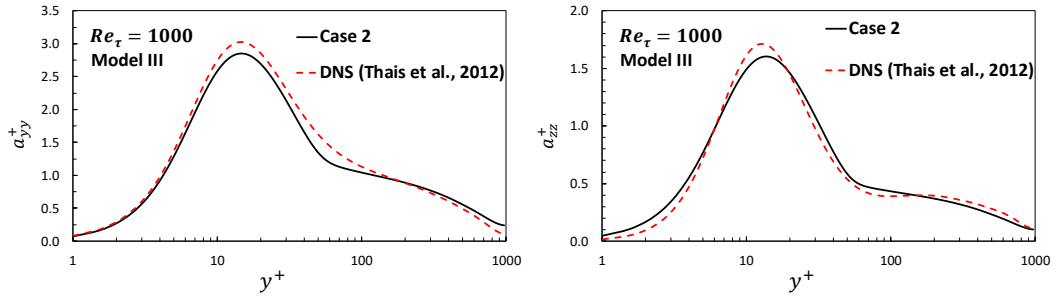

(c) Normal Reynolds stress a_{yy} (d) Normal Reynolds stress a_{zz}

Figure 4.5 – Case 2: Comparison of Reynolds stress tensor components with DNS data (Thais *et al.*, 2012). $\boldsymbol{Re_\tau = 1000}$, Model III of the tensorial model.

Here, a deviation of the velocity field near the symmetry line can be observed in Figure 4.4, where a plateau of the axial velocity near the symmetry line is seen. This occurs, because, the damping function was restricted to the near wall region, and the intensity of the rate of strain is zero at the symmetry line. Since $\dot{\gamma}$ and κ_{DNS}^+ approach zero in an independent form, their ratio present in the models coefficients

is not predicted adequately. As $\dot{\gamma}$ goes to zero faster than κ^+_{DNS}, very high models coefficient are obtained, resulting in constant velocity at the central region. This is a consequence of the damping function restricted to the near wall region, with a constant reference model coefficient C_μ. As shown in Figure 3.3, far from the wall the DNS f_μ presents a strong decay and goes to zero. reducing the diffusion contribution. In the absence of this control, the resulting high diffusion coefficient induces a constant velocity at the center of the domain. The DNS-reference curve, employing Thais *et al*. (2012) data set with $a_{xy} = a^{DNS}_{xy} = 0$, was also added in Figure 4.4, where it can be seen an increase of the mean axial velocity at the symmetry line, also related with $\dot{\gamma}$ approaching zero at the symmetry.

In spite of the problem observed for the axial velocity field, very good results for all components of the Reynolds stress tensor were obtained as shown in Figure 4.5. The shear component is very good because near the symmetry, where the velocity was not well represented, its derivative is small, thus a_{xy} approaches zero as desired.

All three normal components of the Reynolds stress tensor presented a very good agreement with Thais *eta al*. (2012) DNS data, with very small deviation, indicating the importance of considering the contribution of both D^2 and P tensors.

4.2.3 Case 3: Impact of turbulent kinetic energy prediction

As shown in section 3.2.3, the transport equation for the turbulent kinetic energy depends on ε, i.e., the dissipation of κ. In that section, it was also mention that ε equation needs several additional closure terms, increasing its uncertainty. Thus, for the present test, the transport equation for κ proposed by Rodi Mansur, Eq. (3.41), is solved, but ε equation is not solved, instead, its DNS value is used directly in κ equation, as

$$\frac{\partial(\,U_j\,\kappa^+)}{\partial x_j} = \frac{\partial}{\partial x_j}\left[\left(1 + \frac{\mu_t/\,\mu}{\sigma_\kappa}\right)\frac{\partial \kappa^+}{\partial x_j}\right] + G^+_k - \,\varepsilon^+_{DNS} \tag{4.6}$$

Figure 4.6 compares the predicted turbulent kinetic energy with DNS data. A very good agreement was obtained, with a small over prediction, with the exception of the symmetry line, where zero κ was obtained.

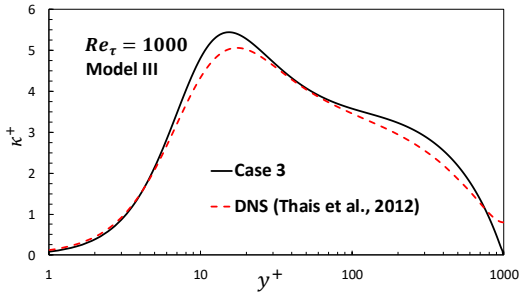

Figure 4.6 – Case 3: Comparison of turbulent kinetic energy with DNS data (Thais *et al.*, 2012). $Re_\tau = 1000$, Model III of the tensorial model.

Figure 4.7 shows the performance of Modell III of the tensorial base to predict the mean axial velocity with the best possible dissipation of turbulent kinetic energy, i.e., by employing its DNS value, ε^+_{DNS}. The shear and normal components of the Reynolds stress tensor, are compared with the DNS data in Figure 4.8.

The velocity profile is shown in Figure 4.7 in log and linear scales. Excellent agreement is obtained near the wall and a very small deviation of the computed solution from the DNS data was obtained along the whole domain. The limitation of κ coupled with the constant f_μ, bounds the ratio with zero $\dot{\gamma}$ rendering a good velocity prediction.

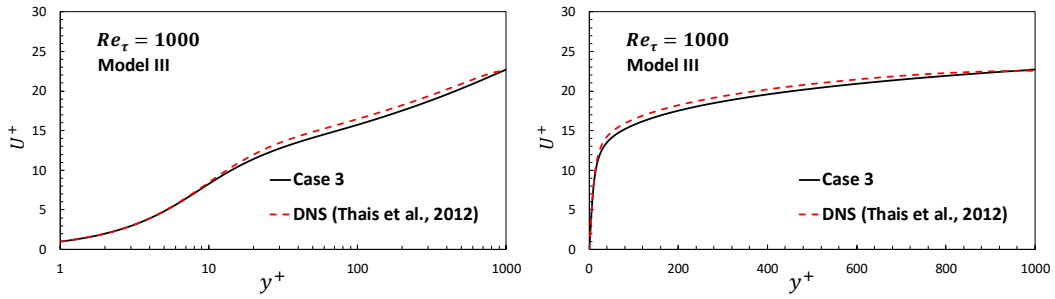

Figure 4.7– Case 3: Comparison of mean axial velocity with DNS data (Thais *et al.*, 2012). $\boldsymbol{Re_\tau = 1000}$, Model III of the tensorial model.

Excellent agreement was also obtained for the shear and normal components of the Reynolds stress tensor, when compared with the DNS data in Figure 4.8. A very small deviation of shear component can be seen for region $y^+ < 20$, where it overestimate DNS data, however, it has an excellent agreement for $y^+ > 20$. The normal components predictions are better than in the previous test. The normal components a_{xx} and a_{yy} present good agreement for $y^+ < 10$, with a minimal error in the rest of domain, while a very small over prediction of a_{zz} is seen along the whole domain.

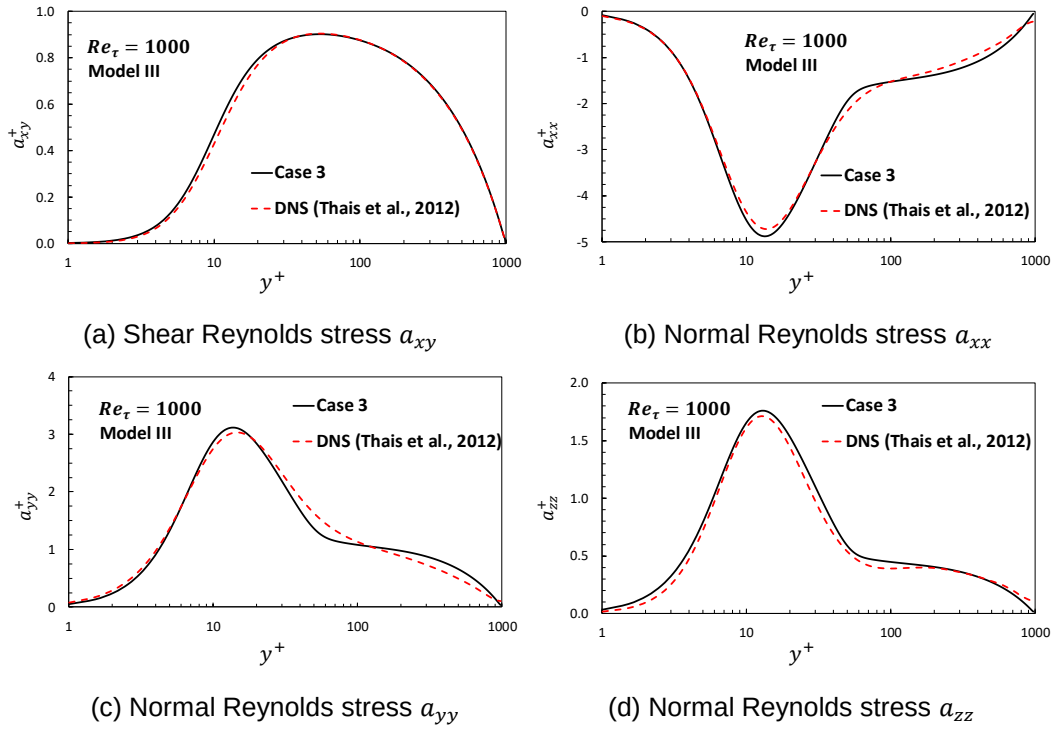

(a) Shear Reynolds stress a_{xy}

(b) Normal Reynolds stress a_{xx}

(c) Normal Reynolds stress a_{yy}

(d) Normal Reynolds stress a_{zz}

Figure 4.8 – Case 3: Comparison of Reynolds stress tensor components with DNS data (Thais *et al.*, 2012). $Re_\tau = 1000$, Model III of the tensorial model.

This test shows that a perfect dissipation model will render very good Reynolds stress tensor components as well as mean axial velocity.

4.3 Non-linear 2 equations $\kappa - \dot{\gamma}$ model

For this test, the complete $\kappa - \varepsilon$ model of Michelassi *et al.* (1993), the Modified Rodi Mansour model, given by Eqs. (3.48) and (3.49), was solved.

The mean axial velocity and shear Reynolds stress component are the same for all non-linear models, as well as for the linear Model I of the tensorial base. The difference between these models is reflected only in the normal components of Reynolds stress tensor. So, first the results obtained corresponding the turbulent variables κ and ε, the mean axial velocity and shear Reynolds stress components, corresponding to Modell III of the tensorial base, are presented. In the sequence, the prediction of the normal Reynolds stress components of all other non-linear models is discussed.

Figure 4.9 compares the predicted dissipation of turbulent kinetic energy and turbulent kinetic energy with DNS data of Thais *et al.* (2012). A small deviation of ε prediction from the DNS data near the wall can be seen, but a very good agreement can be seen for $y^+ > 30$. A good agreement of κ prediction with DNS data can

be seen in the whole domain, with a distribution equivalent to the one obtained in the previous test (Case 3). Note however, an improvement of κ prediction that near the symmetry line, in relation to the previous test.

The mean axial velocity profile along the vertical coordinate is shown in Figure 4.10 in log and linear scale, while the shear Reynolds stress component is presented in Figure 4.11. Examining the velocity result, an increase of the agreement with the DNS data can be seen, in relation to the previous test. An improvement of the prediction of a_{xy} was also obtained (Figure 4.11).

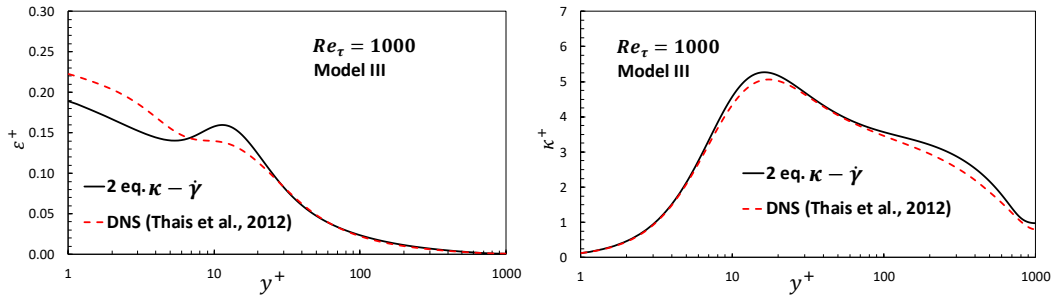

(a) Dissipation of turbulent kinetic energy (b) Turbulent kinetic energy

Figure 4.9 – 2 equations $\kappa - \dot{\gamma}$ model: Comparison of dissipation of turbulent kinetic energy and turbulent kinetic energy with DNS data (Thais *et al.,* 2012). $Re_\tau = 1000$, Model III of the tensorial model.

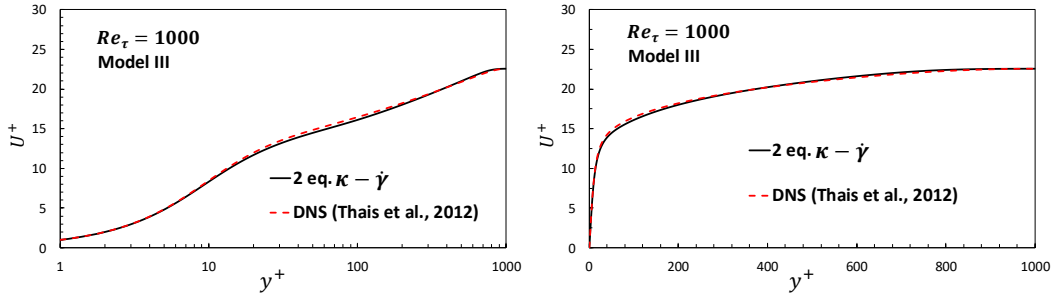

Figure 4.10 – 2 equations $\boldsymbol{\kappa - \dot{\gamma}}$ model: Comparison of mean axial velocity with DNS data (Thais *et al.,* 2012). $\boldsymbol{Re_\tau = 1000}$, Model III of the tensorial model.

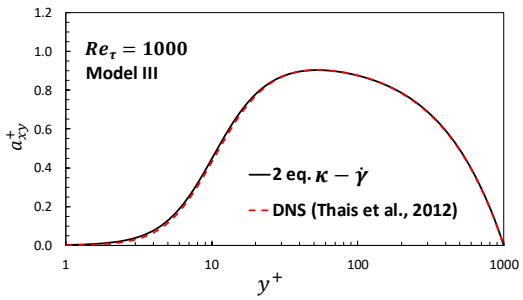

Figure 4.11 – 2 equations $\kappa - \dot{\gamma}$ model: Comparison of shear Reynolds stress tensor component a_{xy} with DNS data (Thais *et al.,* 2012). $Re_\tau = 1000$, Model III of the tensorial model.

Figure 4.12 presents the normal components of Reynolds stress tensor for Model II,III and IV of the tensorial base. Model I is a linear model and it is unable to predict the normal components of Reynolds stress tensor.

The non-linear contribution of Model II is associated with the tensor $\boldsymbol{D}^2$ tensor. Examining Figure 4.12, it can be seen that Models II substantially underestimates a_{xx}. Further, this models fails to predict the correct sign of a_{yy}. The prediction a_{zz} is reasonable, with a slight under prediction along the vertical coordinate, and with a small shift of its peak toward the symmetry line.

Examining Model IV prediction in Figure 4.12, one can observe that a_{xx} is also underestimated, and a_{yy} is overestimated in relation to the DNS data, with a significantly better prediction than Model II. The non-linear contribution of this model comes from the non-persistence tensor $\boldsymbol{P}$, and this model is unable to predict a_{zz}.

At the same Figure 4.12, the normal components of the Reynolds stress tensor predicted by Model III are also shown. This model is formed by the contribution of both tensors $\boldsymbol{D^2}$ and $\boldsymbol{P}$. Note that, by adding the contribution of both non-linear tensors, Model III prediction is significantly better than the prediction of the other two models. The negative contribution of $\boldsymbol{D^2}$ to a_{yy} combined with the overestimation of $\boldsymbol{P}$, results in a very good result for this component with Model III, which combines both tensors. The same is true with respect to component a_{xx}, since both tensors do not contribute enough to its value, but their combination is excellent. Finally, the prediction of Modell II and III for a_{zz} are equal, since tensor $\boldsymbol{P}$, does not add a contribution to this component.

The conclusion of this analysis is that the model which better predicts the normal components of Reynolds stress tensor is Model III, agreeing with Nieckele *et al.*, (2016) and Murad (2018).

The impact of the calculated ε was slightly higher for the normal components, with a small under-prediction of all normal components for Model III, when compared with test Case 3, although it can still be considered that a good agreement was obtained.

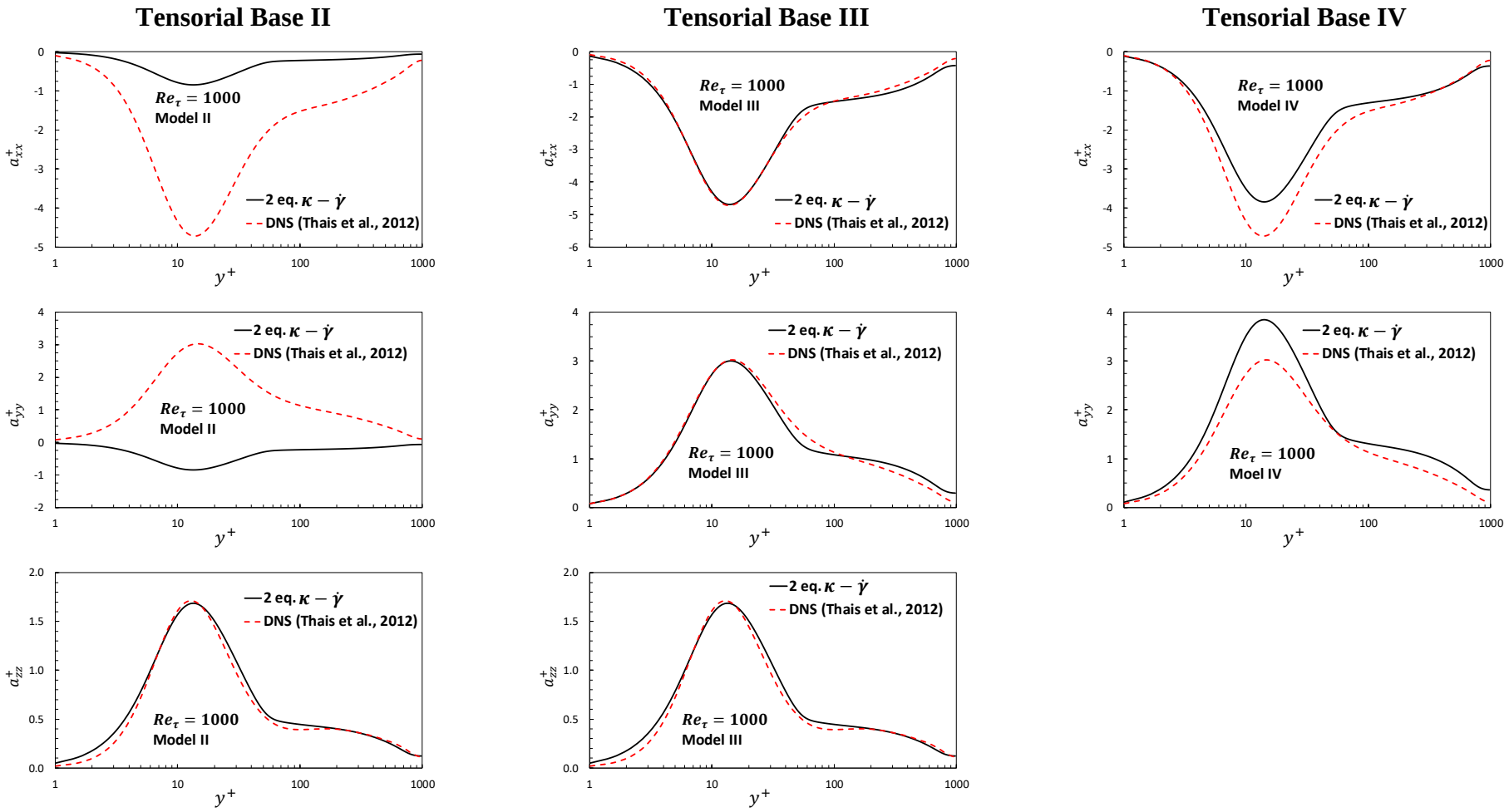

Figure 4.12 – Non-linear models normal Reynolds stress tensor components. 2 equations $\kappa - \dot{\gamma}$ model. $Re_\tau = 1000$, Model II, III and IV of the tensorial base.

4.4 Non-linear 1 equation $\kappa - \dot{\gamma}$ models

In this section the performance of the proposed 1 equation non-linear $\kappa - \dot{\gamma}$ models is presented, by comparing with DNS data from Thais *et al* (2012) for $Re_\tau = 1000$. As mentioned in the previous section, only the normal Reynolds stress components present different results for each model, and Model III of the tensorial basis was selected to present all other variables.

Figure 4.13 presents a comparison of the dissipation of turbulent kinetic energy and turbulent kinetic energy with Thais *et al.* (2012) DNS data. The κ profile is very similar to the one obtained with the 2 equations $\kappa - \dot{\gamma}$ model (shown in Figure 4.9) in most of the domain, with the exception of the symmetry region, where a larger plateau was obtained. The opposite is seen for its dissipation, which is similar to the one obtained in 2 equations $\kappa - \dot{\gamma}$ model (Figure 4.10) in the center of the domain up to the symmetry line, but it increases and approaches the DNS data near the wall.

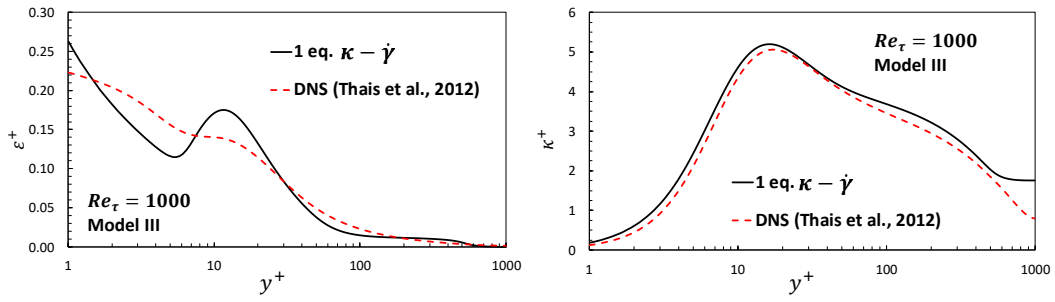

(a) Dissipation of turbulent kinetic energy (b) Turbulent kinetic energy

Figure 4.13 – 1 equation $\kappa - \dot{\gamma}$ model: Comparison of dissipation of turbulent kinetic energy and turbulent kinetic energy with DNS data (Thais *et al.*, 2012). $Re_\tau = 1000$, Model III of the tensorial base.

The axial velocity profile obtained with the 1 equation $\kappa - \dot{\gamma}$ model is shown in Figure 4.14. In the same figure the DNS data of Thais *et al* (2012) was included. Note that, although the profile obtained is close to the DNS data, the dissipation model induced a wavy behavior in the region close to the center of the domain. Further, a large plateau of the axial velocity is obtained in the center region.

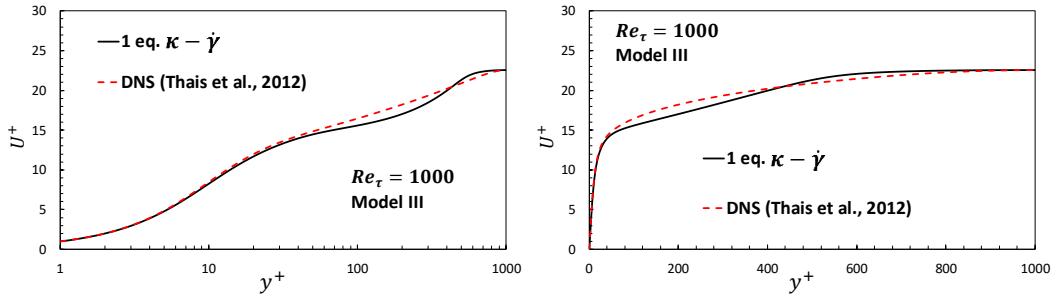

Figure 4.14 – 1 equation $\boldsymbol{\kappa - \dot{\gamma}}$ model: Comparison of axial velocity with DNS data (Thais *et al.,* 2012). $\boldsymbol{Re_\tau = 1000}$, Model III of the tensorial base.

Comparing the present 1 equation $\kappa - \dot{\gamma}$ model prediction of the shear Reynolds stress component a_{xy} in Figure 4.15 with the DNS data, it is observed that an equivalent profile was obtained.

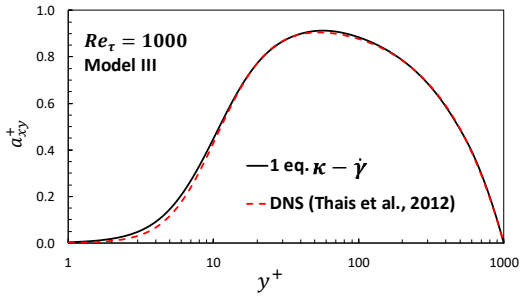

Figure 4.15 – 1 equation $\boldsymbol{\kappa - \dot{\gamma}}$ model: Comparison of shear Reynolds stress $\boldsymbol{a_{xy}}$. with DNS data (Thais *et al.,* 2012). $\boldsymbol{Re_\tau = 1000}$, Model III of the tensorial base.

Figure 4.16 presents normal components of Reynolds stress tensor for Model II, III and IV. The same behavior of the different non-linear models as presented with non-linear 2 equations $\kappa - \dot{\gamma}$ model was obtained, with a slightly better performance for the 1 equation $\kappa - \dot{\gamma}$ model for Model III of the tensorial base, except at the symmetry, where as a consequence to the kinetic energy plateau, a plateau was also obtained for the normal Reynolds stress components

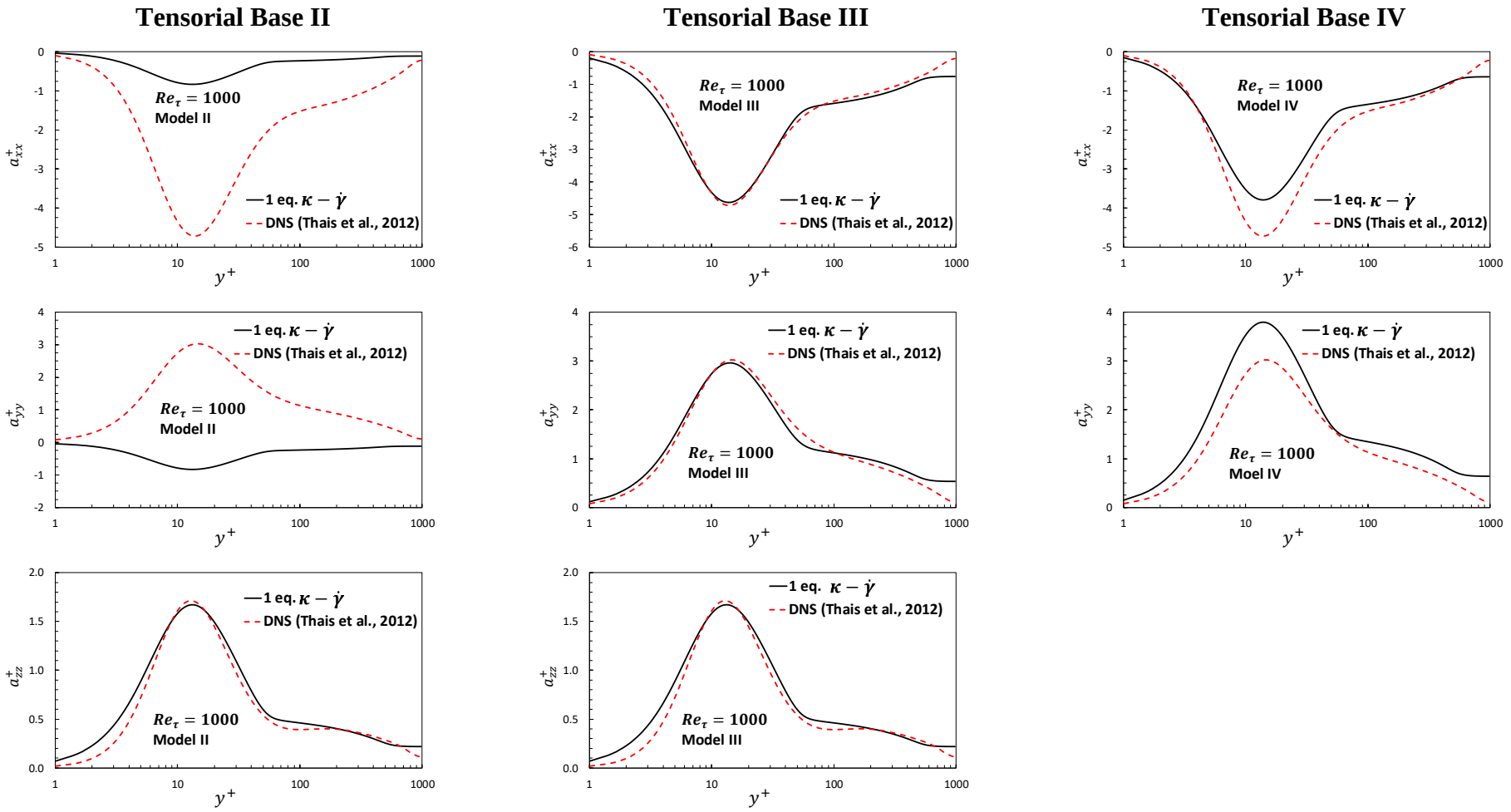

Figure 4.16 – Non-linear models normal Reynolds stress tensor components. $\kappa - \dot{\gamma}$ 1 equation model. $Re_\tau = 1000$, Model II, III and IV of the tensorial base.

4.5 Comparison of Different Models

In this section, the results of the two proposed non-linear $\kappa - \dot{\gamma}$ models develop in this work are compared with the literature. The first model is 2 equations $\kappa - \dot{\gamma}$ model, analyzed in section 4.3, and the second one, is the 1 equation $\kappa - \dot{\gamma}$ model, employing the developed model for ε (section 4.4). Both models are based on the new developed damping functions, detailed in Appendix A.1. The results of models are compared with prediction of Murad (2018), who develop two sets of non-linear models, based on different characteristic velocity and length. The first one, employed κ and ε to define the characteristic velocity and length, as described in section 3.2.2. The second set of models, like the present work employed κ and $\dot{\gamma}$ to define the characteristic velocity and length, with the damping coefficients, as described in section A.2. However, the damping coefficients developed were very cumbersome and they were applied in the whole domain. Further, it was tested only for Re_τ=1000. For all simulations the Modified Rodi Mansour model (Michelassi *et al.*, 1993) was solved to determine κ and ε. Murad (2018) evaluated the models for several Reynolds numbers, and compared with several models available in the literature and showed, in agreement with Nieckele *et al.* (2016) that Model III is the most recommended model, since it better captures the normal Reynolds stress components. Thus, only the results of Model III of the tensorial base are shown here.

Murad (2018) compared the results obtained with his developed model with some $\kappa - \varepsilon$ models found in the literature: four linear Low-Reynolds Models and one Non-Linear Low Reynolds Model. The linear models were Lam BremHorst (Lam & Bremhorst, 1981), Launder Sharma (Launder *et al.*, 1977), Lien Leschziner (Lien & Leschziner, 1993) and Modified Rodi Mansour (Michelasse *et al.*, 1993). The non-linear model was Lien Cubic Model (Lien *et al.*, 1996). The comparison made by Murad (2018) showed that the non-linear Model III of the tensorial basis, with the damping function that he proposed for both characteristic velocity and length ($\kappa - \varepsilon$ and $\kappa - \dot{\gamma}$) presented superior results than these models found in the literature. Therefore, here, the models proposed in this work are compared among themselves, with DNS data and the models proposed by Murad (2018).

Comparison of flow variables obtained with the models develop here (1 equation and 2 equations non-linear $\kappa - \dot{\gamma}$) with Murad (2018) predictions are shown in Figure 4.17 through Figure 4.21. In these figures the predictions of the different models are compare with the DNS data of Thais *et al.* (2012).

The first variable examined is the dissipation of the turbulent kinetic energy ε, shown in Figure 4.17. All two equation models predicted equivalent results for $y^+ \geq 30$, with a slight deviation from the DNS data (below and above) of Model $1eq.\kappa - \dot{\gamma}$. Near $y^+ \approx 12$, a clear transition is observed in the DNS ε profile, with a plateau followed by a stronger increase at the sub-laminar layer. At approximately the same position, all models presented a hump, followed by also an increase of ε at the sub-laminar layer. The increase of ε near the wall of Model 1 eq. $\kappa - \dot{\gamma}$ is too strong, ending up overestimating its value at the wall. Model $\kappa - \dot{\gamma}$ and Model $\kappa - \varepsilon$ of Murad (2018) and the present 2 eq. $\kappa - \dot{\gamma}$ followed the same tendency of the DNS data in this region. The behavior of ε in the near wall is very difficult to predict, and most models prediction disagree in this region as shown by Murad (2018).

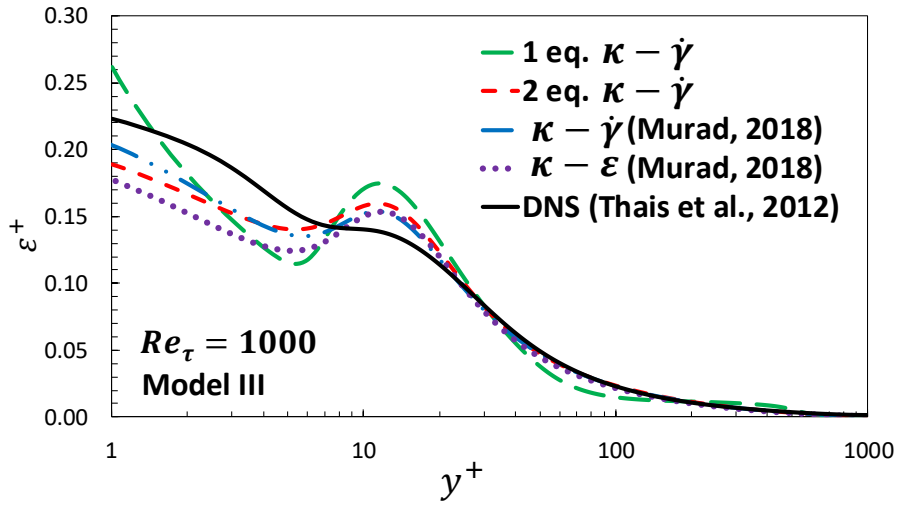

Figure 4.17 –Dissipation rate of turbulent kinetic energy. Models comparison.

The impact of the dissipation behavior in the turbulent kinetic energy in the near wall region is very small, as shown in Figure 4.18, where all models present very close results up to $y^+ \approx 20$. In this region, the present Model 1 eq. $\kappa - \dot{\gamma}$ predicted slightly higher values. All models predict the same peak position with equivalent values. At the center of the domain, the worst prediction is of Model $\kappa - \varepsilon$ (Murad, 2018), and an almost perfect agreement is shown for his $\kappa - \dot{\gamma}$ model.

Although this agreement is very good, his proposed damping function acts in the whole domain, what clearly is not convenient in a general situation. Both 1eq. and 2 eq. $\kappa - \dot{\gamma}$ developed here employ a near wall damping function at $y^+ \leq 100$, and as a consequence, the models are equivalent in the central region ($y^+ > 20$), with a small over estimation of κ. The agreement of 1 equation $\kappa - \dot{\gamma}$ model with 2 equations $\kappa - \dot{\gamma}$ model is very positive, since it solves only one addition equation instead of two, like all other models examined here. However, near the symmetry 1eq. $\kappa - \dot{\gamma}$ presents a small plateau as already discussed.

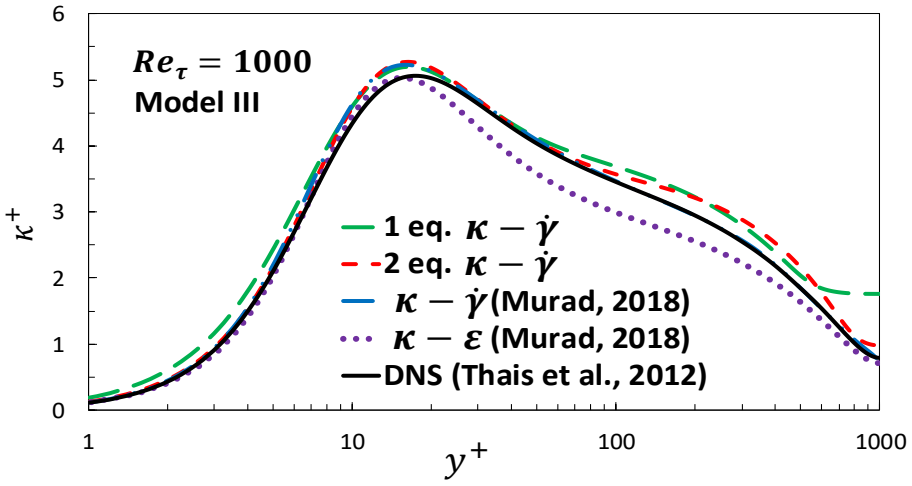

Figure 4.18 – Turbulent kinetic energy. Models comparison.

The models comparison of the mean axial velocity profile can be examined in Figure 4.19. All models present coincident results at the near wall region up to $y^+ \approx 10$. After this distance from the wall, the results obtained by Murad (2018) with both models are slightly lower than the DNS data, while the prediction of present 2 equations $\kappa - \dot{\gamma}$ Model is almost coincident with the DNS data. 1 equation $\kappa - \dot{\gamma}$ Model captures the correct velocity value at the symmetry line, but presented a wave velocity profile for $y^+ > 100$, presenting underestimation in $100 < y^+ < 300$ and an overestimation in $300 < y^+ < 800$.

All models predicted a practically coincident shear Reynolds stress profile with an excellent agreement with the DNS data, as can be seen in Figure 4.20. Very small differences can be observed near the wall, 1 equation $\kappa - \dot{\gamma}$ curve is above the DNS curve, and 2 equations $\kappa - \varepsilon$ below, both 2 equations $\kappa - \dot{\gamma}$ perfectly reproduce the DNS data.

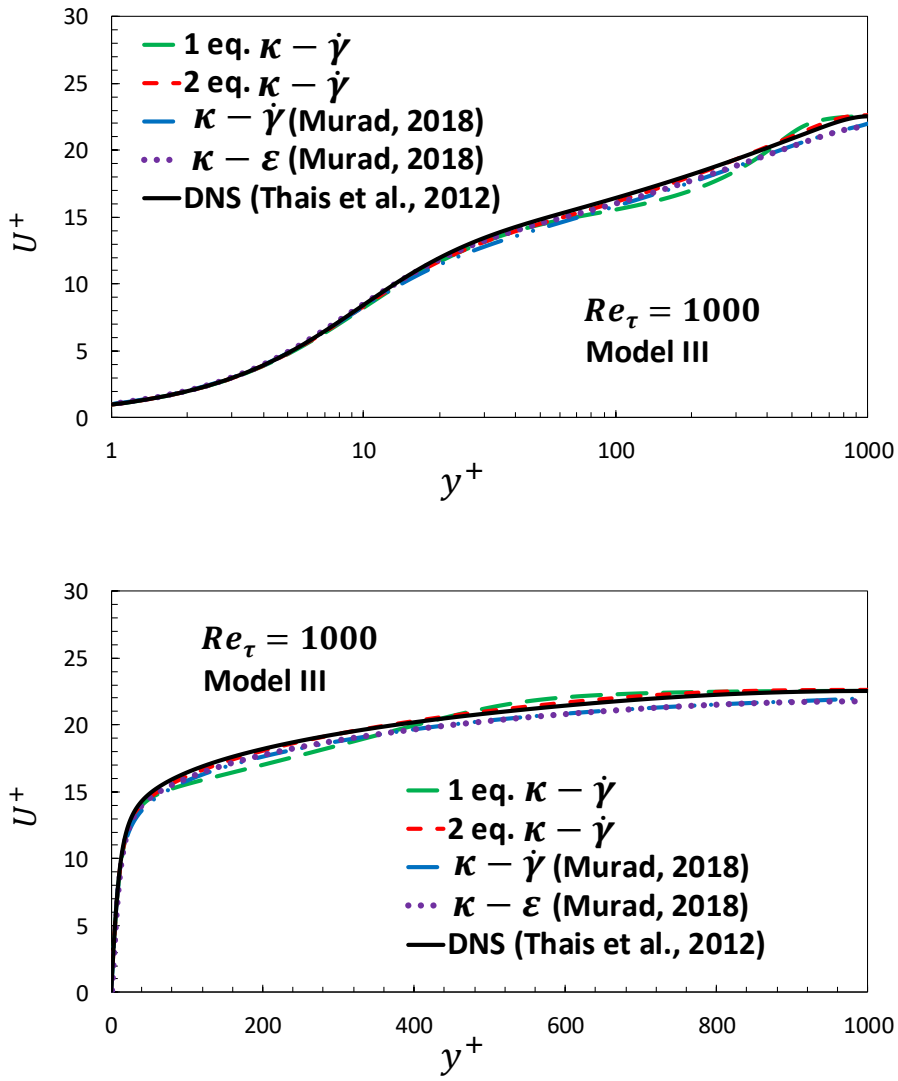

Figure 4.19 – Mean axial velocity for $Re_\tau = 1000$. Models comparison.

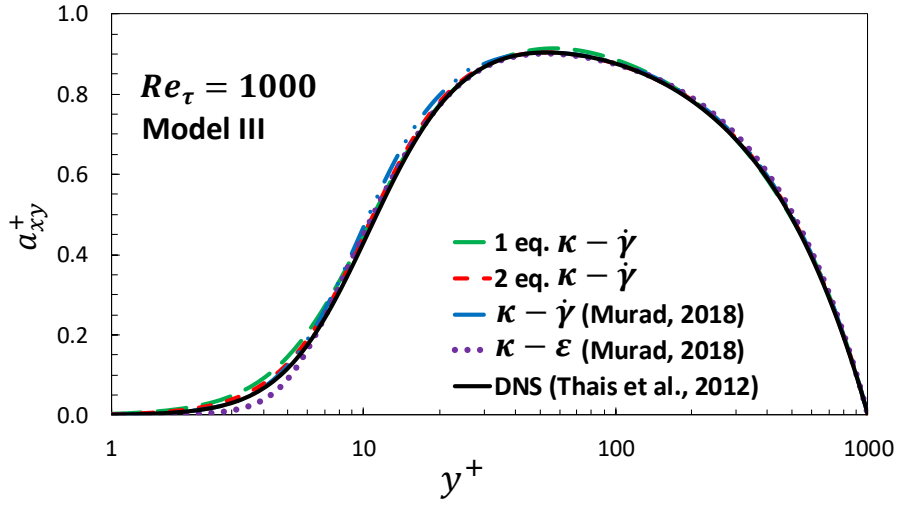

Figure 4.20 – Shear Reynolds stress a_{xy}. $Re_\tau = 1000$.

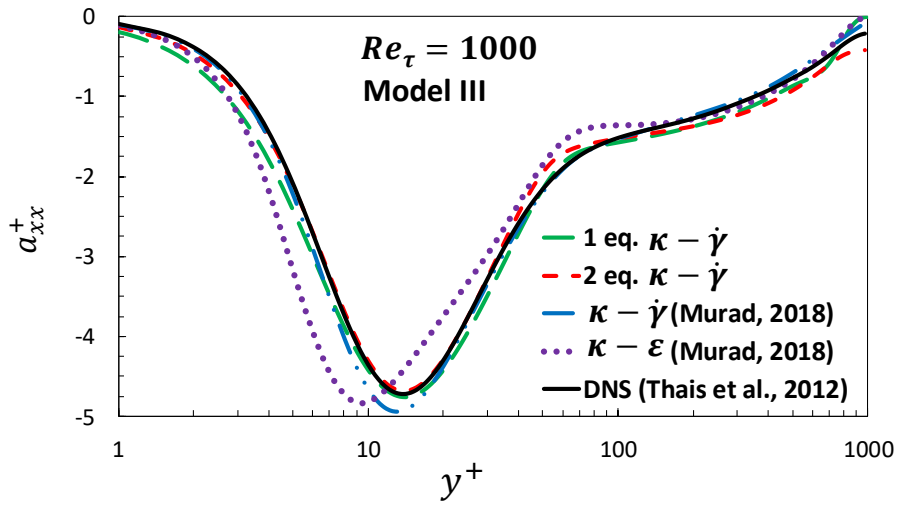

(a) Normal Reynolds stress a_{xx}

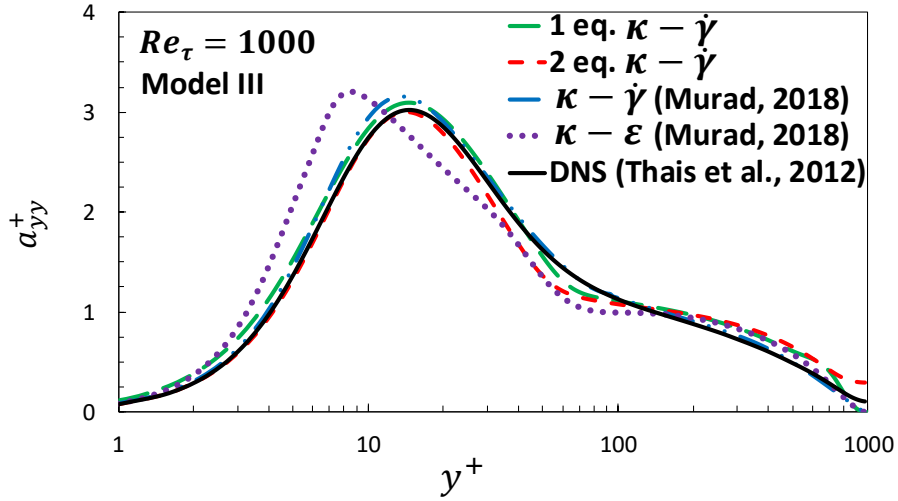

(b) Normal Reynolds stress a_{yy}

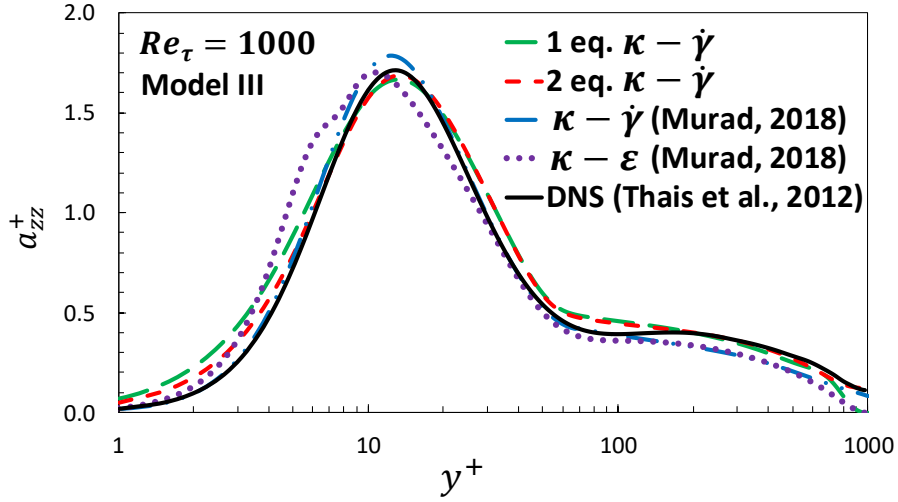

(c) Normal Reynolds stress a_{zz}

Figure 4.21 – Normal Reynolds stress tensor components. $Re_\tau = 1000$.

The comparison of all three normal Reynolds stress tensor components is presented in Figure 4.21. All models showed the same qualitative profile for the three normal components. The $\kappa - \varepsilon$ model of Murad (2018) presented the worst result with the peak of all components shifted to the wall direction. The present 2 equations $\kappa - \dot{\gamma}$ model underestimated all components, Model $\kappa - \dot{\gamma}$ of Murad (2018) and 2 eq. $\kappa - \dot{\gamma}$ presented similar results as the present 1 eq. $\kappa - \dot{\gamma}$ model for the prediction of the normal components of Reynolds stress tensor, and one can say that Model 1 eq. $\kappa - \dot{\gamma}$ prediction was superior for the three components than all other models.

4.6 Influence of Reynolds number Re_τ for Model III $\kappa - \dot{\gamma}$

To better evaluate the proposed non-linear Model III of the tensorial base $\kappa - \dot{\gamma}$, in this section the predictive ability of the model for several Reynolds number is examined. Both 1 equation and 2 equations $\kappa - \dot{\gamma}$ formulation are examined. The models predictions are compared with DNS data of Thais *el al.* (2012) for friction Reynolds number Re_τ=395, 590 and 1000 and Lee and Moser (2015) DNS data for Re_τ=2000, and 5200.

The near wall damping function for the non-linear terms of the Reynolds stress tensor and proposed dissipation of κ for the different friction Reynolds number are shown in Appendix A.1 and A.3, respectively.

In the Figure 4.22, Figure 4.23 and Figure 4.24 are presented the results of 2 equations $\kappa - \dot{\gamma}$ model for all Re_τ. The distribution of the dissipation of the turbulent kinetic energy (Figure 4.22a), obtained by the solution of the Modified Rodi-Mansur model is equivalent for all friction Reynolds numbers, very good for $y^+ > 30$, with an underestimation near the wall, but with similar profile. The resulting turbulent kinetic energy (Figure 4.22b) is also equivalent for the different friction Reynolds number, however, its prediction agreement with DNS data decays as the Reynolds number increases. For $Re_\tau = 2000$ there is a slight increase of the overestimation of κ for $y^+ > 200$, while for $Re_\tau = 5200$, from $100 \leq y^+ \leq 1000$, an approximately constant κ was predicted, reducing abruptly near the symmetry, approaching the DNS value.

In spite of the observed disagreement in κ prediction for the higher friction Reynolds number, the mean axial velocity (Figure 4.23a) and the shear component of the Reynolds stress tensor (Figure 4.23b) were very well capture for all Reynolds number, with a small over estimation of the velocity near the symmetry line for Re_τ =2000 and 5200.

For the normal components of the Reynolds stress tensor (Figure 4.24), the agreement of the predicted values with DNS data of Thais *et al.* (2012) corresponding to $Re_\tau \leq 1000$ is very good and equivalent. For Re_τ =2000, the agreement of the three components with DNS data of Lee and Moser (2015) is also good, with the same peak in the same location, with an increase in the disagreement in the center of the domain. For Re_τ =5200, the peak position of the three components were also well predicted, with a small deviation on its value. However, in the center of the domain, as a direct consequence of the κ prediction, a larger disagreement is observed, but it can also be stated that a reasonable result was obtained.

From the results presented, Model III of the tensorial base is able to predict the channel flow and the proposed near wall damping coefficients for the $\kappa - \dot{\gamma}$ model produced good results for a wide range of Reynolds numbers.

The results for the 1 eq. the $\kappa - \dot{\gamma}$ model III are shown in Figure 4.25, Figure 4.26 and Figure 4.27. For $Re_\tau \leq 1000$, Thais *et al.,* (2012) DNS data base used and for $Re_\tau > 1000$, the DNS data was obtained from Lee & Moser (2015) data base.

Examining the results for ε in Figure 4.25a, it can be seen that $Re_\tau = 590$ and $Re_\tau = 2000$ presented the same behavior as $Re_\tau = 1000$ with a reasonable agreement with DNS data. However, for $Re_\tau = 395$, the dissipation at the wall was significantly underestimated, and for $Re_\tau = 5200$ the dissipation profile predicted by the 1 eq. the $\kappa - \dot{\gamma}$ is very similar to $Re_\tau = 2000$, while the DNS data is more smooth, although very good ε wall value was predicted.

The turbulent kinetic energy is shown in Figure 4.25b. Note an increase of the κ plateau near the symmetry line for the lower friction Reynolds numbers. Once again the prediction for $Re_\tau = 395$ was not satisfactory and for $Re_\tau = 590$ the profile is acceptable only up to $y^+ \leq 200$. On the other hand, the prediction of κ for the $Re_\tau = 2000$ is very good, even superior than for $Re_\tau = 1000$. For $Re_\tau = 5200$, κ prediction of the 1 equation model $\kappa - \dot{\gamma}$ is superior than the 2 equations

$\kappa - \dot{\gamma}$ model, although κ is overprescribed at the center of the domain, but reasonable values were determined. reasonable.

The mean axial velocity for 1 equation $\kappa - \dot{\gamma}$ model is shown in Figure 4.26a, while the shear Reynolds stress component is in Figure 4.26b. Unfortunately, a deterioration of the prediction of the mean velocity with relation to the 2 eq. $\kappa - \dot{\gamma}$ model is clear. A constant velocity is obtained at the center of the domain, up to the symmetry line for $Re_\tau = 395$. For $Re_\tau = 590$, 1000 and 2000, the velocity level is near the DNS data, but a wave profile is obtained. A very poor velocity profile prediction was obtained for $Re_\tau = 5200$. In spite of the velocity profile obtained for all friction Reynolds numbers, the shear Reynolds stress predictions were reasonable. For the lower Reynolds it was slightly underestimated near the wall, and an unrealistic peak is seen for the largest Reynolds number, but very good results for the intermediated ones.

With respect to the normal Reynolds stress prediction of 1 eq. $\kappa - \dot{\gamma}$ model (Figure 4.27), with the exception of $Re_\tau = 395$, good results were obtained for all friction Reynolds number.

A conclusion of this test is that the model for the dissipation of the turbulent kinetic energy needs to be improved. It was well adjusted for $Re_\tau = 1000$ and 2000, that presented the best results, it was reasonable for $Re_\tau = 590$, but it failed for $Re_\tau = 395$ and 5200. The same is true with respect to the damping coefficient of the linear term, since it presents a strong dependence with the friction Reynolds number. On the other hand, the near wall damping coefficients of the non-linear terms was very well designed. Not only, the damping functions are independent of the friction Reynolds number, but good predictions of the normal Reynolds stress components were obtained for all Reynolds.

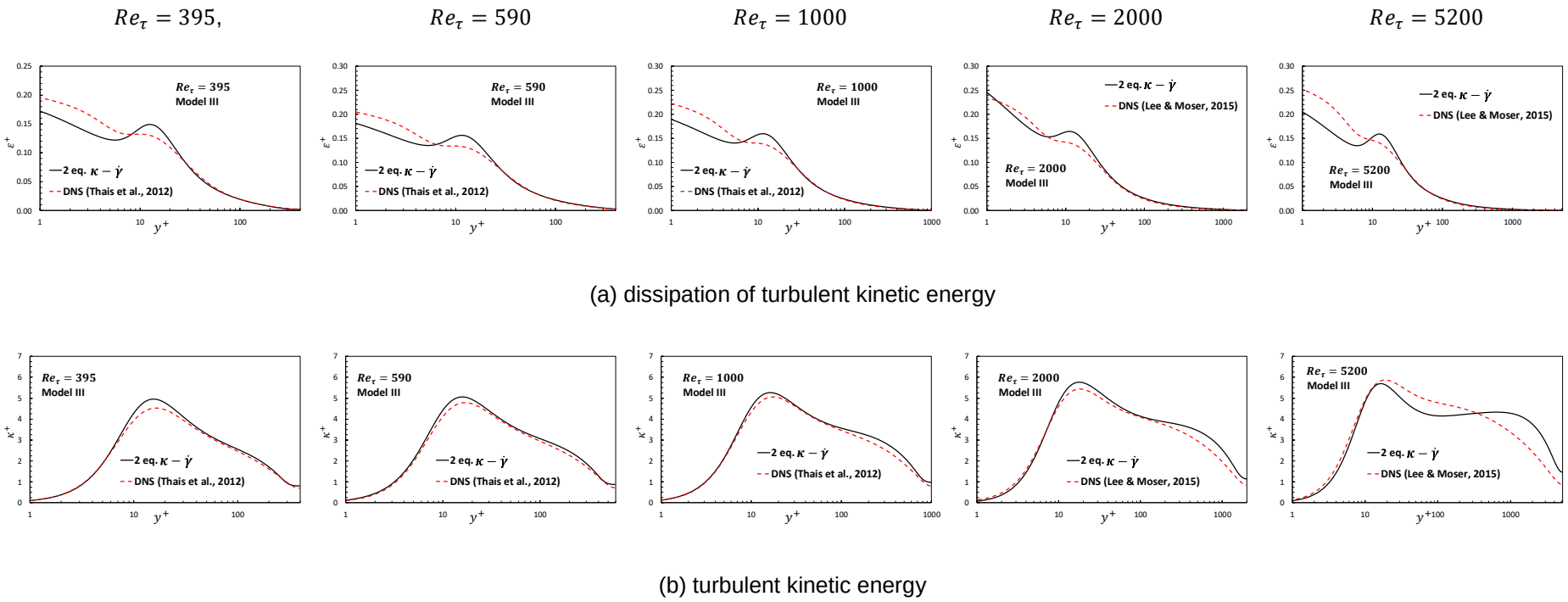

(a) dissipation of turbulent kinetic energy

(b) turbulent kinetic energy

Figure 4.22 –Dissipation of turbulent kinetic energy and turbulent kinetic energy. Non-linear 2 equations $\kappa - \dot{\gamma}$ models. . $Re_\tau = 395$, $Re_\tau = 590$, $Re_\tau = 1000$, $Re_\tau = 2000$, $Re_\tau = 5200$. Model III of the tensorial base.

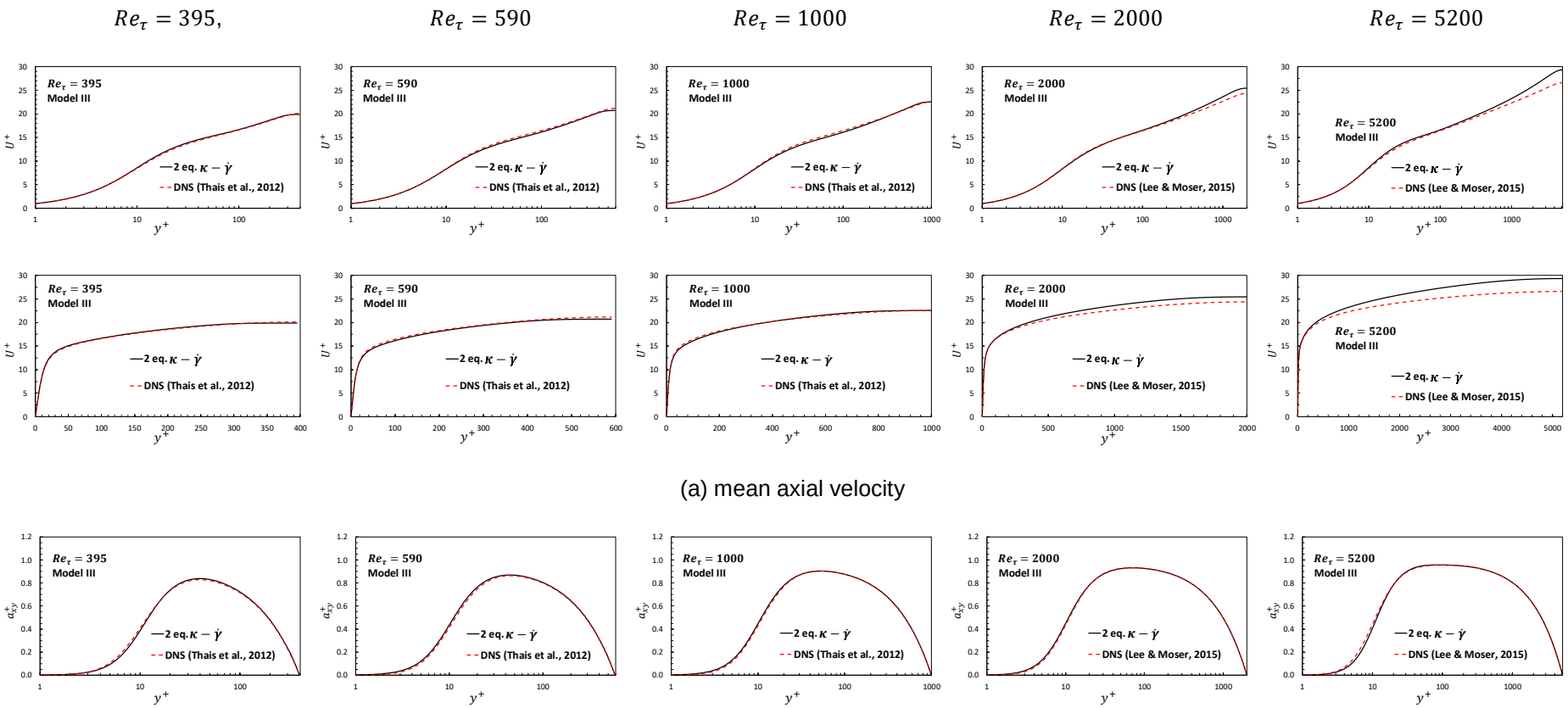

(a) mean axial velocity

(b) shear Reynolds stress a_{xy}.

Figure 4.23 – Mean axial velocity and shear Reynolds stress a_{xy}. Non-linear 2 equations $\kappa - \dot{\gamma}$ model. $Re_\tau = 395$, $Re_\tau = 590$, $Re_\tau = 1000$, $Re_\tau = 2000$, $Re_\tau = 5200$. Model III of the tensorial base.

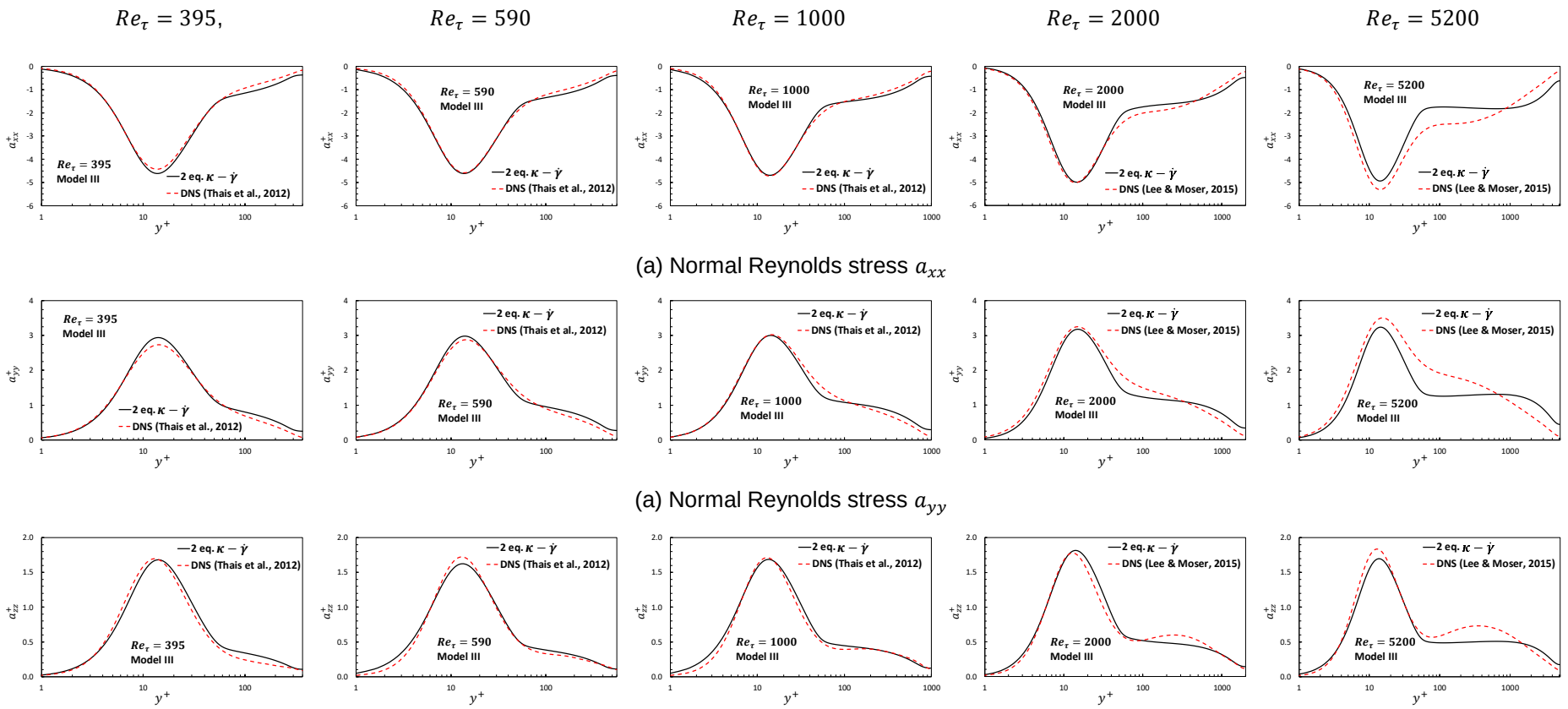

(a) Normal Reynolds stress a_{xx}

(a) Normal Reynolds stress a_{yy}

(c) Normal Reynolds stress a_{zz}.

Figure 4.24 – Normal Reynolds stress a_{xx}, a_{yy}, a_{zz}. Non-linear 2 equations $\kappa - \dot{\gamma}$: $Re_\tau = 395$, $Re_\tau = 590$, $Re_\tau = 1000$, $Re_\tau = 2000$, $Re_\tau = 5200$. Model III of the tensorial base.

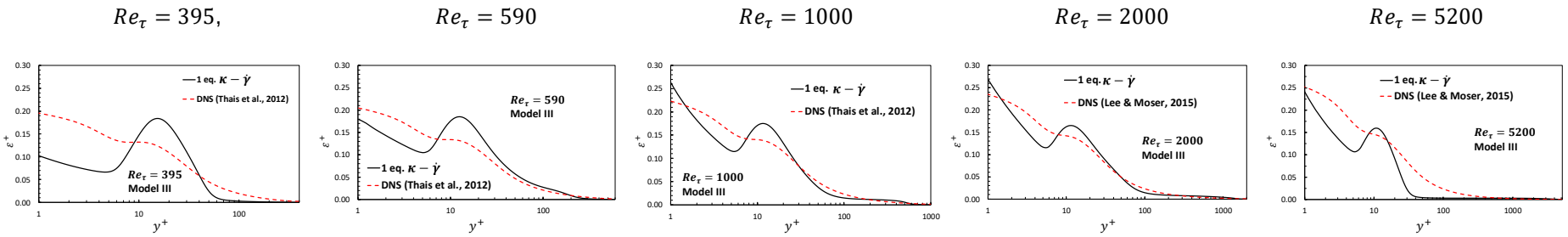

(a) Dissipation of turbulent kinetic energy

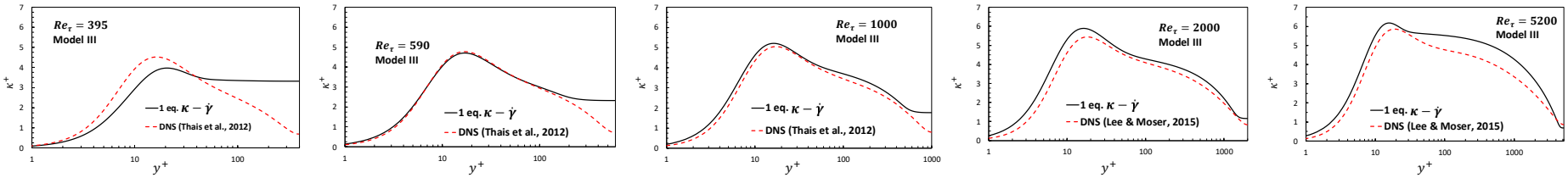

(b) turbulent kinetic energy

Figure 4.25 –Dissipation of turbulent kinetic energy and turbulent kinetic energy. 1 equation $\kappa - \dot{\gamma}$. $Re_\tau = 395$, $Re_\tau = 590$, $Re_\tau = 1000$, $Re_\tau = 2000$, $Re_\tau = 5200$. Model III of the tensorial equation.

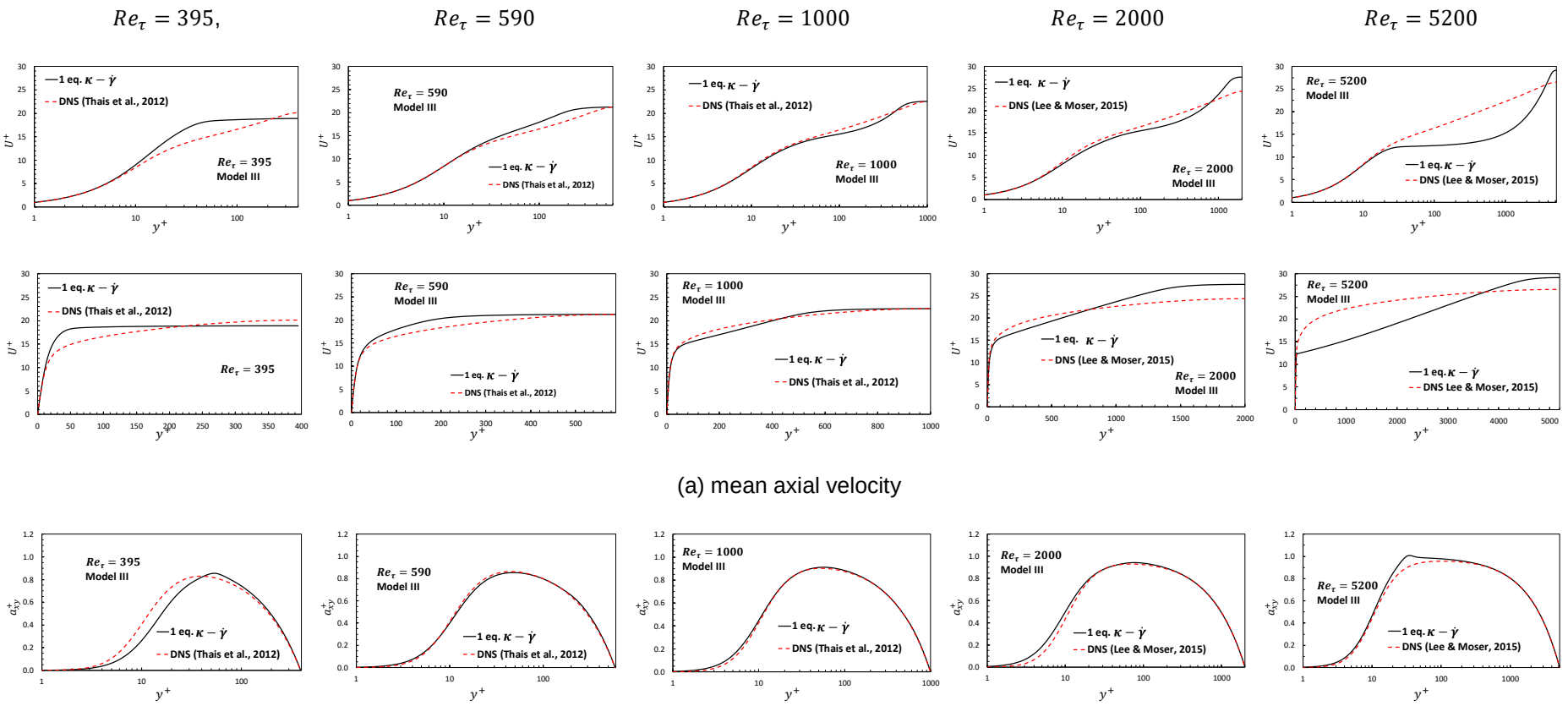

(a) mean axial velocity

(b) Shear Reynolds stress a_{xy}.

Figure 4.26 – Mean axial velocity and shear Reynolds stress a_{xy}. 1 equation $\kappa - \dot{\gamma}$. $Re_\tau = 395$, $Re_\tau = 590$, $Re_\tau = 1000$, $Re_\tau = 2000$, $Re_\tau = 5200$. Model III of the tensorial base.

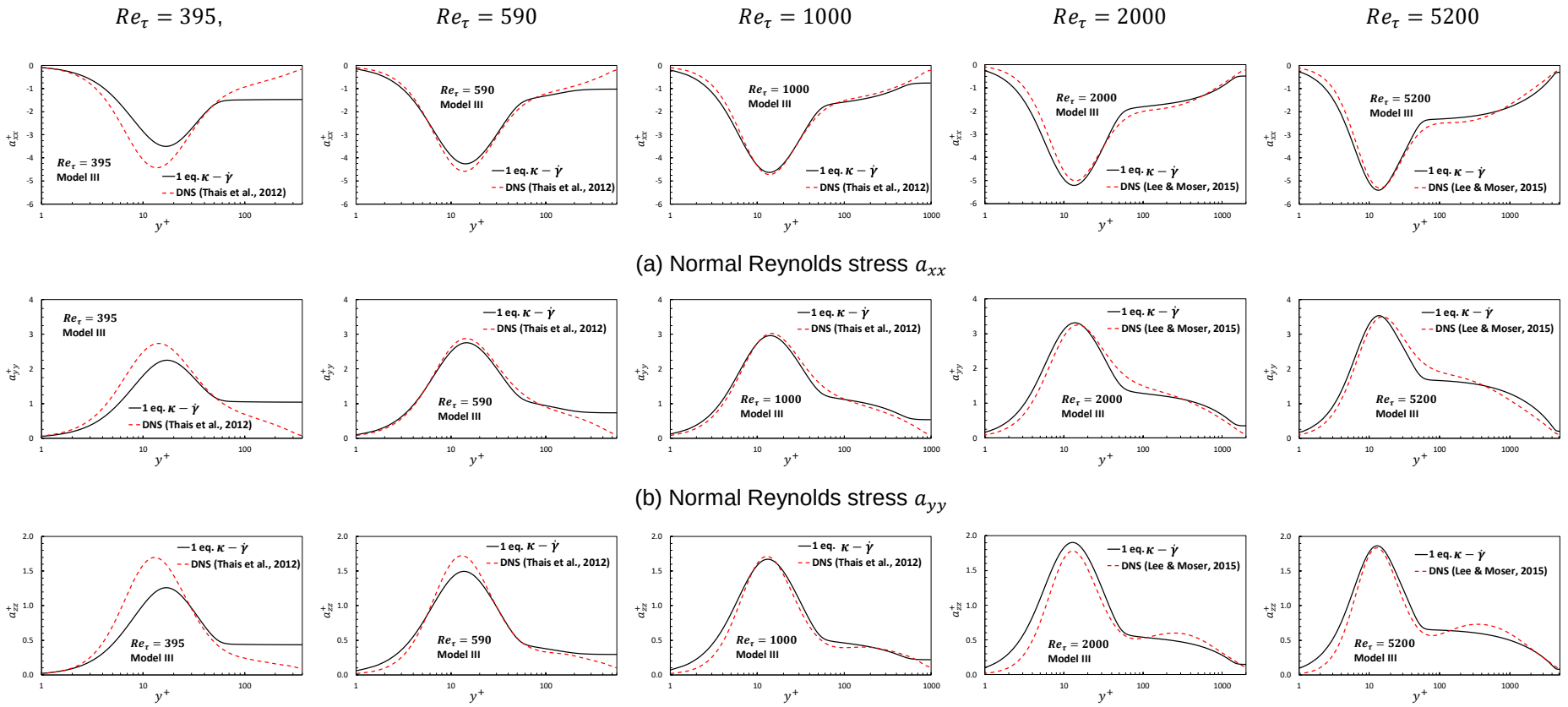

(a) Normal Reynolds stress a_{xx}

(b) Normal Reynolds stress a_{yy}

(c) Normal Reynolds stress a_{zz}.

Figure 4.27 – Normal Reynolds stress a_{xx}, a_{yy}, a_{zz}. 1 equation $\kappa - \dot{\gamma}$. $Re_\tau = 395$, $Re_\tau = 590$, $Re_\tau = 1000$, $Re_\tau = 2000$, $Re_\tau = 5200$. Model III of the tensorial base.

5 Conclusions

The main objective of this work was to develop and evaluate non-linear RANS models to predict channel flow, dependent on the square of the rate of deformation tensor $\boldsymbol{D^2}$ and non-persistence tensor $\boldsymbol{P}$. The characteristic velocity and length of the models are based on the turbulent kinetic energy, κ, and the norm of strain deformation tensor, $\dot{\gamma}$. The transport equation to determine κ was obtained with Modified Rodi Mansour model (Michelassi, 1993). Two different types of models were developed: 2 eq. $\kappa - \dot{\gamma}$ and 1 eq. $\kappa - \dot{\gamma}$. For the later, a model was developed for the dissipation of turbulent kinetic, aiming to avoid the solution of its transport equation. The predictions were compared with DNS data of two different data sets (Thais *et al*., 2012 and Lee & Moser, 2015) for a range of friction Reynolds number from 395 to 5200.

Near wall damping functions corresponding to the linear term, f_μ, and non-linear terms, $f_{\mu 2}$ and f_β, of the models were developed. The near wall damping function f_μ was strongly dependent of the friction Reynolds number, but Reynolds independent near wall damping functions $f_{\mu 2}$ and f_β were determined. Correlations for the limiting parameter C_μ, $C_{\mu 2}$ and C_β as a function of the friction Reynolds number were also developed.

The results obtained with four models from the tensorial base with the proposed 1 equation $\kappa - \dot{\gamma}$ model and 2 equations $\kappa - \dot{\gamma}$ model corroborate the observation of Nieckele *et al.* (2016) and Murad (2018) that the non-linear model based on both $\boldsymbol{D^2}$ and $\boldsymbol{P}$ is the best model. Murad (2018) showed that the models $\kappa - \varepsilon$ and $\kappa - \dot{\gamma}$ that he proposed, with Model III of the tensorial base, were superior to four different $\kappa - \varepsilon$ models found in the literature. It was shown that the present 2 equations $\kappa - \dot{\gamma}$ model developed in the present work was superior to Murad (2018) models. This statement can be made based on the predicted results and by the fact that the present damping functions are restricted to the wall region, therefore, they can be used in other applications, for a wide range of Reynolds number.

A new algebraic model was proposed to determine the dissipation of the turbulent kinetic energy, coupled with a near wall damping function. It must be stressed here that the developed damping function was independent of the friction Reynolds number. Good results were obtained for $Re_\tau = 1000$ and 2000, but the model need improvement for smaller and larger friction Reynolds numbers.

5.1 Future works

As a recommendation of future work, one can suggest to apply the 2 equations $\kappa - \dot{\gamma}$ Tensorial Base III to a wider friction Reynolds number range. Different geometries, like a back step, or the fully developed flow in square channel flow are also good benchmark cases to be examined.

It is also recommended to search a more universal near wall damping function for the linear term. One can also search a methodology to determine the damping function based on the flow solution, as a dynamic type of adjustment.

The present linear 2 equations $\kappa - \dot{\gamma}$ can be compared with other models available in the literature, like $\kappa - \omega$ and $\kappa - \omega\, SST$ models, which presently are very popular. The 2 equations $\kappa - \dot{\gamma}$ Tensorial Base III could also be coupled with $\kappa - \omega$ instead of $\kappa - \varepsilon$.

Although reasonable results were obtained with the proposed model for the dissipation of turbulent kinetic energy for Re_τ =1000, a more general model can be search.

Different propositions found in the literature for the dissipation of turbulent kinetic energy can be tested with the proposed 1 equation $\kappa - \dot{\gamma}$ Tensorial Base III. Further the present 1 equation model can be compared with others 1 equation models available in the literature, like Spallart-Almaras model, to evaluate not only the accuracy but the computing effort.

Bibliography

1. Abe, K.; Jang, Y. J.; Leschziner, M. A. **An Investigation of Wall-Anisotropy Expressions and Length-Scale Equations for Non-Linear Eddy-Viscosity Models.** *International Journal of Heat and Fluid Flow*. V. 24. 2003. Pp. 181-198.
2. Alegre, D. M.; Alves, F. S.; Thompson, R. L.; Mitre, J. F.; Sampaio, L. E. B. **The Use of a General Convected Time Derivative to Compute the Reynolds Stress Tensor for a Compressible Turbulent Flow.** *Journal of Brazilian Society of Mechanical Sciences and Engineering.* V. 42. 2020.
3. Alves, F., V.; Thompson, R., L.; Sampaio, L., B. **O Uso de Base de Dados DNS para Construção de Modelos RANS Utilizando Decomposições Tensoriais e Coeficientes de Bases Normalizadas.** Rio de Janeiro, 2014 Monografia (Mestrado em Engenharia Mecânica) – Universidade Federal Fluminense.
4. Bacchi, R. D. A.; **O que se Deseja de Uma Definição de Vórtex.** Master's thesis. Universidade Federal Fluminense, 2009.
5. Beetham, S.; Capecelatro, J. **Formulating Turbulence Closures Using Sparse Regression with Embedded Form Invariance.** *Physical Review Fluids.* V. 5. 2020.
6. BenSaid, H.; Monpean, G.; Naji, H. **On the Evaluation of Linear and Non-Linear Models Using DNS Data of Turbulent Channels Flow.** *Journal of Brazilian Society of Mechanics Science and Engineering.* pp. 469-476.
7. Bradshaw, P.; **Effects of Streamline Curvature on Turbulent Flow.** AGARD-AG-169, 1973.
8. Carlier, J.; Stanislas, M. **Experimental Study of Eddy Structures in a Turbulent Boundary Layer Using Particles Image Velocimetry.** *Journal Fluid Mechanics.* Vol 535. 2005. pp 143-188.
9. Chen, Y.; Lu, C.; Chen, X. **Quadratic and Cubic Eddy-Viscosity Models in Turbulent Supercavitating Flow Computation.** *Theoretical & Applied Mechannics Letters.* V. 1. 2011.
10. Fadhila, H.; Medina, H.; Aleksandrova, S.; Benjamin, S. **A New Non-Linear RANS Model with Enhanced Near-Wall Treatment of Turbulence**

Anisotropy. *Applied Mathematical Modelling.* V. 82. 2020. Pp. 293-313.

11. Fu, S.; Wang, C., Guo, Y. **On the Minimal Representation of Non-Linear Eddy Viscosity Models.** *Journal of Turbulence.* V12. 2011. Pp. 1-31.
12. Gatski, T. B.; Jongen, T. **Nonlinear Eddy Viscosity and Algebraic Stress Models for Solving Complex Turbulent Flows.** *Progress in Aerospace Sciences.* Vol. 36. 2000. pp 655-682.
13. Kaandorp, M. L. A.; Dwight, R. P. **Data-Driven Modelling of the Reynolds Stress Tensor Using Random Forests with Invariance.** *Computers and Fluids.* V.202. 2020.
14. Kalitzin, G.; Medic, G.; Iaccarino, G.; Durbin, P. **Near-Wall Behavior of RANS Turbulence Models and implications for Wall Functions.** *Journal of Computational Physics.* V.204. 2005. Pp. 265-291.
15. Kundu, P. K.; Cohen, I. M. **Fluid Mechanics.** *Third Edition.Elsevier Academic Press.* 2004.
16. Lam, C.; Bremhorst, K. **Modified form of $\kappa - \varepsilon$ for Predicting Wall Boundary Layers on Spinning and Curved Surfaces.** *Journal of Fluids Engineering, 103,* 1981. P.456-460.
17. Launder, B.; Pridding, C.; Sharma, B. **The Calculation of Turbulent Boundary Layers on Spinning and Curved Surfaces.** *Journal of Lfuids Engineering,* 1977. P.99-231.
18. Lee, M.; Moser, R. D. **Direct Numerical Simulation of Turbulent Channel Flow Up to $Re_\tau = 5200$.** 2015. Journal of Fluid Mechanics. Vol. 774. pp 395-415.
19. Li, F., B.; Pei, B., B., Bai, B., F. **A Non-Linear Turbulence Modelo f Supercritical Fluid Considering Local Non-Equilibrium of Reynolds Stress Transport.** *Physics of Fluids.* V.32. 2020.
20. Lien, F.; Chen, W.; Leschziner, M. **Low-Reynolds-Number Eddy-Viscosity Modelling Based on Non-Linear Stress-Strain/Vorticity Relations.** *Engineering Turbulence Modelling and Experiments*, 1996. pp 1598-1605.
21. Lien, F.; Leschziner, M. **A Pressure-Velocity Solution Strategy for Compressible Flow and Its Application to Shock/Boundary-Layer Interaction Using Second-Moment Turbulence Closure.** *Journal of Fluids Engineering,*1993. P. 717-725
22. Lumley, J. L.; **Toward a Turbulent Constitutive Equation.** *Journal of Fluid Mechanics,* 1970, Vol. 41. pp 413-434.
23. Luo, G.; Yao, Z.; Shen, H. **A New Hybrid Turbulence Model Applied to Highly Turbulent Taylor-Cowette Flow.** *Physics of Fluids.* V. 30. 2018.

24. Menter, F. R. **Two-Equations Eddy-Viscosity Turbulence Models for Engineering Applications.** *AIAA Journal,* 1994. Vol. 32, Nº 8.
25. Michelassi, V.; Rodi, W.; Zhu, J.; **Testing a Low Reynolds Number $\kappa - \varepsilon$ Turbulence Model Based on Direct Simulation Data.** *AIAA Journal,* 1993. p 1720-1723.
26. Mukin, R. V.; Alipchenkov, V. M.; Zaichik, L. I.; Mukina, L. S.; Strizhov, V. F. **Non-Linear Algebraic Reynolds Stress Model for Two-Phase Turbulent Flows Laden with Small Heavy Particles in Circular Tube.** *Journal of Physics: Conference Series*. 2011.
27. Murad, F., W.; Nieckele, A., O.; Sampaio, L., E., B.; Thompson, R., L. **Evaluation of Different Levels of Approximation of the Reynolds Stress Tensor for Channel Flow Employing DNS Data.** *ASTFE*. 2020.
28. Murad, F., W.; Sampaio, L., E., B.; Thompson, R., L.; Nieckele, A., O. **Evaluation of a Quadratic Rate of Strain Reynolds Stress Tensor Model for a Channel Flow Employing DNS Data.** *Turbulence, Heat and Mass Transfer.* V. 9. 2018.
29. Murad, F.; Nieckele, A.; Sampaio, L. **Performance evaluation of nonlinear explicit algebraic Reynolds stress models to predict channel flow.** Rio de Janeiro, 2018 Monografia (Mestrado em Engenharia Mecânica) – Pontifícia Universidade Católica do Rio de Janeiro.
30. Nieckele, A.; Thompson, R.; Mopean, G. **Anisotropic Reynolds stress tensor representation in shear floes using DNS and experimental data.** *Journal of Turbulence, (2016)*. p.1-29.
31. Otereo, R., G., J.; Patel, A.; Diez, R., S.; Pecnik, R. **Turbulence Modelling for Flows with Strong Variations in Thermo-Physical Properties.** *International Journal of Heat and Fluid Flow.* V.73. 2018. Pp.114-123.
32. Park, T. S.; Sung, H. J.; Suzuki, K. **Development of a Nonlinear Near-Wall Turbulence Model for Turbulent Flow and Heat Transfer.** *International Journal of Heat and Fluid Flow*, Vol. 24. 2003. pp 29-40.
33. Patankar, S. **Numerical Heat Transfer and Fluid Flow.** 1980. Hermisphere Publishing Co.
34. Patankar, S. V.; Liu, C. H.; Sparrow, E. M. **Fully Developed Flow and Heat Transfer in Ducts Streamwise Periodic Variations of Cross-Sectional Area.** 1977. *ASME J. Heat Transfer.* Vol. 99. pp 180-186.
35. Pope, S. B. **A More Genreal Effective-Viscosity Hypothesis.** *J. Fluid Mech. 72.,* 1975. pp 331-340

    Pope, S. B. **Turbulent Flows.** Cambridge University Press. 2000.

36. Rahman, M. M.; Keskinen, K.; Vuorinen, V.; Larmi, M.; Siikonen, T. **Consistently Formulated Eddy-Viscosity Coefficient for κ −Equation Model.** *Journal of Turbulence.*2019.
37. Resende, P. R.; Pinho, F. T.; Cruz, D. O. **A Reynolds Stress Model for Turbulent Flows of Viscoelastic Fluids.** *Journal of Turbulence*. V. 14. 2013. Pp. 1-36.
38. Ribeiro, B., L., R.; Lopes, L., B., F., Mitre, J., F., Thompson, R., L. **Model Analysis of the Turbulent Flows in a Convergent-Divergent Channel and Around a Sphere.** *Journal of the Brazilian Society of Mechanical Sciences and Engineering.* V. 40. 2018.
39. Rodi, W; Mansour, N.; **Low Reynolds number $\kappa - \varepsilon$ Modelling With the Aid of DNS Data.** *J. Fluid Mech,* 1993. pp 509-529.
40. Santos, T., L., A. **Modelagem Linear e Não-Linear para o Tensor de Reynolds em Escoamentos Turbulentos em Dutos.** Dissertação de Mestrado apresentada ao Programa de Pós-Graduação em Engenharia Mecânica, COPPE, UFRJ, 2019.
41. Settari, A.; Aziz, K. **A Generalization of the Additive Correction Methods for the Iterative Solution of Matrix Equations.** *SIAM J. Numer. Anal.* Vol. 10, No. 3, June 1973. Pp. 506-521
42. Stanislas, M.; Perret, L.; Foucaut, J. **Vortical Structures in the Turbulent Boundary Layer: a possible Route to a Universal Representation.** *Journal of fluid Mechanics.* Vol 602. 2008. pp 327-382.
43. Tennekes, H.; Lumley, J. L. **A First Course in Turbulence.** *The MIT Press.* 1972.
44. Thais, L.; Gatski, T. B.; Mompean, G. **Some Dynamical Features of the Turbulent Flow of a Viscoelastic Fluid for Reduceddrag.** J. Turbulence. 2012. Vol. 13. pp 1-26.
45. Thompson R. L. **Some Perspectives on the Dynamic History of a Material Element.** *International Journal of Engineering Science.* (2008). p.224-249.
46. Thompson, R. L.; Mompean, G.; Thais, L. **A Methodology to Quantify the Nonliearity of the Reynolds Stress Tensor.** *Journal of Turbulence.* 2010. p.1-27.
47. Thompson, R. L.; Sampaio, L. B.; Alves, F. A.; Thais, L.; Mompean, G. **A Methodology to Evaluate Statistical Errors in DNS Data of Plane Channel Flows.** *Computers and Fluids*, 2016. p. 1-7.

48. Tian, X., Q.; Rahman, M., M.; Pan, H. C.; Islam, A., K., M., S. **A Simplified One-Equation Elliptic-Relaxation Model.** *8th BSME International Conference on Thermal Engineering.* V.2121. 2019.
49. Versteeg, H. K.; Malalasekera, W. **An Introduction to Computational Fluid Dynamics, THE FINITE VOLUME METHOD.** PEARSON Prantice Hall. 2007.
50. Walling, S.; Johansson, A. V. **Modelling Streamlines Curvature Effects in Explicit Algebraic Reynolds Stress Turbulence Models.** *International Journal of Heat and Fluid Flow.* Vol. 23. 2002. pp 721-730.
51. Weatheritt, J.; Sandberg, R. **A Novel Evolutionary Algorithm Applied to Algebraic Modifications of the RANS Stress-Strain Relationship.** *Journal of Computational Physics.* V. 35. 2016. Pp. 22-37.
52. Wei, Q.; Chen, H.; Zheng, M. A. **An Hybrid RANS/LES Model for Simulation of Complex Turbulent Flow.** *Journal of Hydrodinamics.* V. 28. 2015. Pp. 811-820.
53. Wilcox, D.; **Turbulence Modeling for CFD.** *San Diego: DWC Industries,* 1994.
54. Yang, X. L.; Liu, Y.; Yang, L. **A Shear Stress Transport Incorporated Elliptic Blending Turbulence Model Applied to Near-Wall, Separated and Impinging Jet Flows and Heat Transfer.** Computers and Mathematics with Apllications. 2020.
55. Zhang, Y.; Rahman, M., M.; Chen, G. **Development of $\kappa - R$ Turbulence Model for Wall-Bounded Flows.** *Aerospace Science and Technology.* V.98. 2020.

Appendix A – Models $\kappa - \dot{\gamma}$ Coefficients

As mentioned in chapter 3, this appendix will discuss the definition of the constants and damping functions of $\kappa - \dot{\gamma}$ model.

The DNS data for $Re_\tau \leq 1000$ is from Thais *et al.* (2012) and for $Re_\tau \geq 2000$ is from Lee & Moser (2015).

A.1 Linear and non-linear models $\kappa - \dot{\gamma}$ coefficients

For all f_μ used, the same equation, Eq(3.56), repeated below,

$$f_\mu = \tanh\left(a_1 y^{+b_1}\right)$$

was applied, but for each Re_τ there are different constants. The damping function correlation parameters are shown in Table A.**1** for all friction Reynolds number Re_τ evaluated here.

Table A.1 – Constants for f_μ and C_μ.

Re_τ	a_1	b_1	C_μ
395	0.04*0*	0.890	0.298
590	0.062	0.772	0.280
1000	0.070	0.750	0.261
2000	0.091	0.639	0.248
5200	0.049	0.870	0.242

Equations for the damping function of the non-linear terms given by Eq(3.54) and Eq. (3.55), are repeated below

$$f_{\mu 2} = a_2\left\{b_2 + \exp\left[c_2 + d_2 y^+ + g_2 y^{+2}\right]\right\}^{h_2}$$

$$f_\beta = a_3\left\{b_3 + \exp\left[c_3 + d_3 y^+ + g_3 y^{+2}\right]\right\}^{h_3}$$

The coefficients for $f_{\mu 2}$ and f_β are independent for the Reynolds number and are:

$$a_2 = 0.0155; b_2 = 1.2;\ c_2 = -0.0425;\ \ d_2 = -0.0013; g_2 = 0.21; h_2 = 2.4$$

$$a_3 = 0.0155; b_3 = -0.32;\ c_3 = -0.02;\ d_3 = -0.0013; g_3 = 0.21; h_3 = 2.4$$

Figure A.1 shows the constants C_{μ_2} and C_β for each Re_τ. Since the reference values of $C_{\mu 2}$ and C_β are function of the friction Reynolds number Re_τ, correlations of these variable with Re_τ were developed, as

$$C_\beta = Re_\tau^{-g(Re_\tau)} \tag{A.1}$$

$$g(Re_\tau) = 1.1 \times 10^{-10} Re_\tau^2 - 2.3 \times 10^{-6} Re_\tau + 4.74 \times 10^{-2}$$

$$C_{\mu 2} = 3 \times 10^{-9} Re_\tau^2 + 7 \times 10^{-6} Re_\tau + 7.45 \times 10^{-1} \tag{A.2}$$

The comparison of the adjusted coefficients and the proposed functions are presented in graphical form in Figure A.1. A reasonable agreement of the correlation with the adjusted constants from the DNS data was obtained, with the exception of $Re_\tau = 395$, where it is substantially overestimated, perhaps because it corresponds to a low Re_τ.value.

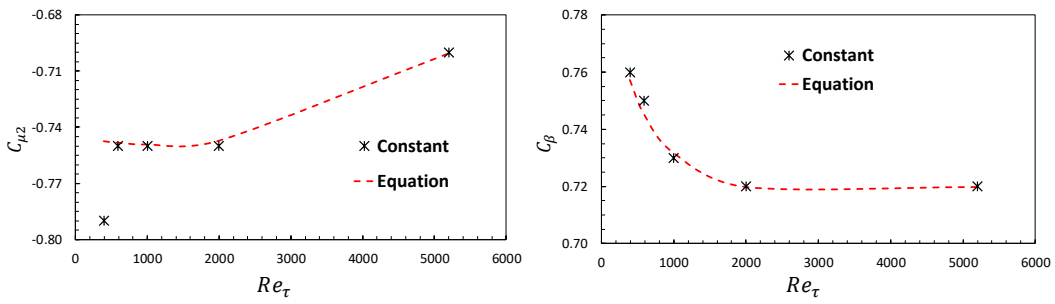

(a) $C_{\mu 2}$ (b) C_β

Figure A.1 – C_β and $C_{\mu 2}$ dependence on Re_τ.

The behaviors all three damping parameters are shown for all friction Reynolds in Figure A.2, Figure A.2, Figure A.3 and Figure A.4.

Table A.2 – Constants of non-linear coefficients $C_{\mu 2}$ and C_β.

Re_τ	395	590	1000	2000	5200
$-C_{\mu 2}$	0.79	0.75	0.75	0.75	0.70
C_β	0.76	0.75	0.73	0.72	0.72

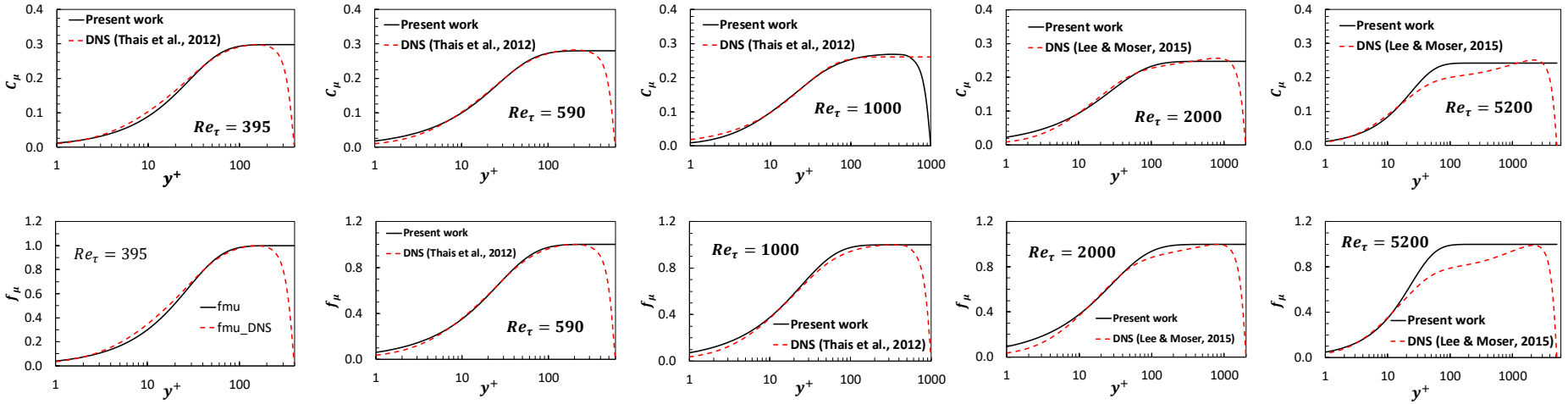

(a) $Re_\tau = 395$ (b) $Re_\tau = 590$ (c) $Re_\tau = 1000$ (d) $Re_\tau = 2000$ (e) $Re_\tau = 5200$

Figure A.2 – C_μ and f_μ from DNS data and fitted for $Re_\tau = 395$ to 5200.

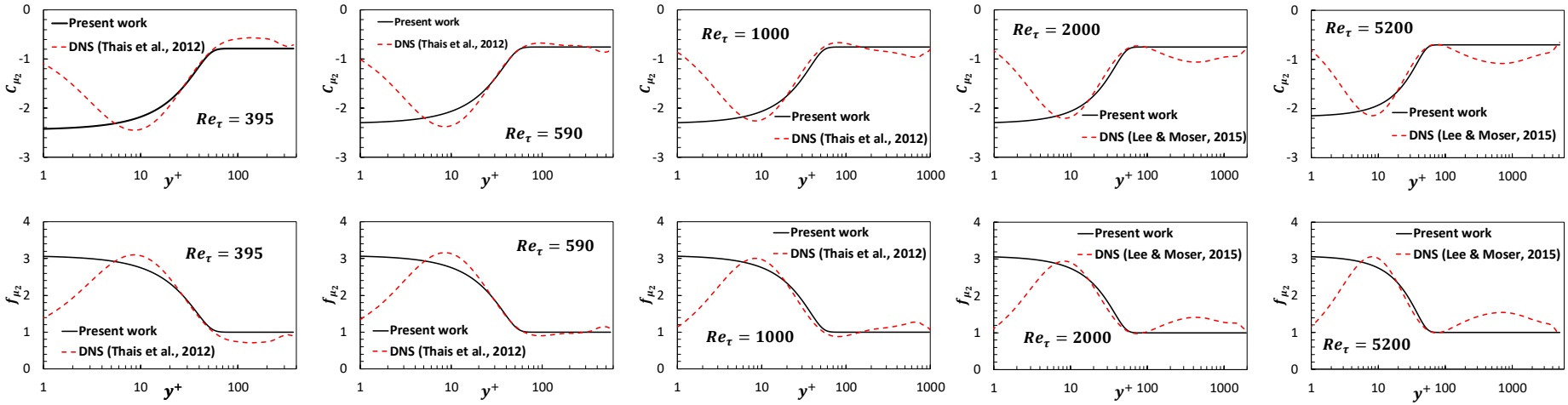

(a) $Re_\tau = 395$ (b) $Re_\tau = 590$ (c) $Re_\tau = 1000$ (d) $Re_\tau = 2000$ (e) $Re_\tau = 5200$

Figure A.3 – $C_{\mu 2}$ and f_{μ_2} from DNS data and fitted from DNS data and fitted for $Re_\tau = 395$ to 5200.

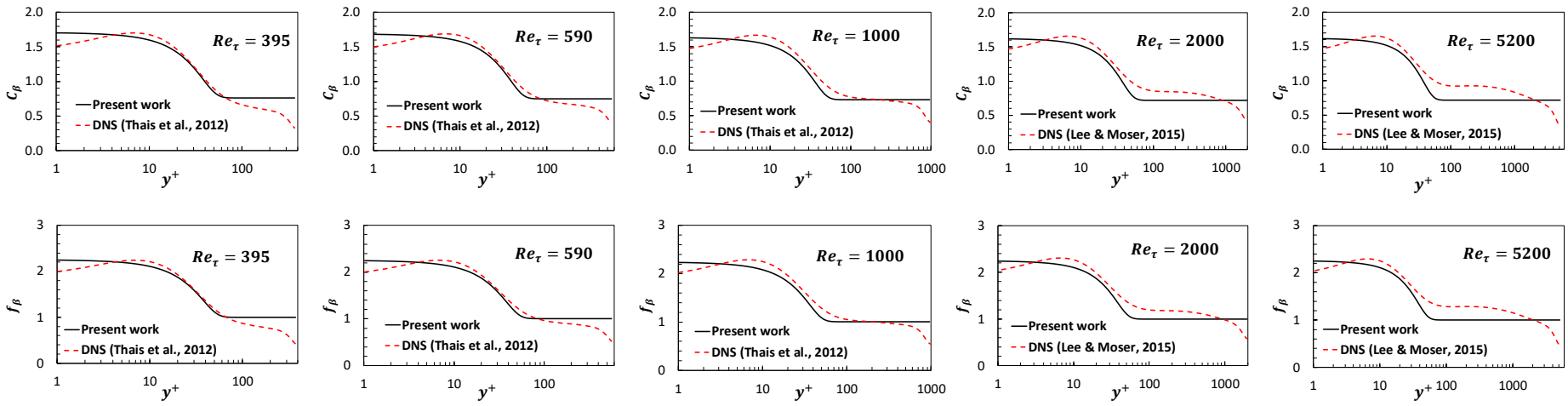

(a) $Re_\tau = 395$ (b) $Re_\tau = 590$ (c) $Re_\tau = 1000$ (d) $Re_\tau = 2000$ (e) $Re_\tau = 5200$

Figure A.4 – f_β and C_β from DNS data and fitted for $Re_\tau = 395$ to $Re_\tau = 5200$.

A.2 Murad (2018) model $\kappa - \dot{\gamma}$ coefficients

The coefficients for the non-linear terms proposed by Murad (2018) are presented next. The functions for C_{μ}^{γ} are

$$
\begin{aligned}
C_{\mu-\gamma} &= 0.0054y^{+};\ y^{+} < 3 \\
C_{\mu-\gamma} &= \frac{-0.007 + 0.0086y^{+}}{1 + 0.056y^{+} + 1.5x10^{-5}(y^{+})^{2}};\ 3 < y^{+} \leq \hat{y}^{+} \\
C_{\mu-\gamma} &= 5.6x10^{-10}\left(y_{eff}^{+}\right)^{3} + 9x10^{-8}\left(y_{eff}^{+}\right)^{2} + C_{\mu}^{\gamma}(y_{eff}^{+});\ \hat{y}^{+} < y^{+}
\end{aligned}
\tag{A.1}
$$

where y_{eff}^{+} is written as the following difference $y_{eff}^{+} = y^{+} - \hat{y}^{+}$ and $\hat{y}^{+}$ is the y^{+} value of maximum $C_{\mu-\gamma}$ which can be defined as a function of the Reynolds Number: $\hat{y}^{+} = 0.2734Re + 44.745$.

The coefficient of $C_{\mu 2-\gamma}$ of the non-linear term D_{ij}^{2} is

$$
\begin{aligned}
C_{\mu 2-\gamma} &= 0.2277;\ y^{+} < 1 \\
C_{\mu 2-\gamma} &= 0.5622\left(y_{log}^{+}\right)^{4} - 2.0685\left(y_{log}^{+}\right)^{3} + 1.948\left(y_{log}^{+}\right)^{2} \\
&\quad - 0.1167\left(y_{log}^{+}\right) + 0.2277;\ 1 < y^{+} \leq 69 \\
C_{\mu 2-\gamma} &= C_{\mu 2-\gamma}(y^{+} = 69);\ 69 < y^{+}
\end{aligned}
\tag{A.2}
$$

where $y_{log}^{+} = log_{10}(y^{+})$.

Finally the coefficient C_{β}^{γ} is

$$
\begin{aligned}
C_{\beta-\gamma} &= 0.3716;\ y^{+} < 1 \\
C_{\beta-\gamma} &= 0.04835\left(y_{log}^{+}\right)^{5} - 0.0859\left(y_{log}^{+}\right)^{4} - 0.1759\left(y_{log}^{+}\right)^{3} \\
&\quad + 0.2784\left(y_{log}^{+}\right)^{2} - 0.0269\left(y_{log}^{+}\right) + 0.3716;\ 1 < y^{+} \\
&\quad \leq 95 \\
C_{\beta-\gamma} &= 2.38x10^{-10}(y^{+})^{3} + 2.38x10^{-7}(y^{+})^{2} + 1.117x10^{-4}\,y^{+} \\
&\quad + 0.1993;\ 95 < y^{+}
\end{aligned}
\tag{A.3}
$$

Figure A.5 shows a comparison with the damping function of the present work with developed by Murad (2018). Note that the functions proposed by Murad (2018) act in the entire domain.

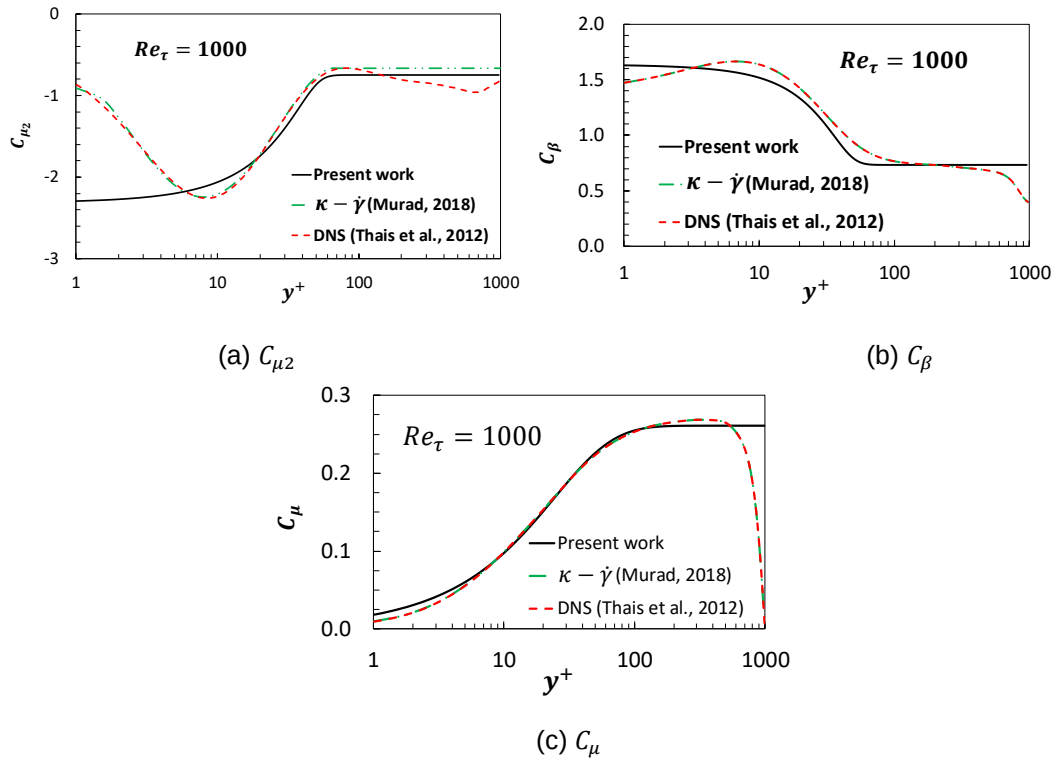

(a) $C_{\mu 2}$ (b) C_β

(c) C_μ

Figure A.5 – Comparison of $C_\mu, C_{\mu 2}$ and C_β from Murad (2018) and the present work.

A.3 Model ε coefficients

The equation proposed for the dissipation rate of the turbulent kinetic energy and its near wall damping function f_ε described in Chapter 3 are repeated here

$$\varepsilon^+ = f_\varepsilon \, C_\varepsilon \, \kappa^+ \, \dot{\gamma}$$

$$f_\varepsilon = \left\{ a \frac{\tanh[b(y^+)^c]}{\tanh[d(y^+)^e]} \right\}^\Theta + g \left\{ \exp\left[\lambda - \frac{y^+}{h} \right] \right\}$$

Table A.3 shows the constants used in the damping function f_ε for all Re_τ,

Table A.3 – Constants for f_ε.

a	b	c	d	e	Θ	g	λ	h
0.95	0.0035	1.5	−0.00038	4.6	0.68	0.05	0.1	100

Although the f_ε equation is equal for all friction Reynolds number studied in this work, the constant C_ε is different for each friction Reynolds number. For this case, it also was developed a correlation with Re_τ to predict these constants. The constant C_ε for the $Re_\tau = 395; Re_\tau = 590; Re_\tau = 1000; Re_\tau = 2000; Re_\tau = 5200$ are, respectively $C_\varepsilon = 0.291; C_\varepsilon = 0.279; C_\varepsilon = 0.26; C_\varepsilon = 0.234; C_\varepsilon = 0.205$. The obtain the C_ε constant, the following correlation with Re_τ was developed

$$C_\varepsilon = 0.6707 Re_\tau^{-0.138} \tag{A.6}$$

Figure A.6 shows that a very good fit was obtained for the dependence of C_ε with Re_τ by the comparison with the adjusted values employing DNS data of Thais *et al*. (2012) and Lee and Moser (2015) for all Re_τ.

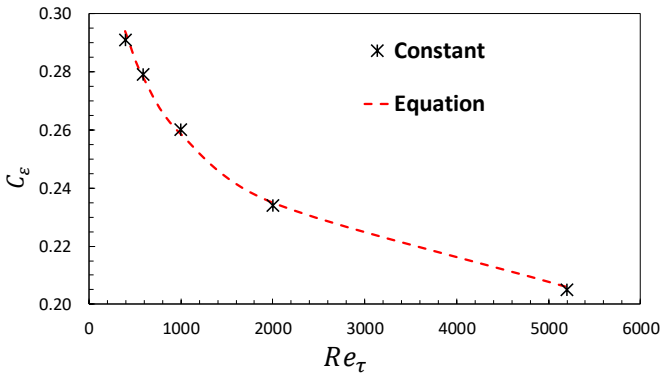

Figure A.6 – C_ε dependence on Re_τ.

The profile of the damping function f_ε with the distance to the wall is shown in Figure A.**7**. For all Re_τ, it is possible to observe a little disagreement in $y^+ < 10$, with an underestimate of the correlation when compared with DNS data. An special attention has to be given to the case $Re_\tau = 5200$, because the DNS behavior far from the wall is not constant, it is slightly tilted., causing a disagreement near the center line.

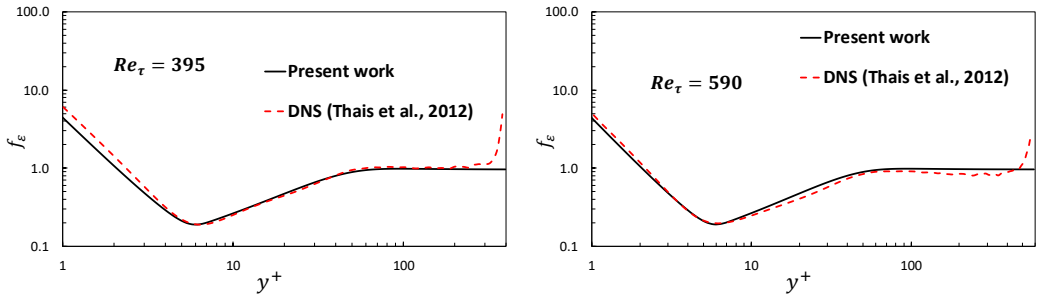

(a) $Re_\tau = 395$

(b) $Re_\tau = 590$

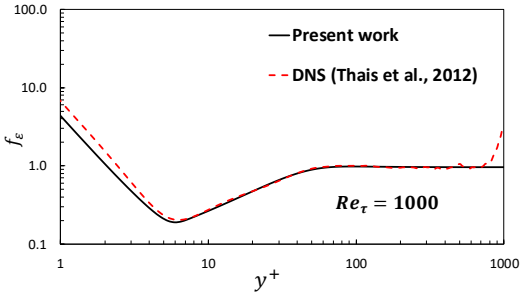

(c) $Re_\tau = 1000$

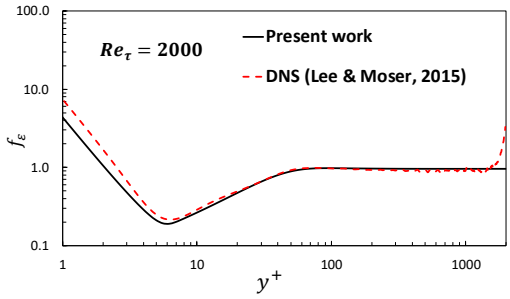

(d) $Re_\tau = 2000$

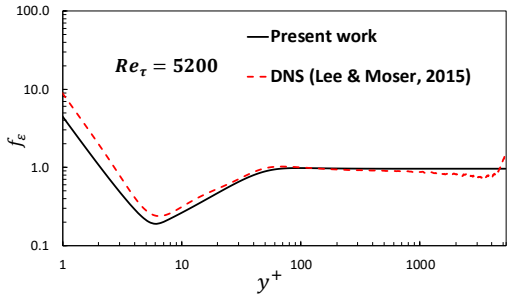

(e) $Re_\tau = 5200$

Figure A.7 – f_ε from DNS data (Thais *et al.*, 2012 and Lee & Moser, 2015) and fitted $Re_\tau = 395$ to $Re_\tau = 5200$.

Appendix B – Grid Test

To evaluate the non-linear models, the same mesh size employed in the DNS data base of Thais *et al.* (2012) and Lee and Moser (2015) was defined to simplify the comparison. However, DNS mesh is a very refined mesh to capture all scales of the flow. In RANS approach all scales are modelled and a coarse mesh can be employed. Therefore, to evaluate if the non-linear models are able to reproduce the DNS data with a coarser mesh, a new solution was obtained.

Once again, the case with friction Reynolds number $Re_\tau = 1000$ was selected, and comparison with DNS data of Thais *et al.*(2012) was performed. The DNS mesh for this Reynolds number was equal to 257 points in the vertical direction. Here, a mesh size 25% smaller, with193 points was tested.

Solution was obtained with the 1-equation $\kappa - \dot{\gamma}$ model, solving κ equation of the Modified Rodi Mansur model, with the present model for the dissipation of κ.

Turbulent variables, κ and ε are shown in Figure B.1. A very good agreement between the solutions was obtained. A slight difference can be seen for ε very close to the wall $y^+ < 10$, and for κ near the symmetry line.

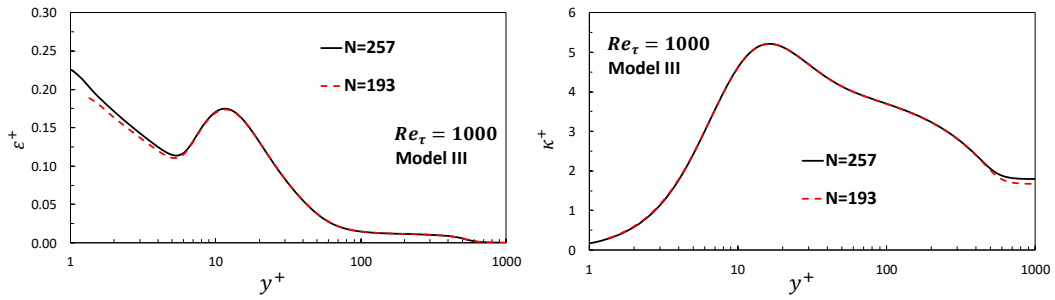

(a) Dissipation of turbulent kinetic energy (b) Turbulent kinetic energy

Figure B.1 – Grid Test:: Dissipation of turbulent kinetic energy and turbulent kinetic energy for. $Re_\tau = 1000$. Model III of the tensorial base.

The mean axial velocity is shown in Figure B.2 where a very small difference between the two meshes can be seen near the symmetry line due to the difference observe in the turbulent kinetic energy in that regions.

Finally the components of the Reynolds stress tensor can be examined in Figure B.3, where an excellent agreement between the solution with both mesh sizes, indicating that a mesh independent solution was obtained and a coarser mesh is able to predict the flow with reasonable agreement with DNS data.

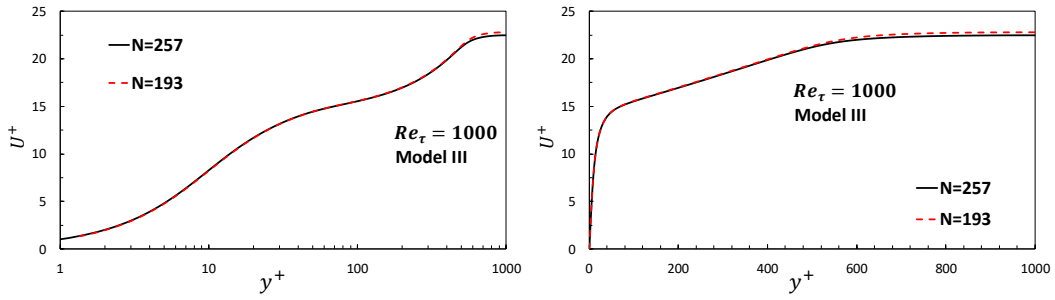

Figure B.2 – Grid Test: Comparison of axial velocity with DNS data (Thais *et al.*, 2012). $\boldsymbol{Re_\tau = 1000}$. Model III of the tensorial base.

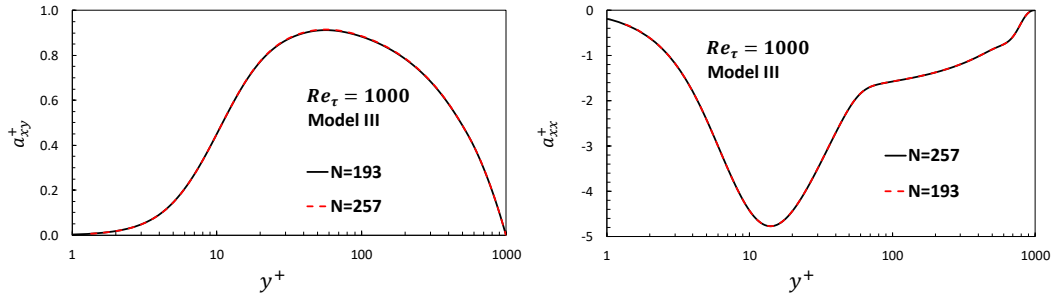

(a) Shear Reynolds stress a_{xy}

(b) Normal Reynolds stress a_{xx}

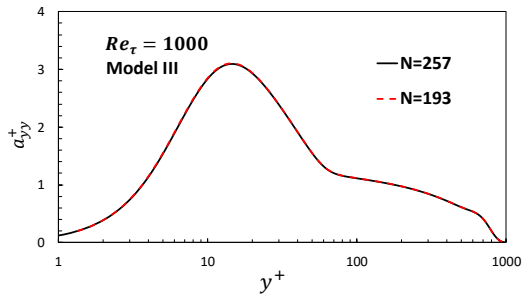

(c) Normal Reynolds stress a_{yy}

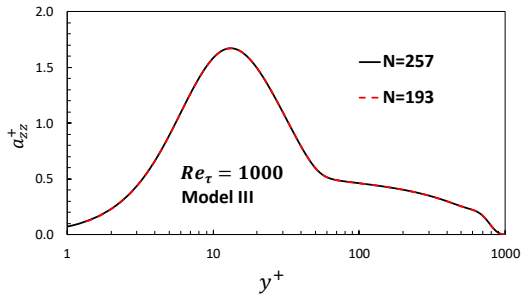

(d) Normal Reynolds stress a_{zz}

Figure B.3 – Grid Test: Comparison of Reynolds stress tensor components with DNS data (Thais *et al.*, 2012). $Re_\tau = 1000$. Model III of the tensorial base.

The results of both mesh are almost the same of the DNS mesh, with a very small disagreement in the region of center line, for the turbulent kinetic energy and mean axial velocity, where the coefficients became singular because $\dot{\gamma} \to 0$. Excellent agreement was obtained for all Reynolds stress tensor components.

Appendix C – Comparison of 1D and 2D formulation

As mentioned in section 3.4.1, the problem has been solved as 2D flow, but in fact, it is a 1D flow. The simulation of 1D problem is computationally cheaper, not only because the computer does not process data in one of the directions, but since the velocity in vertical direction (y^+ direction) is null, all process with this component of the velocity can be ignored, considering only the mean axial velocity. Further all derivatives in the axial direction can also be neglected, eliminating a high number of calculation and iterations to obtain zero for several variables.

For the present test, the Modified Rodi Mansur model for the differential equations of turbulent kinetic energy and dissipation of turbulent kinetic energy presented in section 3.2.3 was employed, as in 2 equations $\kappa - \dot{\gamma}$ model. The 1D solution was obtained with the equations shown in section 3.4.1.

A comparison of 1D and 2D flows predictions for the turbulent quantities, κ and ε, mean axial velocity, and components of the Reynolds stress tensor are shown in Figure C.1 through Figure C.3 for $Re_\tau = 1000$. For all variables, the same results were obtained within the convergence tolerance defined.

The same test was performed for the total range of friction Reynolds number investigated here (from 395 to 5200) for Model III of the tensorial base, with 2 equations $\kappa - \dot{\gamma}$ model. The graphs are not presented, because again perfect agreement within the convergence tolerance was obtained for all variables.

This test indicates that to evaluate the non-linear models prediction for the channel, the1D solution is totally acceptable and, as said before, computationally cheaper, then, all simulations for this work were performed with the 1D model.

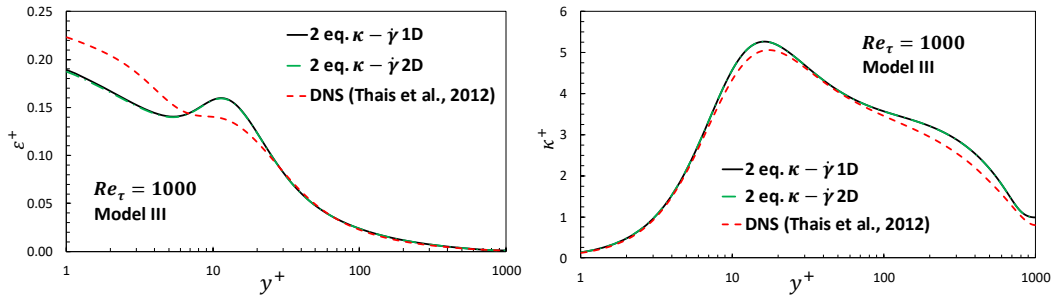

(a) Dissipation of turbulent kinetic energy (b) Turbulent kinetic energy

Figure C.1 – Comparison of 1D and 2D prediction for dissipation of turbulent kinetic energy and turbulent kinetic energy. $Re_\tau = 1000$. Model III of the tensorial base.

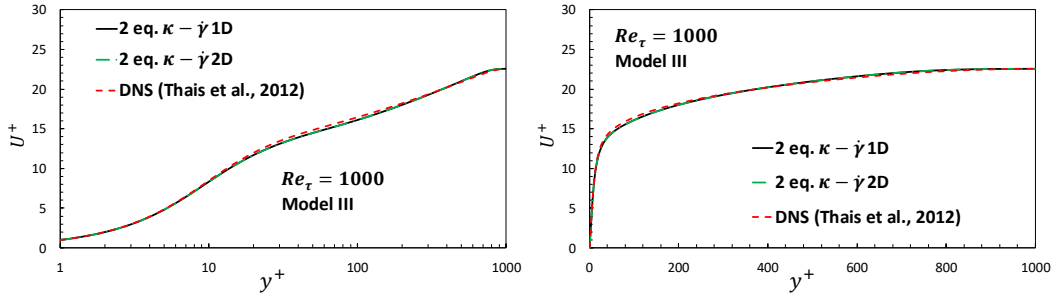

Figure C.2 – Comparison of 1D and 2D of axial velocity with DNS data (Thais *et al.*, 2012). $\boldsymbol{Re_\tau = 1000}$. Model III of the tensorial base.

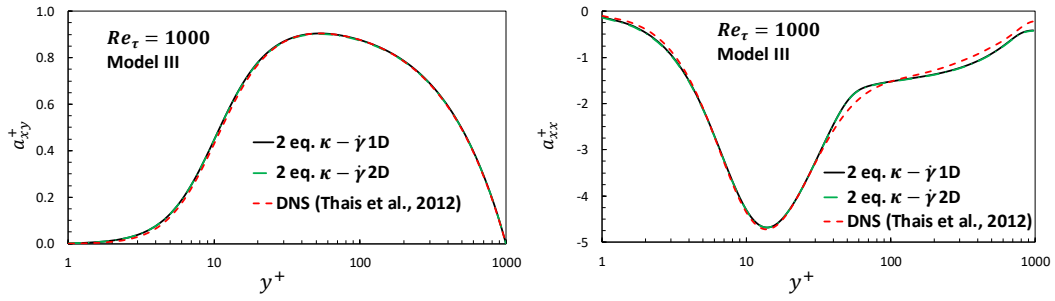

(a) Shear Reynolds stress a_{xy} (b) Normal Reynolds stress a_{xx}

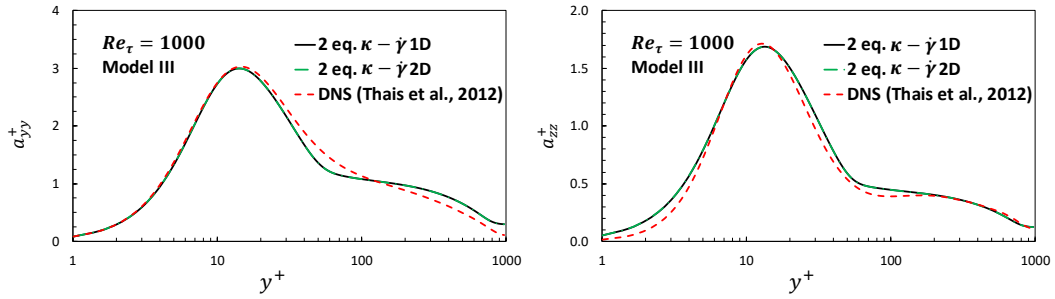

(c) Normal Reynolds stress a_{yy} (d) Normal Reynolds stress a_{zz}

Figure C.3 – Comparison of 1D and 2D of Reynolds stress tensor components with DNS data (Thais *et al.*, 2012). $Re_\tau = 1000$. Model III of the tensorial base.